BOUNDARY MATCHING TECHNIQUES FOR TERAHERTZ LOSSY GUIDING STRUCTURES

YEAP KIM HO

DOCTOR OF PHILOSOPHY IN ENGINEERING

FACULTY OF ENGINEERING AND SCIENCE
UNIVERSITI TUNKU ABDUL RAHMAN
MAY 2011

BOUNDARY MATCHING TECHNIQUES FOR TERAHERTZ LOSSY GUIDING STRUCTURES

By

YEAP KIM HO

A thesis submitted to the Department of Electrical and Electronic Engineering,
Faculty of Engineering and Science,
Universiti Tunku Abdul Rahman,
in partial fulfillment of the requirements for the degree of
Doctor of Philosophy in Engineering
May 2011

ABSTRACT

BOUNDARY MATCHING TECHNIQUES FOR TERAHERTZ LOSSY GUIDING STRUCTURES

Yeap Kim Ho

In THz radio astronomy, waveguide heterodyne receivers are often used in signal mixing. To ensure that the energy of the waves from the incoming waveguide couples efficiently to the microstrip probe, an accurate and versatile mathematical model that computes losses in waveguides is desirable in the development of a mixer circuit.

In this thesis, a new and novel method to compute the propagation constants in guiding structures is presented. This method is based on matching the fields at the boundary with the constitutive properties of the wall material. Compared to existing methods which assume lossless fields, the field expressions in the new method can accommodate both lossless and lossy cases. Unlike the existing methods which are geometry specific, the new method is applicable to various structures including the circular and rectangular waveguides, superconducting waveguides, and microstrip lines.

For circular and rectangular waveguides, simulation and experimental measurements were carried out to validate the new method. It is found that this method is able to account the additional loss induced by mode coupling effects in degenerate modes. This is in contrast to existing methods which fail to account for multimode propagation.

In the study of superconducting waveguides, the real conductivity is replaced with a complex conductivity derived from the Bardeen-Cooper-Schrieffer theory. It is found that at frequencies below the gap frequency, the waveguide exhibited lossless transmission behaviour while above the gap frequency, Cooper pairs breaking dominates and the loss increases considerably. Considering that THz signals from astronomical sources are extremely weak, the result suggests that superconducting waveguides that operate at frequencies below the gap frequency can be applied in SIS receivers to minimize the loss of such signals.

A full-wave analysis has also been performed on microstrip lines. Since the new method accounts for the propagation of hybrid modes and fringing loss, it is found to be more accurate compared to the conventional quasi-static methods which only assume TEM mode propagation. Superconducting microstrips are found to be dispersionless and exhibit a much lower loss. A comparison is also made between the performance of a microstrip line and coplanar waveguide (CPW). Preliminary studies suggest that at dimensions comparable with the wavelength, CPW exhibits lower loss than a microstrip. The lower loss found in CPWs strongly suggests that CPWs can be considered as a better alternative to microstrip line for THz waves coupling in heterodyne receivers.

ACKNOWLEDGEMENT

I hope to convey profound gratitude to my family – especially my Mom and Dad, my wife, my twin brother, sisters, and sister-in-law, for their support and encouragement throughout all these years of my research.

I am also greatly indebted to my supervisor Dr. Yeong Kee Choon. Dr. Yeong has been a great mentor as well as a colleague and friend to me. Every advice that he told me would surely entrench deeply in my heart. I must also thank him for willing to become my supervisor when my former supervisor Dr. Tham resigned to join another university.

I would also like to thank Dr. Tham and Ghassan for their discussion and guidance. Thanks to both of them for offering me the opportunity to visit and perform research in University of Oxford. I am deeply grateful to Dr. Tham for reading my thesis and giving constructive comments on how to improve the quality of it.

I am also thankful to Dr. Lim for becoming my co-supervisor, Prof. Poljak, Dr. Sekimoto, and Dr. Lau for being my examiners, Brock and Mike for their help in drawing and fabricating the chokes, Kok Hen and Thompson for their words of support, and, not forgetting, Boon Kok, Amorn, Chris, Mrs. Nirrenski, Paul, and Jamie for their assistance when I was in Oxford.

Lastly and not the least, I would like to thank my fellow colleagues in the Department of Electronic Engineering for their support. Thanks to Dr. Yap for lending me his ears, listening to my frustration every now and then.

I am truly blessed, being able to know all of them. Every one of them plays a significant role in painting my life – making it so wonderful, interesting, and not to mention, colourful.

APPROVAL SHEET

This thesis entitled "**BOUNDARY MATCHING TECHNIQUES FOR TERAHERTZ LOSSY GUIDING STRUCTURES"** was prepared by YEAP KIM HO and submitted as partial fulfillment of the requirements for the degree of Doctor of Philosophy in Engineering at Universiti Tunku Abdul Rahman.

Approved by:

_____
(Assoc. Prof. Dr. Yeong Kee Choon)
Date:……..
Associate Professor/Supervisor
Department of Electronic Engineering
Faculty of Engineering and Green Technology
Universiti Tunku Abdul Rahman

_____
(Asst. Prof. Dr. Lim Eng Hock)
Date:……..
Assistant Professor/Co-supervisor
Department of Electrical and Electronic Engineering
Faculty of Engineering and Science
Universiti Tunku Abdul Rahman

FACULTY OF ENGINEERING AND SCIENCE
UNIVERSITI TUNKU ABDUL RAHMAN

Date: _____

PERMISSION SHEET

It is hereby certified that **YEAP KIM HO** (ID No: **07UED08533**) has completed this thesis/dissertation entitled "BOUNDARY MATCHING TECHNIQUES FOR TERAHERTZ LOSSY GUIDING STRUCTURES" under the supervision of Dr. Yeong Kee Choon (Supervisor) from the Department of Electronic Engineering, Faculty of Engineering and Green Technology, and Dr. Lim Eng Hock (Co-Supervisor) from the Department of Electrical and Electronic Engineering, Faculty of Engineering and Science.

I hereby give permission to the University to upload softcopy of my thesis in pdf format into UTAR Institutional Repository, which will be made accessible to UTAR community and public.

Yours truly,

_____
(YEAP KIM HO)

DECLARATION

I hereby declare that the thesis is based on my original work except for quotations and citations which have been duly acknowledged. I also declare that it has not been previously or concurrently submitted for any other degree at UTAR or other institutions.

Name _____YEAP KIM HO_____

Date _____

TABLE OF CONTENTS

LIST OF TABLES

LIST OF FIGURES

LIST OF ABBREVIATIONS

THz	Terahertz
TEM	Transverse Eletromagnetic
TE	Transverse Electric
TM	Transverse Magnetic
CMB	Cosmic Microwave Background
JCMT	James Clerk Maxwell Telescope
CSO	Caltech Submillimeter Oscilloscope
ALMA	Atacama Large Millimeter Array
LO	Local Oscillator
IF	Intermediate Frequency
CPW	Coplanar Waveguide
PPM	Papadopoulos' Perturbation Method
HFSS	High Frequency Structure Simulator
FEM	Finite Element Method
ALPS	Adaptive Lanczos-Pade Sweep
VNA	Vector Network Analyzer
SIS	Superconductor-Insulator-Superconductor
OMT	Ortho-Mode Transducer
BCS	Bardeen-Cooper-Schrieffer
MIC	Microwave Integrated Circuits
SDA	Spectral Domain Approach
LSE	Longitudinal Section Electric
LSM	Longitudinal Section Magnetic
HB	Hammerstad and Bekkadal

SGB	Schneider, Glance, and Bodtman
PMH	Pucel, Masse, and Hartwig
MMIC	Monolithic Microwave Integrated Circuits
FET	Field Effect Transistor

LIST OF SYMBOLS

Symbols

T_R	Front-end receiver noise temperature
T_M	Mixer noise temperature
C_{Loss}	Conversion loss
T_{IF}	Noise temperature of the first IF amplifier
η_{IF}	Coupling efficiency between the IF port of the junction and the input port of the first IF amplifier
r	Radial distance
F	Signal frequency
f_c	Cutoff frequency
ω	Angular frequency
k_z	Propagation constant
β_z	Phase constant
α_z	Attenuation constant
∇^2	Lapalcian operator
k_0	Wavenumber in free-space
k_x	Transverse wavenumber in the x direction
k_y	Transverse wavenumber in the y direction
$\alpha_{z(d)}$	Attenuation due to the lossy dielectric material
$\alpha_{z(c)}$	Attenuation due to the imperfectly conducting wall
P_z	Time average power flowing through the cross section
P_L	Time average power lost per unit length
$\alpha_{z(\mathrm{TM})}$	Attenuation for TM modes
$\alpha_{z(\mathrm{TM})}$	Attenuation for TE modes

E_t	Transverse electric fields in lossy waveguides
E_{ts}	Transverse electric fields in lossless waveguides
Z_s	Surface impedance of the wall material
a_n	Normal direction to the wall
ϕ_y	Penetration factor in the *y* direction
ϕ_x	Penetration factor in the *x* direction
μ_0	Permeability of free space
ε_0	Permittivity of free space
μ_c	Permeability of the wall material
ε_c	Permittivity of the wall material
σ_c	Frequency dependent conductivity
τ	Mean free time
b	Width of the waveguide
a	Height of the waveguide
λ_g	Guide wavelength
P_{av}	Average power density
l	Length of the waveguide
J_n	Bessel function of the first kind
H_n	Hankel function of the first kind
a_r	Inner radius of the circular waveguide
f_g	Gap frequency
Nb	Niobium
λ_L	London penetration depth
T	Temperature
T_c	Critical temperature

Δ	Gap energy
$\hbar$	Reduced Planck's constant
E_F	Fermi energy
k	Boltzmann's constant
γ_E	Euler's constant
σ_n	Normal conductivity
Δ	Skin depth
μ_{nb}	Permittivity of Nb
σ_{nb}	Conductivity of Nb
R_s	Surface resistance
n_n	Number density of quasiparticles
α	Attenuation constant in microstrips
L_i	Inductance induced by the magnetic field
Z_0	Characteristic impedance
w	Width of the strip
Δw	Edge correction factor
ε_{eff}	Effective dielectric constant
Z	Series impedance
Y	Shunt admittance
Z_{ss}	Surface impedance of the strip
Z_{sg}	Surface impedance of the groundplane
σ_s	Conductivity of the strip
σ_g	Conductivity of the groundplane
t_s	Strip thickness
t_g	Groundplane thickness

χ	Yassin-Withington's penetration factor
ε_r	Dielectric constant
Z_η	Intrinsic impedance of free space
K	Elliptic integral of the first kind

CHAPTER 1

INTRODUCTION*

1.1 Scientific Motivation

Wave guiding structures such as circular and rectangular waveguides and microstrip transmission lines are widely used in radio receiver systems to channel and couple signals to the mixer circuits. In order to ensure that the received signal is converted in the mixer circuit with minimum loss, accurate and versatile mathematical formulations are used as a guide to compute and predict the losses in the guiding structures. The detection of extremely weak extraterrestrial signals at millimeter and submillimeter wavelengths poses an interesting challenge (Withington, 2003). The millimeter and submillimeter bands of the electromagnetic spectrum hold the most important spectral and spatial signatures in the field of astrophysics. For example, the study of the cosmic microwave background (CMB) radiation which peaks in the frequency range of 100 GHz to 300 GHz provides an in depth understanding on the physics of the Big Bang theory and the formation of the early universe (Withington, 2003; Komatsu *et al.*, 2010). Besides, the cold material (10 K – 30 K) associated with the early stages of star and planet formation, as well as the earliest stages of galaxy formation, has its peak emission in the millimeter and submillimeter range as well (Barychev, 2005). By analyzing and mapping the lines in the millimeter and submillimeter bands, it is essential to build

*Parts of this chapter were published in "K. H. Yeap, C. Y. Tham, G. Yassin, and K. C. Yeong, *Propagation in Lossy Rectangular Waveguides*, Electromagnetic Waves Propagation in Complex Matter, Intech, July 2011, pp. 255 – 272."

models of astrophysical objects, which include temperature, density, large scale movement of material, magnetic field strengths, isotope abundance, etc.

In general, presently available formulations to compute the loss in guiding structures are rather limited in three ways. The first limitation is that the formulations (especially that for a rectangular waveguide) are mostly derived from the perturbation of the lossless case. Since the fields' expression in these methods is assumed to be identical with those of a lossless waveguide, they do not give an accurate insight on the actual propagation characteristics of waves in practical lossy waveguides. The second limitation is that these formulations are designed only for very specific geometrical structures. For example, Stratton's equation (Stratton, 1941) can be implemented only in circular waveguides but not rectangular waveguides. Conformal mapping methods (Wheeler, 1964; Wheeler, 1965; Wheeler, 1977; Yassin and Withington, 1995; Yassin and Withington, 1996a; Withington and Yassin, 1996; Hammerstad and Jansen, 1980; Schneider, 1969; Assadourian and Rimai, 1952) are only applicable for planar waveguides such as microstrips. The third limitation of these formulations is due to simplifications in mode transmissions. For example, the power loss methods (Stratton, 1941; Seida, 2003; Collin, 1991; Cheng, 1989) that are applied in circular and rectangular waveguides assume the propagation of single modes and thus do not take into account the mode coupling effects of the concurrent propagation of degenerate modes (Imbriale *et al*., 1998). Similarly, the quasi-static methods (Wheeler, 1964; Wheeler, 1965; Wheeler, 1977; Yassin and Withington, 1995; Yassin and Withington, 1996a; Withington and Yassin, 1996; Hammerstad and

Jansen, 1980; Schneider, 1969; Assadourian and Rimai, 1952; Yamashita and Mittra, 1968; Yamashita, 1968; Green, 1965; Stinehelfer, 1968; Schneider, 1965; Matick, 1969; Kautz, 1978) in microstrips assume the propagation of the transverse electromagnetic (TEM) mode. At frequencies where the wavelengths are comparable with the dimensions of the structures, the longitudinal components of the hybrid modes can no longer be neglected. This means that these methods are inaccurate at higher frequencies.

In this thesis, a new formulation in computing losses in wave guiding structures that is novel and fundamental is proposed. The main advantage of this formulation is that it can be easily generalized to solve for characteristic equations with more than one unknown variables. By matching hybrid fields to the material property at the boundary of the structures this method is found to account for the superposition of both Transverse Electric (TE) and Transverse Magnetic (TM) modes. This is an added advantage as the formulation can be implemented at higher frequencies (millimeter and submillimeter wavelengths). In addition, the formulation is general and can be applied to any structure as long as the geometry can be put into the formulation. In this thesis, this formulation has been applied to compute the loss in rectangular waveguides, circular waveguides, and microstrip lines.

1.2 Technological Background

Millimeter and submillimeter waves are attenuated by significant levels of precipitation and are absorbed in the atmosphere by water vapor and

oxygen. Hence, to be able to observe stellar sources effectively, radio telescopes and interferometers are usually built at places with high altitude and dry climate. Examples of such observatories are the James Clerk Maxwell Telescope (JCMT) and the Caltech Submillimeter Observatory (CSO), both of which situated at the summit of Mauna Kea, Hawaii. Another example is the Atacama Large Millimeter Array (ALMA), an interferometer which is still under construction at the Plano de Atacama in Chile. Comprises 64 antennas, each 12 m in diameter, ALMA is going to be the world's most powerful interferometer at millimeter and submillimeter wavelengths (Withington, 2003; Tarenghi, 2008).

Figure 1.1 shows the functional block diagram of a typical heterodyne receiver in radio telescopes (Chattopadhyay *et al.*, 2002; Kraus, 1986). The RF signal from the antenna is directed down to the receiver system via mirrors and beam waveguides (Paine *et al.*, 1994). At the front-end of the receiver system, the RF signal is channeled and coupled to a mixer circuit via hollow waveguides and microstrips. A superconductor-insulator-superconductor (SIS) heterodyne mixer is commonly implemented to down convert the RF signal to an intermediate frequency IF signal. After going through multiple stages of amplification, the IF signal is fed to a data analysis system such as an acousto-optic spectrometer. The data analysis system will be able to perform Fourier transformation and record spectral information about the input signal.

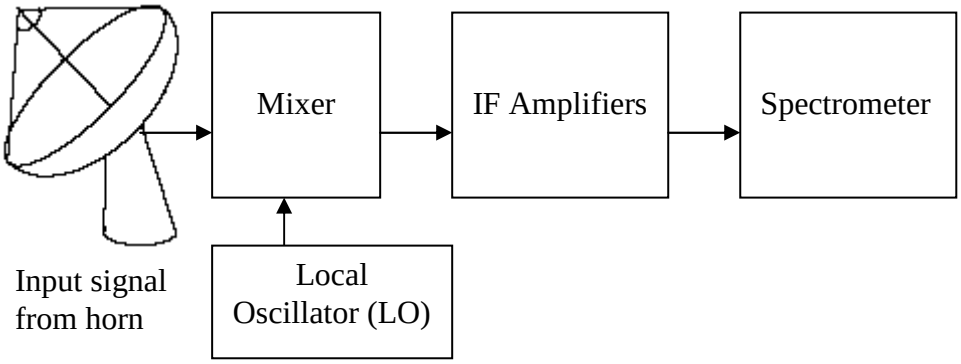

Figure 1.1. Block diagram of a heterodyne receiver

To illustrate in detail the applications of wave guiding structures in receiver systems, the side band separating SIS mixer designed and fabricated by the Onsala Space Observatory, for the ALMA 85 – 115 GHz band 7 cartridge (Vassilev *et al.*, 2004; Vassilev and Belitsky, 2001a; Vassilev and Belitsky, 2001b) has been taken as an example. As can be seen in Figure 1.2, the received RF signal is channeled from the aperture of the horn through a circular and subsequently a rectangular waveguide, before being coupled to the SIS mixer, built in the same substrate as the microstrip. Figure 1.3 shows the RF power being coupled to the microstrip in the middle of the substrate and divided between the two mixer junctions by the rectangular waveguide to microstrip double probe transition. Similarly, the local oscillator LO signal is channeled to a waveguide branch line coupler via a rectangular waveguide. The waveguide coupler provides a 90º phase shift, splitting the LO power so as to be coupled to both ends of the substrate via the waveguide-to-microstrip transition. As depicted in Figure 1.4, a three section transformer in the microstrip matches the impedance of the LO probe to the LO injection coupler. To keep the signal path loss small, the LO power is coupled to the RF

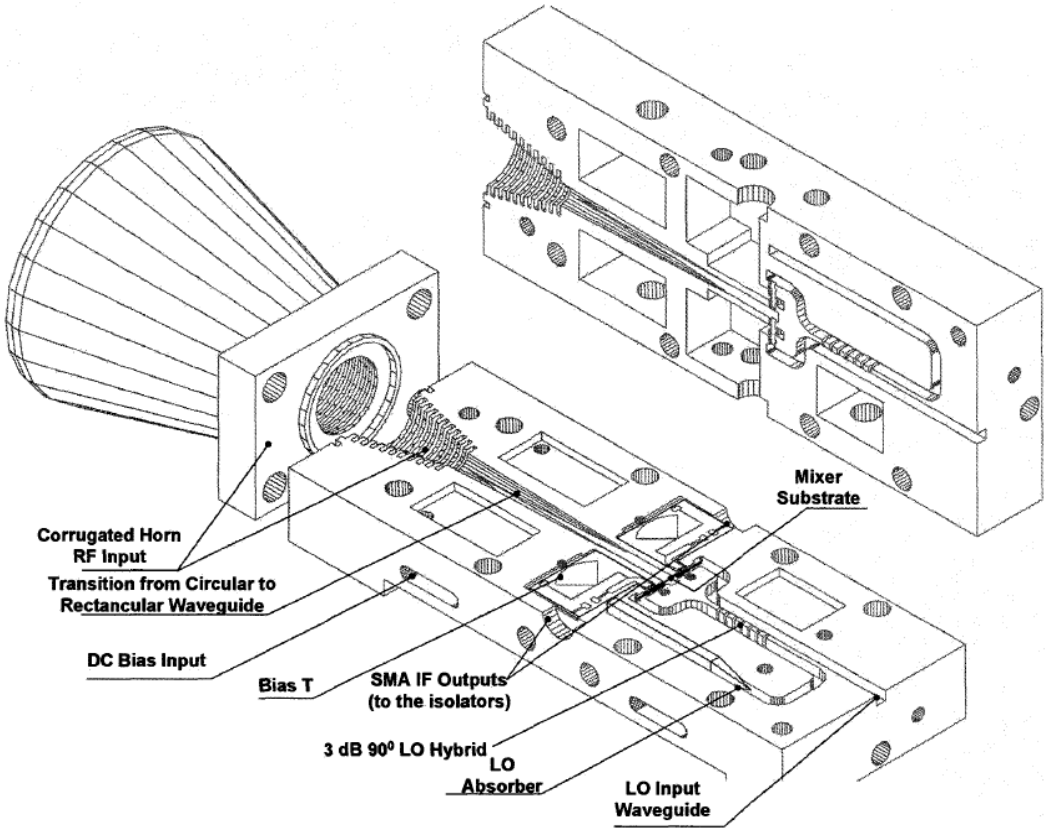

Figure 1.2. Layout of the SIS receiver for ALMA band 7 cartridge (Vassilev *et al.*, 2004).

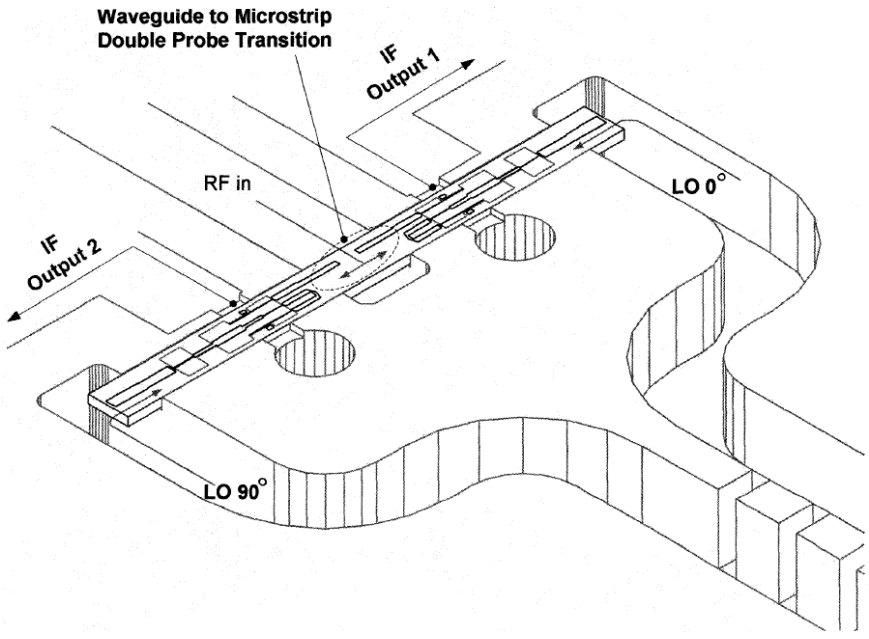

Figure 1.3. A mixer substrate is coupled to the waveguides in the ALMA band 7 receiver (Vassilev and Belitsky, 2001b).

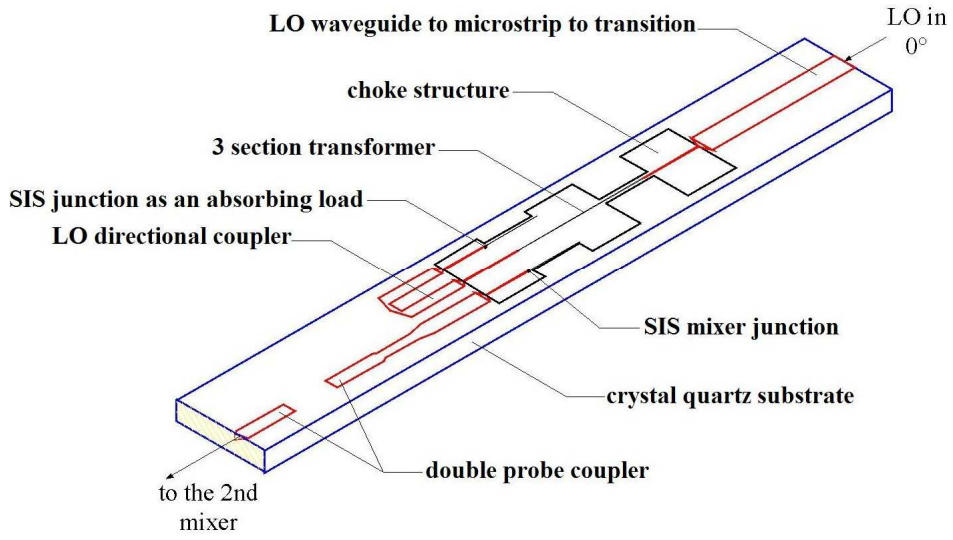

Figure 1.4. Layout of the quartz substrate with the SIS mixer built onto it (Vassilev and Belitsky, 2001b).

signal via the LO directional coupler. The RF and LO signals are subsequently fed to each of the mixer junctions tuning circuitry. At the SIS mixer, both the RF and LO signals are then mixed and down converted to a lower intermediate frequency IF signal. The rest of the LO power at the idle port of the coupler is terminated by a second SIS junction. Since the SIS termination absorbs 15 dB more LO power than the mixer junction, it becomes over-pumped. The nonlinear current-voltage (*I*-*V*) curve of the second SIS junction straightens and thus allowing it to behave as a pumped resistor.

The front-end receiver noise temperature T_R is determined by a number of factors. These include the mixer noise temperature T_M, the conversion loss C_{Loss}, the noise temperature of the first IF amplifier T_{IF}, and the coupling efficiency between the IF port of the junction and the input port of the first IF amplifier η_{IF}. A comparison of the performance of different SIS waveguide

receivers is listed in Table 1.1 (Walker *et al.*, 1992). It can be seen that the value of T_R for the 230 GHz system is a factor of 3 to 4 less than that achieved with the 492 GHz system. The decrease in system performance at 492 GHz is due to the increase of C_{Loss} and T_M by a factor of approximately 3.

Since the input power level of the weak THz signal is quite small, i.e. of the order of 10^{-18} to 10^{-20} W (Shankar, 1986), it is therefore of primary importance to minimize the conversion loss C_{Loss} of the mixer circuit. One way is to ensure that the energy of the LO and, in particular, the RF signals is channeled and coupled from the waveguides to the mixer circuit in a highly efficient manner. It is simply too time consuming and too expensive to develop wave guiding structures in a receiver system on a trial-and-error basis. To minimize the loss of the propagating signals, the availability of an accurate and easy-to-use mathematical model to compute the loss of such signals in wave guiding structures is, of course, central to the development of receiver circuits.

Table 1.1. Comparison of SIS receiver performance.

SIS Junction	**Nb**	**Pb**	**Nb**
Center Frequency (GHz)	230	345	492
$\boldsymbol{T_R}$ **(K)**	48	159	176
$\boldsymbol{T_M}$ **(K)**	34	129	123
$\boldsymbol{C_{Loss}}$ **(dB)**	3.1	8.1	8.9
$\boldsymbol{T_{IF}}$ **(K)**	7.0	4.2	6.8

1.3 Overview of Thesis

The theme of this thesis is to develop a new formulation to investigate the loss of waves in wave guiding structures, operating in particular in the millimeter and submillimeter frequencies range. The thesis is organized as follows:

Chapter 2 describes the formulation of a set of characteristic equations used to compute the propagation constant of waves in rectangular waveguides. The equations are obtained by matching the tangential electromagnetic fields with the electrical properties of waves, expressed as surface impedance. To account for the penetration of fields into the wall materials, two new phase parameters are introduced in the field equations. In addition, the transverse and longitudinal wavenumbers in a lossy waveguide are also allowed to take complex forms.

Chapter 3 extends the approach implemented in Chapter 2 for rectangular waveguides to the case of circular waveguides. It can be seen that the new method has the flexibility of being implemented in waveguides with different geometry – especially in circular and rectangular waveguides.

Chapter 4 gives a detail analysis of superconducting waveguides based on the equations derived in Chapters 2 and 3. In the computation of loss, the complex conductivity of a superconductor is substituted into the transcendental equations developed in Chapters 2 and 3. The complex

conductivity is obtained by solving Mattis-Bardeen equations (Mattis and Bardeen, 1958).

Chapter 5 describes a new full-wave analysis developed to compute the loss in a microstrip transmission line. The microstrip is assumed to be partially encapsulated in a metallic box. A transcendental equation is formulated by matching the fields at the dielectric-air interface and also matching the fields with the surface impedance at the dielectric-conductor interface. To account for the finite thickness of the strip and groundplane, the surface impedance formulated by Kerr (1999) is incorporated into the equation.

Chapter 6 shows an analysis between the performance of normal and superconducting coplanar waveguides (CPWs) and microstrip lines, designed at different dimensions. The conduction loss in a CPW is computed based on the quasi static equation in Ghione (1993). To account for the dispersive effect of a lossy CPW, the frequency dependent effective dielectric constant ε_{eff} given by Hasnain *et al.* (1986) is incorporated into the loss equation.

Chapter 7 concludes with a summary the findings of Chapters 2, 3, 4, 5, and 6. Some of the future work is also proposed and discussed here.

CHAPTER 2

RECTANGULAR WAVEGUIDES*

In this chapter, the characteristics of electromagnetic waves propagating in a rectangular waveguide with finite conducting walls are investigated. A set of transcendental equation was developed based on matching the tangential fields at the boundaries of the waveguide with the electrical properties of the wall material. A significant contribution from this new proposed method is that it successfully demonstrates the mode coupling effects in degenerate mode waves.

2.1 Introduction

Propagation of electromagnetic waves in circular waveguides has been widely investigated, for waveguides with lossy (Glaser, 1969) and superconducting (Yassin *et al.*, 2001; Yassin *et al.*, 2003) walls, unbounded dielectric rod (Claricoats, 1960a), bounded dielectric rod in a waveguide (Claricoats, 1960b), and multilayered coated circular waveguide (Chou and Lee, 1988). The computation given by these authors were based on a method suggested by Stratton (1941). The circular symmetry of the waveguide allows the boundary matching equations to be expressed in a single variable which is the propagation constant k_z. The eigenmodes could therefore be obtained from a single transcendental equation. This approach, however, cannot be

*Parts of this chapter were published in "K. H. Yeap, C. Y. Tham, G. Yassin, and K. C. Yeong, "Attenuation in Rectangular Waveguides with Finite Conductivity Walls", *Radioengineeringl*, Vol. 20(2), June 2011, pp. 472 - 478."

implemented in the case of rectangular symmetry where a 2D Cartesian coordinate system must be used (Krammer, 1976). A similar rigorous technique to study the attenuation of rectangular waveguides is not available hitherto. It is to be noted, however, that in practice, rectangular waveguides are more widely used than circular waveguides. This is especially true in receivers of radio telescopes (Carter *et al.,* 2004; Boifot *et al.,* 1990; Withington *et al.,* 2003) where rectangular waveguide-to-microstrip transition is commonly used to couple the field to the detector circuit. Indeed, rectangular waveguides are much easier to manipulate than circular waveguides (bend, twist, etc.) and also offer significantly lower cross polarization component.

The approximate power-loss method has been widely used in analyzing wave attenuation in lossy rectangular waveguides as a result of its simplicity and because it gives reasonably accurate result, when the frequency of the signal is well above cutoff (Stratton, 1941; Seida, 2003; Collin, 1991; Cheng, 1989). In this method, the fields' expression are derived assuming perfectly conducting walls, allowing the solution to be separated into pure TE and TM modes. For a practical waveguide with finite conductivity, however, a superposition of both TE and TM modes is necessary to satisfy the boundary conditions (Stratton, 1941; Yassin *et al.,* 2003). To calculate the attenuation using the power-loss method, ohmic losses are assumed to exist due to small field penetration into the conductor walls. Results however show that this method fails near cutoff, as the attenuation obtained diverges to infinity when the signal frequency f approaches the cutoff frequency f_c. Clearly, it is more

realistic to expect losses to be high but finite rather than diverging to infinity. The inaccuracy in the power-loss method at cutoff is due to the fact that the fields' equation is assumed to be the same as those of a lossless waveguide. A lossless waveguide behaves exactly like an ideal high pass filter where signal ceases to propagate at frequency f below the cutoff f_c. Since waveguides are commonly used as filters, an accurate calculation of the power loss at frequencies at the vicinity of cutoff would hence be substantial.

Robson (1963) and Bladel (1971) discussed degenerate modes propagation in lossy rectangular waveguides, but neither of them was able to compute the attenuation values accurately near cutoff. Like the power-loss method, their theories predict infinite attenuation at cutoff. An expression valid at all frequencies is given by Kohler and Bayer (1964) and reiterated by Somlo and Hunter (1996). This expression however is only applicable to the TE_{10} dominant mode. The perturbation solution developed by Papadopoulos (1954) shows that the propagation of a mode does not merely stop at f_c. Rather, as the frequency approaches f_c, transition from a propagating mode to a highly attenuated mode takes place. The propagation of waves will only cease when $f = 0$. Papadopoulos' perturbation method (PPM) shows that the attenuation at frequencies well above f_c remains in close agreement with that computed using the power loss method for non-degenerate modes. Because of this reason, PPM is perceived as a more accurate technique in computing the loss of waves travelling in waveguides. A similar solution has been derived by Gustincic using the variational approach (Collin, 1991; Gustincic, 1963). Nevertheless, the PPM is merely an approximate solution based on the

perturbation from the lossless case. Therefore, it is not an accurate derivation from fundamental principles. Although this method takes into account the co-existence of TE and TM modes, the boundary conditions are still assumed to be the same as those of the perfectly conducting waveguide.

It can be seen that almost all analysis techniques are based on certain approximations and assumptions. The most commonly used assumption is that based on the boundary conditions of lossless waveguides. Due to such assumption, most methods fail to give an insight or deeper understanding on the mechanism of the propagation of waves in lossy waveguides. Moreover, at very high frequency – especially that approaches the millimeter and submillimeter wavelengths – the loss tangent of the conducting wall decreases. Therefore, such assumption turns out to be inaccurate at very high frequency. Although Stratton (1941) has developed a truly fundamental approach to analyze waveguides, his approach is only restricted to the case of circular waveguides and could not be applied to rectangular waveguides. Because of these reasons, a more accurate approach – one that does not assume lossless boundary condition, is essential to accurately compute the loss of waves in waveguides – in particular, at frequencies operating in the millimeter and submillimeter wavelengths.

In this chapter, a novel and fundamental technique to compute the attenuation of waves in rectangular waveguides with imperfectly conducting walls is introduced. The method is derived from fundamental principles without assumptions made in its formulation. In this method, the solution for

the attenuation constant is found by solving two transcendental equations derived from matching the tangential components of the electromagnetic field at the waveguide walls with the constitutive properties of the wall material, expressed as surface impedance. The attenuation constants for the dominant non-degenerate TE_{10} mode and the degenerate TE_{11} and TM_{11} modes are computed and compared with the power-loss method and the PPM. As demonstrated in the subsequent sections, the new method gives more realistic values for the degenerate modes since the formulation allows co-existence and exchange of power between these modes while other methods treat each one independently.

2.2 General Wave Behaviours along Uniform Guiding Structures

As depicted in Figure 2.1, a time harmonic field propagating in the *z* direction of a uniform guiding structure with arbitrary geometry can be expressed as a combination of elementary waves having a general functional form (Cheng, 1989, Marcuvitz, 1986)

$$\vec{\psi} = \vec{\psi}^{0}\ (x, y)\exp[\mathrm{j}(\omega t + k_z z)], \tag{2.1}$$

where $\vec{\psi}^{0}\ (x, y)$ is a two dimensional vector phasor that depends only on the cross-sectional coordinates, $\omega = 2\pi f$ the angular frequency, and k_z is the propagation constant.

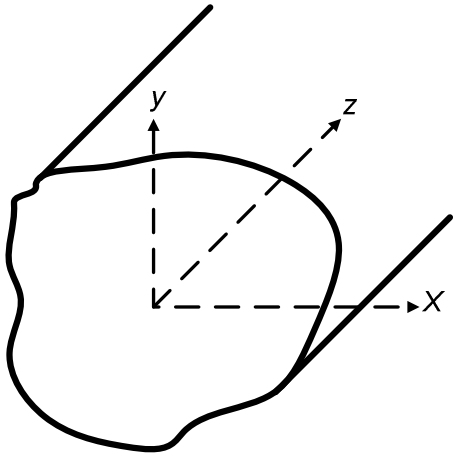

Figure 2.1. A waveguide with arbitrary geometry.

In using phasor representation in equations relating field quantities, the partial derivatives with respect to t and z may be replaced by products with jω and jk_z, respectively; i.e.

$$\frac{\partial}{\partial t}\left(\exp\left(j\omega t\right)\right) = j\omega \exp\left(j\omega t\right), \tag{2.2}$$

$$\frac{\partial}{\partial z}\left(\exp\left(jk_z z\right)\right) = jk_z \exp\left(jk_z z\right). \tag{2.3}$$

Hence, the common factor exp[j(ωt + $k_z z$)] can be dropped. Here, the propagation constant k_z is a complex variable, which consists of a phase constant β_z and an attenuation constant α_z

$$k_z = \beta_z - \mathrm{j}\alpha_z . \tag{2.4}$$

The field intensities in a charge-free dielectric region (such as free-space), satisfy the following homogeneous vector Helmholtz's equation (Cheng, 1989; Marcuvitz, 1986)

$$\nabla^2 \psi_z + (k^2 - k_z^2)\psi_z = 0, \tag{2.5}$$

where ψ_z is the longitudinal component of $\vec{\psi}$, ∇^2 is the Laplacian operator for the transverse coordinates, and k is the wavenumber in the material. For waves propagating in a hollow waveguide, $k = k_0$, the wavenumber in free-space.

It is convenient to classify propagating waves into three types, in correspond to the existence of the longitudinal electric field E_z or longitudinal magnetic H_z field:

(i) Transverse electromagnetic (TEM) waves. A TEM wave consists of neither electric fields nor magnetic fields in the longitudinal direction.

(ii) Transverse magnetic (TM) waves. A TM wave consists of a nonzero electric field but zero magnetic field in the longitudinal direction.

(iii) Transverse electric (TE) waves. A TE wave consists of a zero electric field but nonzero magnetic field in the longitudinal direction.

Single-conductor waveguides, such as a hollow (or dielectric-filled) circular and rectangular waveguide, cannot support TEM waves. As graphically shown in Figure 2.2, this is because according to Ampere's

circuital law in (2.6), the line integral of a magnetic field $\vec{H}$ around any closed loop in a transverse plane must equal the sum of the longitudinal conduction $\vec{J}$ and displacement currents $\frac{\partial \vec{D}}{\partial t}$ through the loop; i.e.

$$\oint_c \vec{H} \bullet d\vec{l} = \int_s \left(\vec{J} + \frac{\partial \vec{D}}{\partial t} \right) \bullet d\vec{s} . \tag{2.6}$$

However, since a single-conductor waveguide does not have an inner conductor and that the longitudinal electric field is zero, there are no longitudinal conduction and displacement current. Hence, transverse magnetic field of a TEM mode cannot propagate in the waveguide (Cheng, 1989).

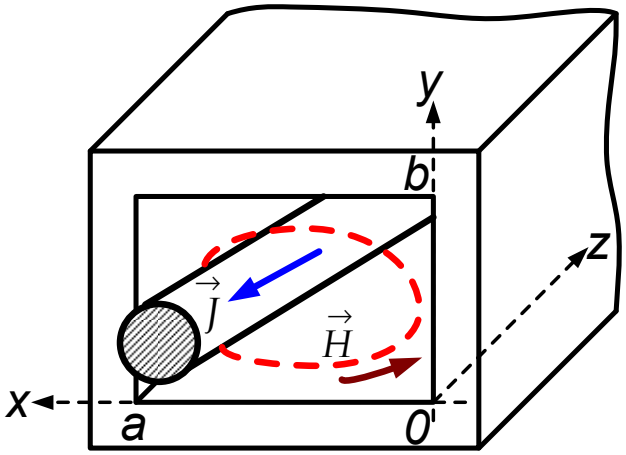

Figure 2.2. The presence of an inner conductor within a rectangular waveguide allows the propagation of TEM wave.

2.3 Fields in Cartesian Coordinates

For waves propagating in a rectangular waveguide, such as that shown in Figure 2.3, Helmholtz's equation in (2.5) can be written in Cartesian coordinates to give

$$\frac{\partial^2 \psi_z}{\partial x^2} + \frac{\partial^2 \psi_z}{\partial y^2} + h^2 \psi_z = 0, \tag{2.7}$$

where $h = \sqrt{k^2 - k_z^{\,2}}$.

By applying the method of separation of variables, ψ_z can be expressed as

$$\psi_z = X(x)Y(y). \tag{2.8}$$

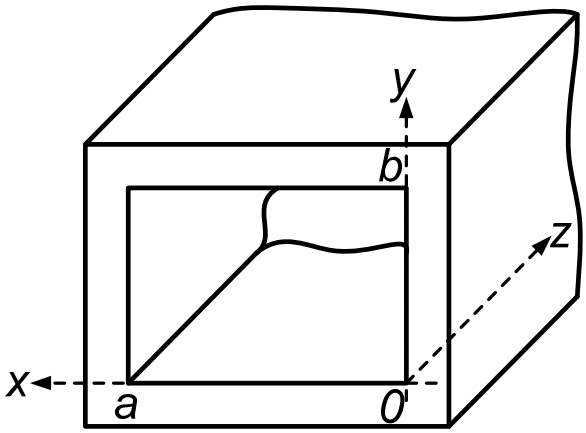

Figure 2.3. The cross section of a rectangular waveguide

Equation (2.7) can thus be separated into two sets of linearly independent second order differential equations, as shown below (Cheng, 1989)

$$\frac{d^2X(x)}{dx^2} + k_x^2 X(x) = 0, \tag{2.9}$$

$$\frac{d^2Y(y)}{dy^2} + k_y^2 Y(y) = 0, \tag{2.10}$$

where k_x and k_y are the transverse wavenumbers in the x and y directions, respectively. The longitudinal fields can be obtained by solving (2.9) and (2.10) based on a set of boundary conditions and substituting the solutions into (2.8).

The transverse field components can be derived by substituting the longitudinal field components into Maxwell's source free curl equations

$$\nabla \times \vec{E} = -\mathrm{j}\omega\mu \vec{H}, \tag{2.11}$$

$$\nabla \times \vec{H} = \mathrm{j}\omega\varepsilon \vec{E}, \tag{2.12}$$

where ε and μ are the permittivity and permeability of the material, respectively and $\vec{E}$ the electric field intensity. Expressing the transverse field components in term of the longitudinal field components E_z and H_z, the following equations can be obtained (Cheng, 1989)

$$H_x = -\frac{1}{h^2}\left(jk_z \frac{dH_z}{dx} - j\omega\varepsilon \frac{dE_z}{dy} \right), \tag{2.13}$$

$$H_y = -\frac{1}{h^2}\left(jk_z \frac{dH_z}{dy} + j\omega\varepsilon \frac{dE_z}{dx} \right), \tag{2.14}$$

$$E_x = -\frac{1}{h^2}\left(jk_z \frac{dE_z}{dx} + j\omega\mu \frac{dH_z}{dy} \right), \tag{2.15}$$

$$E_y = -\frac{1}{h^2}\left(jk_z \frac{dE_z}{dy} - j\omega\mu \frac{dH_z}{dx} \right). \tag{2.16}$$

2.4 A Review of Some Conventional Methods

In the subsequent sections, analysis and comparison among the power-loss method, PPM, and the proposed method shall be performed. Hence, in order to present a complete scheme, derivations of the former two conventional approximate methods are briefly outlined in this section.

The attenuation of electromagnetic waves in waveguides can be caused by two factors, i.e. the attenuation due to the lossy dielectric material $\alpha_{z(d)}$, and that due to the ohmic losses in imperfectly conducting walls $\alpha_{z(c)}$ (Cheng, 1989)

$$\alpha_z = \alpha_{z(d)} + \alpha_{z(c)}. \tag{2.17}$$

For a conducting waveguide, the inner core is usually filled with low-loss dielectric material, such as air. Hence, $\alpha_{z(d)}$ in (2.17) shall be assumed zero in the following approximate methods and the loss in a waveguide is assumed

to be caused solely by the conduction loss. It could be seen later that such assumption is not necessary in the proposed method. The new boundary-matching method inherently accounts for both kinds of losses in its formulation.

2.4.1 The Power-Loss Method

The approximate power-loss method assumes that the fields' expression in a highly but not perfectly conducting waveguide, to be the same as those of a lossless waveguide. Hence, k_x, k_y, and k_z are given as (Cheng, 1989)

$$k_x = \frac{m\pi}{a}, \tag{2.18}$$

$$k_y = \frac{n\pi}{b}, \tag{2.19}$$

$$k_z = \beta_z, \tag{2.20}$$

where a and b are the width and height, respectively, of the rectangular waveguide; whereas m and n denote the number of half cycle variations in the x and y directions, respectively. Every combination of m and n defines a possible mode for TE_{mn} and TM_{mn} waves.

Conduction loss is assumed to occur due to small fields' penetration into the conductor surfaces. According to the law of conservation of energy,

the attenuation constant due to conduction loss can be derived as (Cheng, 1989)

$$\alpha_z = \frac{P_L}{2P_z}, \tag{2.21}$$

where P_z is the time-average power flowing through the cross-section and P_L the time-average power lost per unit length of the waveguide.

Solving for P_L and P_z based on Poynting's theorem, the attenuation constant α_z for TM and TE modes, i.e. $\alpha_{z(\mathrm{TM})}$ and $\alpha_{z(\mathrm{TE})}$, respectively, can thus be expressed as (Collin, 1991; Marcuvitz, 1986)

$$\alpha_{z(TM)} = \frac{2R_s(m^2b^3 + n^2a^3)}{\eta ab\sqrt{1-\left(\frac{f_c}{f}\right)^2}\left(m^2b^2 + n^2a^2\right)}, \tag{2.22}$$

$$\alpha_{z(TE)} = \frac{2R_s}{\eta b\sqrt{1-\left(\frac{f_c}{f}\right)^2}}\left\{\left(1+\frac{b}{a}\right)\left(\frac{f_c}{f}\right)^2 + \frac{b}{a}\left[1-\left(\frac{f_c}{f}\right)^2\right]\left[\frac{m^2ab + n^2a^2}{(mb)^2 + (na)^2}\right]\right\}, \tag{2.23}$$

where R_s is the surface resistance, f_c the cutoff frequency, and η the intrinsic impedance of free space.

2.4.2 Papadopoulos' Perturbation Method

Papadopoulos' perturbation method (PPM) assumes that the transverse electric fields propagating in a waveguide with finite conducting walls ($\vec{E}_t$) can be expressed as a linear combination of transverse electric fields ($\vec{E}_{ts}$) for different modes in a lossless waveguide (Papadopoulos, 1954)

$$\vec{E}_t = \sum_S A_s \vec{E}_{ts} \quad . \tag{2.24}$$

where the sum is extended over all the TE and TM modes and A_s is an unknown amplitude coefficient. $\vec{E}_{ts}$ consists of transverse wavenumbers which are assumed to be real, as given by (2.18) and (2.19).

A system of equations for determining the coefficients A_s and propagation constant k_z may be obtained by first scalar multiplying the homogeneous Helmholtz's equation for $\vec{E}_t$ with $\vec{E}_{ts}$, and vice-versa, $\vec{E}_{ts}$ with $\vec{E}_t$. A characteristic equation can then be derived by subtracting both equations and, subsequently, integrating the result over the cross section of the waveguide

$$(\beta_z^{\,2} - k_z^{\,2}) \int_S \vec{E}_t \bullet \vec{E}_{ts} \quad dS = \int_S (\vec{E}_t \bullet \nabla_t^{\,2} \vec{E}_{ts} - \vec{E}_{ts} \bullet \nabla_t^{\,2} \vec{E}_t) \quad dS \tag{2.25}$$

Applying (2.25) into the case of a rectangular waveguide, the following two homogeneous equations are obtained (Papadopoulos, 1954)

$$\left\{\frac{\left(\beta_{mn}{}^2 - k_z{}^2\right)j\omega\mu_0 ab}{Z_s\varepsilon_{0n}\varepsilon_{0m}} + k_c{}^2\left(\frac{2b}{\varepsilon_{0m}} + \frac{2a}{\varepsilon_{0n}}\right) + \frac{\beta_{mn}{}^2}{k_c{}^2}\left[b\left(\frac{n\pi}{b}\right)^2 + a\left(\frac{m\pi}{a}\right)^2\right]\right\}A_{mn}$$
$$+\left\{\frac{k_0{}^2}{k_{c,}{}^2}\frac{mn\pi^2}{ab}(b-a)\right\}A_{mn}{}' = 0 \quad , \tag{2.26a}$$

$$\left\{\frac{\beta_{mn}{}^2}{k_c{}^2}\frac{mn\pi^2}{ab}(b-a)\right\}A_{mn}$$
$$+\left\{\frac{\left(\beta_{mn}{}^2 - k_z{}^2\right)j\omega\mu_0 ab}{Z_s\varepsilon_{0n}\varepsilon_{0m}} + \frac{k_0{}^2}{k^2{}_c}\left[a\left(\frac{n\pi}{b}\right)^2 + b\left(\frac{m\pi}{a}\right)^2\right]\right\}A_{mn}{}' = 0 \qquad ; m = n \neq 0 \quad , \tag{2.26b}$$

where Z_s is the surface impedance of the wall material, A_{mn} and A_{mn}' are the coefficients of TE and TM modes, respectively, $\beta_{mn}{}^2 = k_0{}^2 - k_c{}^2$, $k_c{}^2 = \left[\left(\frac{m\pi}{a}\right)^2 + \left(\frac{n\pi}{b}\right)^2\right]$, and

$$\varepsilon_{0m} = \begin{cases} 1 & m = 0 \\ 2 & m > 0 \end{cases}, \tag{2.27a}$$

$$\varepsilon_{0n} = \begin{cases} 1 & n = 0 \\ 2 & n > 0 \end{cases}. \tag{2.27b}$$

If m = 1 and n = 0, (2.26a) reduces to a single term and gives the propagation constant k_z for the dominant TE_{10} mode as:

$$k_z = \sqrt{{k_0}^2 - \left(\frac{\pi}{a}\right)^2 - \frac{jZ_s\left[\left(\frac{\pi\beta_0}{\pi}\right)^2 a + \left(\frac{\pi}{a}\right)^2 (2b + a)\right]}{\pi f \mu_0 ab}}\,. \qquad (2.28)$$

If $m \neq 0$ and $n \neq 0$, (2.26a) and (2.26b) determine a solution for A_{nm} and A_{nm}', provided the determinant vanishes. The vanishing of the determinant leads to two roots for k_z as shown below:

$$k_z = \sqrt{\frac{-jZ_m \varepsilon_{0m} \varepsilon_{0n}}{2\omega\mu_0 ab}\left\{T + R \pm \sqrt{(T+R)^2 - 4\left[TR - \left(\frac{k_0 \beta_{mn} mn\pi^2}{{k_c}^2 ab}\right)^2 (b-a)^2\right]}\right\} + {\beta_{mn}}^2}\,. \qquad (2.29)$$

where $R = \left(\frac{{k_0}^2 P}{{k_c}^2}\right)$, $T = \left({k_c}^2 S + \frac{{\beta_{mn}}^2 Q}{{k_c}^2}\right)$, $P = \left[a\left(\frac{n\pi}{b}\right)^2 + b\left(\frac{m\pi}{a}\right)^2\right]$,

$Q = \left[b\left(\frac{n\pi}{b}\right)^2 + a\left(\frac{m\pi}{a}\right)^2\right]$, and $S = \left(\frac{2b}{\varepsilon_{0m}} + \frac{2a}{\varepsilon_{0n}}\right)$.

For the root where $A_{mn} > A_{mn}$', the propagation constant k_z corresponds to a perturbed TE_{mn} mode. The other root where $A_{mn}' > A_{mn}$, corresponds to a perturbed TM_{mn} mode.

2.5 The Proposed Method

It is apparent that, in order to derive the approximate characteristic equations illustrated in the previous sections, the field equations must be assumed to be exactly the same as those propagating in a lossless waveguide.

In a lossless waveguide where the conductivity σ is infinity, the boundary condition requires that the resultant tangential component of the electric field E_t and the normal derivative of the tangential magnetic field H_t to vanish at the waveguide wall,

$$E_t = \frac{\partial H_t}{\partial a_n} = 0; \sigma = \infty, \tag{2.30}$$

where a_n is the normal direction to the waveguide wall. In reality, however, this is not exactly the case. The conductivity of a practical waveguide is finite. Hence, both E_t and $\frac{\partial H_t}{\partial a_n}$ are not exactly zero at the boundary of the waveguide,

$$E_t = \frac{\partial H_t}{\partial a_n} \neq 0; \sigma \neq \infty, \tag{2.31}$$

Besides, the loss tangent of a material decreases in direct proportion with the increase of frequency. Hence, a highly conducting wall at low frequency may exhibit the properties of a lossy dielectric at high frequency, resulting in inaccuracy using the assumption at millimeter and submillimeter wavelengths.

In order to model the fields' expression closer to those in a lossy waveguide and to account for the presence of fields inside the walls, two phase parameters have been introduced in the proposed method. The phase parameters – i.e ϕ_x and ϕ_y, are referred to as the field's penetration factors in

the x and y directions, respectively. It is worthwhile noting that, with the introduction of the penetration factors, E_t and $\frac{\partial H_t}{\partial a_n}$ do not necessarily decay to zero at the boundary, therefore allowing the effect of not being a perfect conductor at the waveguide wall.

2.5.1 Fields in a Lossy Rectangular Waveguide

For waves propagating in a lossy hollow rectangular waveguide, as shown in Figure 2.1, a superposition of TM and TE waves is necessary to satisfy the boundary condition at the wall (Stratton, 1941; Yassin *et al.*, 2003). The longitudinal electric and magnetic field components E_z and H_z, respectively, can be derived by solving Helmholtz's homogeneous equation in Cartesian coordinate. Using the method of separation of variables (Cheng, 1989), the following set of field equations is obtained:

$$E_z = E_0 \sin(k_x x + \phi_x)\sin(k_y y + \phi_y), \tag{2.32}$$

$$H_z = H_0 \cos(k_x x + \phi_x)\cos(k_y y + \phi_y), \tag{2.33}$$

where E_0 and H_0 are constant amplitudes of the fields.

The propagation constant k_z for each mode will be found by solving for k_x and k_y and substituting the results into the dispersion relation

$$k_z = \sqrt{{k_0}^2 - {k_x}^2 - {k_y}^2}\ . \tag{2.34}$$

Equations (2.32) and (2.33) must also apply to a perfectly conducting waveguide. In that case E_z and $\frac{\partial H_z}{\partial a_n}$ are either at their maximum magnitude or zero at both $x = \frac{a}{2}$ and $y = \frac{b}{2}$, i.e. the centre of the waveguide, therefore

$$\sin\left(\frac{k_x a}{2} + \phi_x\right) = \sin\left(\frac{k_y b}{2} + \phi_y\right) = \begin{cases} \pm 1 \\ 0 \end{cases} . \tag{2.35}$$

Solving (2.35), the penetration factors are obtained as,

$$\phi_x = \frac{(m\pi - k_x a)}{2} , \tag{2.36a}$$

$$\phi_y = \frac{(n\pi - k_y b)}{2} , \tag{2.36b}$$

For waveguides with perfectly conducting wall, $k_x = \frac{m\pi}{a}$ and $k_y = \frac{n\pi}{b}$, (2.36a) and (2.36b) result in zero penetration and E_z and H_z in (2.32) and (2.33) are reduced to the fields of a lossless waveguide. To take the finite conductivity into account, k_x and k_y are allowed to take complex values yielding non-zero penetration of the fields into the waveguide material:

$$k_x = \beta_x - j\alpha_x , \tag{2.37}$$

$$k_y = \beta_y - j\alpha_y , \tag{2.38}$$

where β_x and β_y are the phase constants and α_x and α_y are the attenuation constants in the *x* and *y* directions, respectively. This in turn results in complex value for the propagation constant of the waveguide k_z (see equation (2.4)) which yields loss in propagation.

Substituting (2.32) and (2.33) into (2.13) to (2.16), the fields are obtained as:

$$H_x = \frac{j}{h^2}\left[k_z k_x H_0 + \omega\varepsilon_0 k_y E_0\right]\sin(k_x x+\phi_x)\cos(k_y y+\phi_y)\ , \qquad (2.39)$$

$$H_y = \frac{j}{h^2}\left[k_z k_y H_0 - \omega\varepsilon_0 k_x E_0\right]\cos(k_x x+\phi_x)\sin(k_y y+\phi_y)\ , \qquad (2.40)$$

$$E_x = -\frac{j}{h^2}\left[k_z k_x E_0 - \omega\mu_0 k_y H_0\right]\cos(k_x x+\phi_x)\sin(k_y y+\phi_y)\ , \qquad (2.41)$$

$$E_y = -\frac{j}{h^2}\left[k_z k_y E_0 + \omega\mu_0 k_x H_0\right]\sin(k_x x+\phi_x)\cos(k_y y+\phi_y)\ , \qquad (2.42)$$

where μ_0 and ε_0 are the permeability and permittivity of free space, respectively.

2.5.2 Constitutive Relations for TE and TM Modes

Using Maxwell equations it can be shown that the ratio of the tangential component of the electric field to the surface current density at the conductor surface is given by (Tham *et al.*, 2001; Tham *et al.*, 2003)

$$\frac{E_t}{a_n \times H_t} = \sqrt{\frac{\mu_c}{\varepsilon_c}}, \tag{2.43}$$

where μ_c and ε_c are the permeability and permittivity of the wall material, respectively, and $\sqrt{\frac{\mu_c}{\varepsilon_c}}$ is the intrinsic impedance of the wall material. The dielectric constant is complex and ε_c may be written as

$$\varepsilon_c = \varepsilon_0 - j\frac{\sigma_c}{\omega}, \tag{2.44}$$

where σ_c is the conductivity of the wall.

In order to estimate the loss of waves in millimeter and submillimeter wavelengths more accurately, a more evolved model than the conventional constant conductivity model used at microwave frequencies is necessary. Here, Drude's model is applied for the frequency dependent conductivity σ_c (Booker, 1982)

$$\sigma_c = \frac{\sigma}{(1 + j\omega\tau)}, \tag{2.45}$$

where σ is the conventional constant conductivity of the wall material and τ the mean free time. For most conductors, such as Copper, the mean free time τ is in the range of 10^{-13} to 10^{-14} s (Kittel, 1986).

At the width surface of the waveguide, $y = b$, $\frac{E_z}{H_x} = -\frac{E_x}{H_z} = \sqrt{\frac{\mu_c}{\varepsilon_c}}$.

Substituting (2.32), (2.33), (2.39), and (2.41) into (2.43), the following relationships are obtained:

$$\frac{-E_x}{H_z} = \frac{j}{h^2}\left(\frac{E_0}{H_0}k_z k_x - \omega\mu_0 k_y\right)\tan\left(k_y b + \phi_y\right) = \sqrt{\frac{\mu_c}{\varepsilon_c}}, \tag{2.46a}$$

$$\frac{H_x}{E_z} = \frac{j}{h^2}\left(\frac{H_0}{E_0}k_z k_x + \omega\varepsilon_0 k_y\right)\cot\left(k_y b + \phi_y\right) = \sqrt{\frac{\varepsilon_c}{\mu_c}}. \tag{2.46b}$$

Similarly, at the height surface where $x = a$, we obtain $\frac{E_y}{H_x} = -\frac{E_z}{H_y} = \sqrt{\frac{\mu_c}{\varepsilon_c}}$. Substituting (2.32), (2.33), (2.40), and (2.42) into (2.43), the following relationships are obtained:

$$\frac{E_y}{H_z} = \frac{-j}{h^2}\left(\frac{E_0}{H_0}k_z k_y + \omega\mu_0 k_x\right)\tan\left(k_x a + \phi_x\right) = \sqrt{\frac{\mu_c}{\varepsilon_c}}, \tag{2.47a}$$

$$\frac{-H_y}{E_z} = \frac{-j}{h^2}\left(\frac{H_0}{E_0}k_z k_y - \omega\varepsilon_0 k_x\right)\cot\left(k_x a + \phi_x\right) = \sqrt{\frac{\varepsilon_c}{\mu_c}}. \tag{2.47b}$$

In order to obtain nontrivial solutions for (2.46) and (2.47), the determinant of the equations must be zero. By letting the determinant of the coefficients of E_0 and H_0 in (2.46) and (2.47) vanish the following transcendental equations are obtained

$$\left[\frac{j\omega\mu_0 k_y \tan\left(k_y b+\phi_y\right)}{h^2}+\sqrt{\frac{\mu_c}{\varepsilon_c}}\right]\left[\frac{j\omega\varepsilon_0 k_y \cot\left(k_y b+\phi_y\right)}{h^2}-\sqrt{\frac{\varepsilon_c}{\mu_c}}\right]=\left[\frac{k_z k_x}{h^2}\right]^2,$$

(2.48a)

$$\left[\frac{j\omega\mu_0 k_x \tan\left(k_x a+\phi_x\right)}{h^2}+\sqrt{\frac{\mu_c}{\varepsilon_c}}\right]\left[\frac{j\omega\varepsilon_0 k_x \cot\left(k_x a+\phi_x\right)}{h^2}-\sqrt{\frac{\varepsilon_c}{\mu_c}}\right]=\left[\frac{k_z k_y}{h^2}\right]^2.$$

(2.48b)

In the above equations, k_x and k_y are the unknowns and k_z can then be obtained from (2.34). The Powell Hybrid root-searching algorithm in a NAG routine was used to find the roots of k_x and k_y. The routine requires initial guesses of k_x and k_y for the search. For good conductors, suitable guess values are clearly those close to the perfect conductor values.

For TE_{10} mode, m and n are set to 1 and 0, respectively, hence the search starts with $k_x = \frac{\pi}{a}$ and $k_y = 0$. Substituting $m = 1$ and $n = 0$ into the penetration factors in (2.36), the transcendental equations in (2.48) for TE_{10} mode can be simplified to

$$\left[\sqrt{\frac{\mu_c}{\varepsilon_c}}+\frac{j\omega\mu_0 k_y \tan\left(k_y \frac{b}{2}\right)}{h^2}\right]\left[\sqrt{\frac{\varepsilon_c}{\mu_c}}-\frac{j\omega\varepsilon_0 k_y \cot\left(k_y \frac{b}{2}\right)}{h^2}\right]=\left[\frac{jk_z k_x}{h^2}\right]^2,$$

(2.49a)

$$\left[\sqrt{\frac{\mu_c}{\varepsilon_c}}-\frac{j\omega\mu_0 k_x \cot\left(k_x\frac{a}{2}\right)}{h^2}\right]\left[\sqrt{\frac{\varepsilon_c}{\mu_c}}+\frac{j\omega\varepsilon_0 k_x \tan\left(k_x\frac{a}{2}\right)}{h^2}\right]=\left[\frac{jk_z k_y}{h^2}\right]^2 .$$

(2.49b)

For TE_{11} and TM_{11} modes, m and n are both set to 1 and the initial guess values are $\frac{\pi}{a}$ and $\frac{\pi}{b}$ respectively for both modes. Similarly, substituting $m = n = 1$ into (2.36), (2.48a) and (2.48b) for TE_{11} and TM_{11} modes, the equations in (2.48) can be simplified to:

$$\left[\sqrt{\frac{\mu_c}{\varepsilon_c}}-\frac{j\omega\mu_0 k_y \cot\left(k_y\frac{b}{2}\right)}{h^2}\right]\left[\sqrt{\frac{\varepsilon_c}{\mu_c}}+\frac{j\omega\varepsilon_0 k_y \tan\left(k_y\frac{b}{2}\right)}{h^2}\right]=\left[\frac{jk_z k_x}{h^2}\right]^2 ,$$

(2.50a)

$$\left[\sqrt{\frac{\mu_c}{\varepsilon_c}}-\frac{j\omega\mu_0 k_x \cot\left(k_x\frac{a}{2}\right)}{h^2}\right]\left[\sqrt{\frac{\varepsilon_c}{\mu_c}}+\frac{j\omega\varepsilon_0 k_x \tan\left(k_x\frac{a}{2}\right)}{h^2}\right]=\left[\frac{jk_z k_y}{h^2}\right]^2 .$$

(2. 50b)

When solving for these two degenerate modes with a set of initial guess, it is not obvious that the solution will converge to which of the two modes. However when the guess for one is very slightly changed a second set of result is obtained. By comparing with results from any of the approximate methods the two solutions can then be identified. Clearly, the solutions of (2.50) account for the interaction between TE_{11} and TM_{11} modes.

It is worthwhile noting that when the search started with exactly these values, the solution did not always converge to the required mode. It was often necessary to refine the initial values slightly in order to force convergence to the correct mode.

It could be seen that solving for the root of (2.49a) and (2.49b) only gives the propagation constant k_z of one non-degenerate mode, i.e. the dominant TE_{10} mode, since TM_{10} mode does not exist. However, for the concurrent presence of modes, such as the degenerate TE_{11} and TM_{11} modes, the transcendental equations in (2.50) actually combines both TE and TM modes in its formulation, therefore, allowing cross coupling effects in degenerate modes. This solution is certainly different from most existing methods, such as the power-loss method, PPM, and even Stratton's rigorous approach, where separate sets of equations are required to solve for the loss in TE mode and TM mode.

2.6 HFSS Simulation

To obtain a preliminary insight on the validity of the new independently derived transcendental equations, the attenuation constant of a rectangular waveguide has been simulated using Ansoft's High Frequency Structure Simulator (HFSS). HFSS is a high performance full-wave electromagnetic field simulator for volumetric passive device modeling. It employs the Finite Element Method (FEM), adaptive meshing, and Adaptive Lanczos-Pade Sweep (ALPS) for electromagnetic simulation.

In the simulation, a 10 cm copper rectangular waveguide with an arbitrary size of 2.29 × 1.02 cm^2 has been drawn on the 3D modeler window. A pair of waveports is connected to both ends of the waveguide. The waveports are necessary for exciting electromagnetic waves into the waveguide. Once the setup is completed as shown in Figure 2.4, the attenuation constant α_z of the dominant TE_{10} mode are then acquired, by simulating the model on a range of frequencies. As shown in Figure 2.5, the loss predicted by the proposed method is in close agreement with the simulated loss result. Both the electric and magnetic fields intensity are also shown in Figures 2.6 and 2.7, respectively.

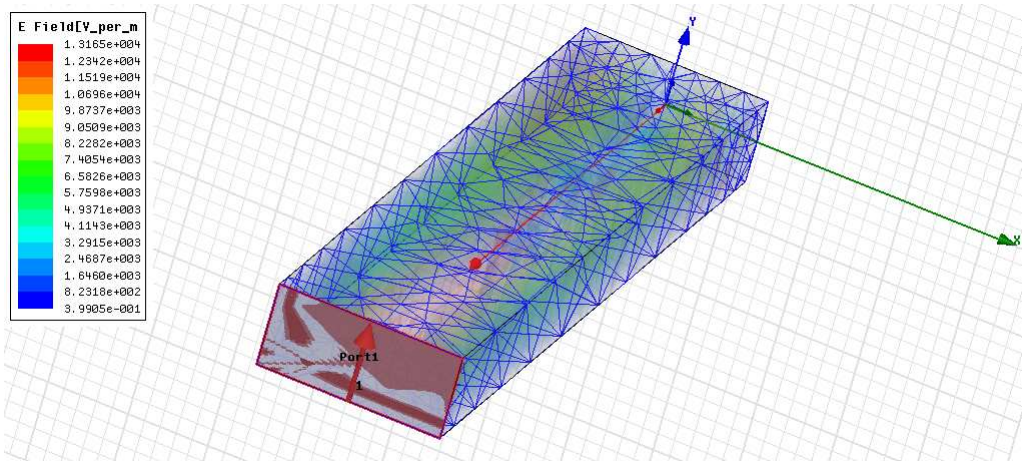

Figure 2.4. The meshes of a 10 cm long, 2.29 × 1.02 cm^2 copper rectangular waveguide, simulated using Finite Element Method (FEM) in HFSS.

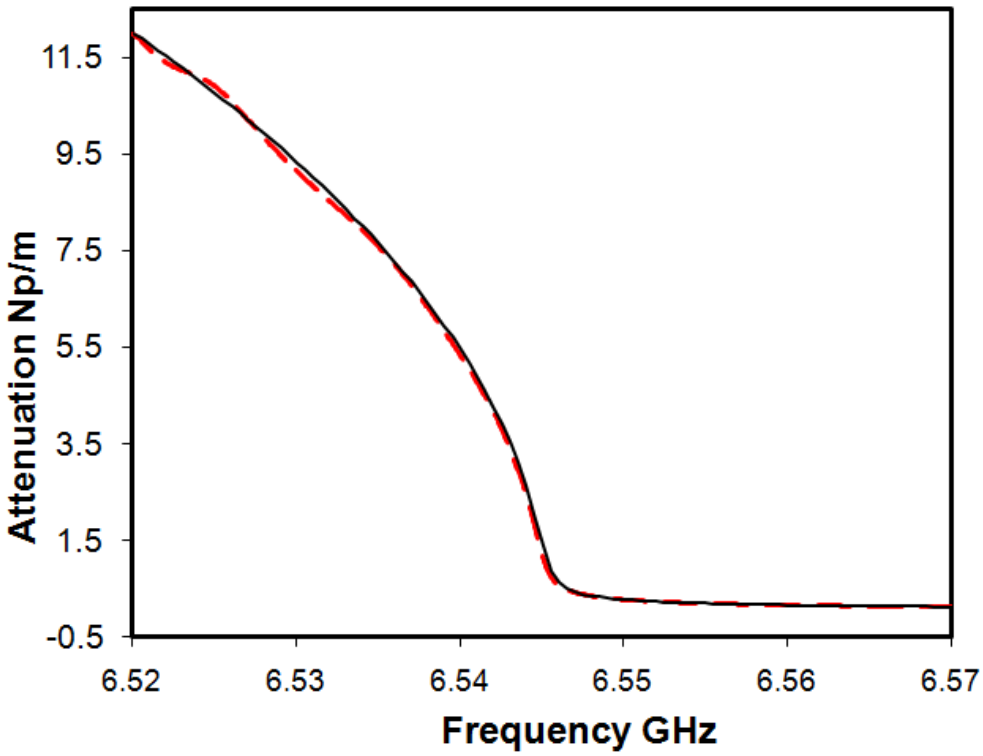

Figure 2.5. Attenuation of TE_{10} wave in a 2.29 × 1.02 cm^2 rectangular waveguide near cutoff. — — — — simulation result. ———— the proposed method.

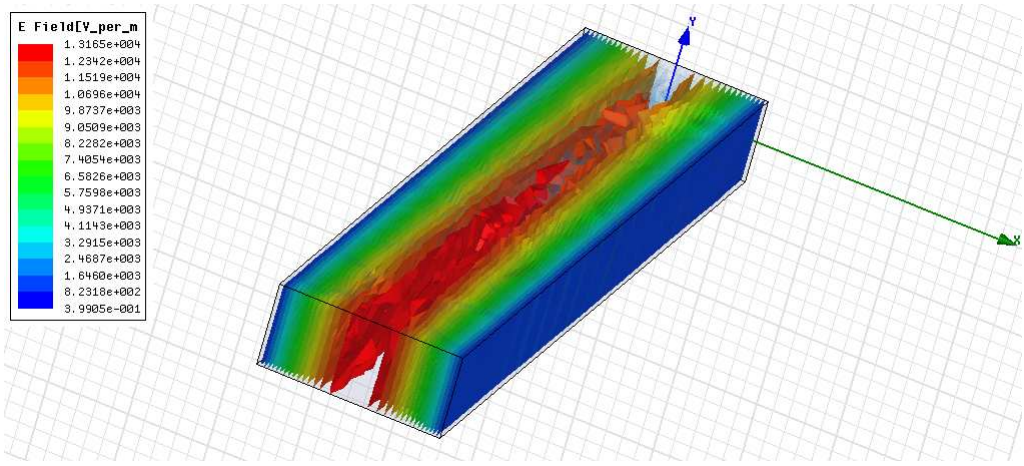

Figure 2.6. Electric field of TE_{10} mode in a 2.29 × 1.02 cm^2 rectangular waveguide.

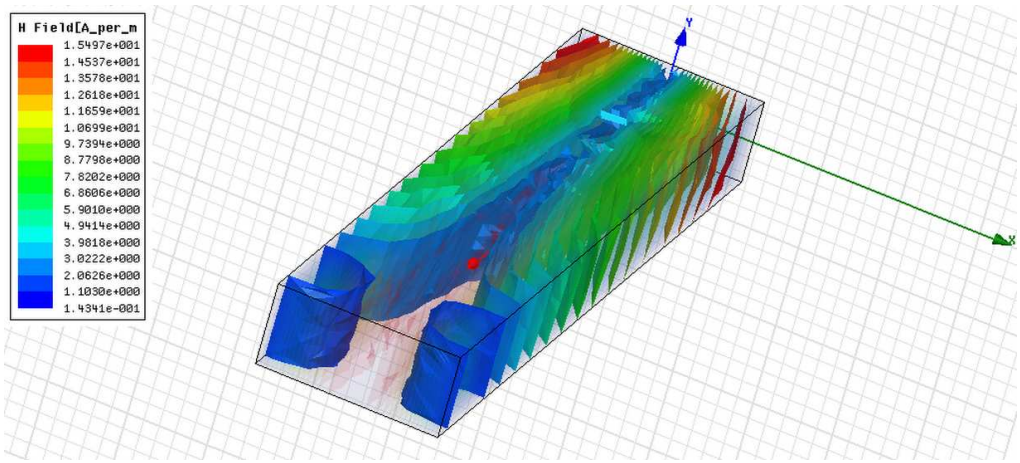

Figure 2.7. Magnetic field of TE_{10} mode in a 2.29 × 1.02 cm^2 rectangular waveguide.

2.7 Experimental Setup

To further validate the results, experimental measurements had been carried out in the experimental cosmology laboratory of the University of Oxford. It is in this laboratory where the millimeter wave instrumentation for studying the Cosmological Microwave Background and the Sunyaev-Zel'dovich effect were developed. The loss as a function of frequency for a rectangular waveguide was measured using a Vector Network Analyzer (VNA). A 20 cm copper rectangular waveguide with dimensions of a = 1.30 cm and b = 0.64 cm such as that shown in Figure 2.8 were used in the measurement.

To minimize noise in the waveguide, a pair of chokes had also been designed and fabricated as shown in Figure 2.9(a). The choke was machined to form an effective radial transmission line in the narrow gap between the

Figure 2.8. Rectangular waveguides with width a = 1.30 cm and height b = 0.64 cm.

chokes and the flanges of both the waveguide and the adapters. As illustrated in Figure 2.9(b), the radial transmission line is approximately $\frac{\lambda_g}{4}$ in length between the choke and the point of contact for the flanges, where $\lambda_g = \frac{2\pi}{\beta}$ is the guide wavelength. Another $\frac{\lambda_g}{4}$ line is formed by a circular axial groove in the choke. So the short circuit at the end of this groove is transformed to an open circuit at the contact point between the choke and the flanges. Any resistance in this contact is in series with an infinite (or very high) impedance and thus has little effect. This high impedance is then transformed back to a short circuit (or very low impedance) at the edges of the waveguides, to provide a very low-resistance path for current flow across the joint. Since there is a negligible voltage drop across the ohmic contact between the flanges and the choke, voltage breakdown is avoided (Pozar, 2005). A detail design of the choke drawn using AutoCAD is shown in Figure 2.10.

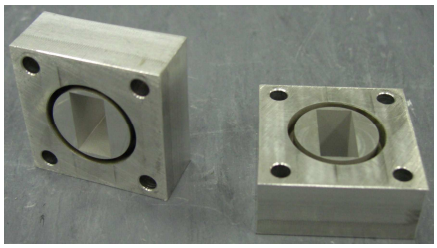

(a)

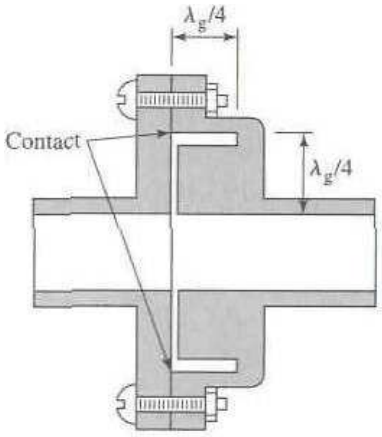

(b)

Figure 2.9. (a) Chokes and (b) cover-to-choke connection (Pozar, 2005).

Figure 2.10. Schematic of a choke.

In order to allow the waveguide to be connected to the adapters which are of different sizes, a pair of taper transitions had also been used as shown in Figure 2.11. Figure 2.12 depicts the complete setup of the experiment where the rectangular waveguide was connected to the VNA via tapers, chokes, coaxial cables, and adapters. Before measurement was carried out, the coaxial cables and waveguide adapters were calibrated to eliminate noise from the two devices. The loss in the waveguide was then observed from the S_{21} parameter of the scattering matrix. The measurement was performed in the frequency range where only TE_{10} mode could propagate, while other higher order modes were in evanescence.

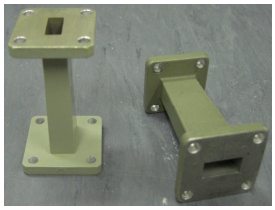

Figure 2.11. Taper transitions.

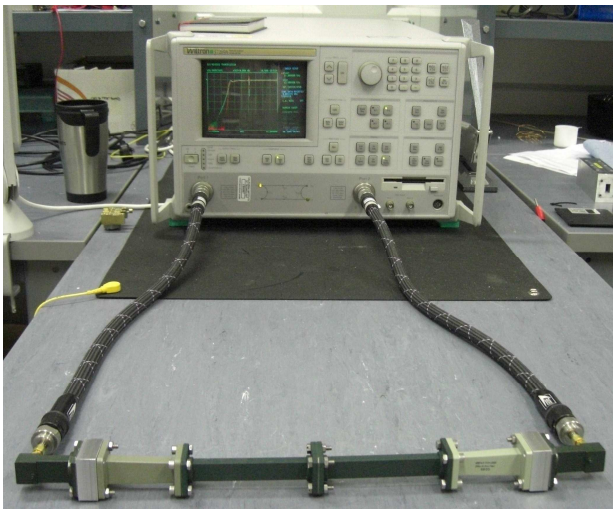

Figure 2.12. A 20 cm rectangular waveguide connected to the VNA, via tapers, chokes, adapters, and coaxial cables.

2.8 Results and Discussion

Figure 2.13 depicts the geometrical dimensions and material properties of the hollow rectangular waveguide implemented here for analysis. As shown in Figure 2.14, a comparison among the attenuation of the TE_{10} mode near cutoff as computed by the proposed new method, the conventional power-loss method, the PPM, and the measured S_{21} result was performed. As can clearly be seen, the attenuation constant α_z computed from the power-loss method diverges sharply to infinity, as the frequency approaches f_c, and is very different to the measured results, which show clearly that the loss at frequencies below f_c is high but finite. The attenuation curves computed using the proposed method and the PPM in Figure 2.14 match very well and in fact are indistinguishable on the plot.

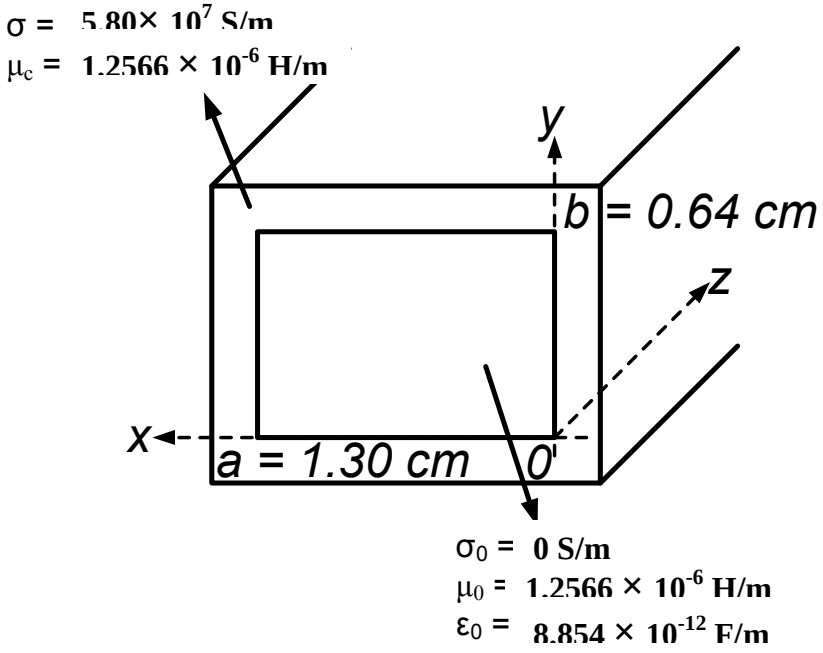

Figure 2.13. Cross section of a1.30 × 0.64 cm^2 rectangular waveguide.

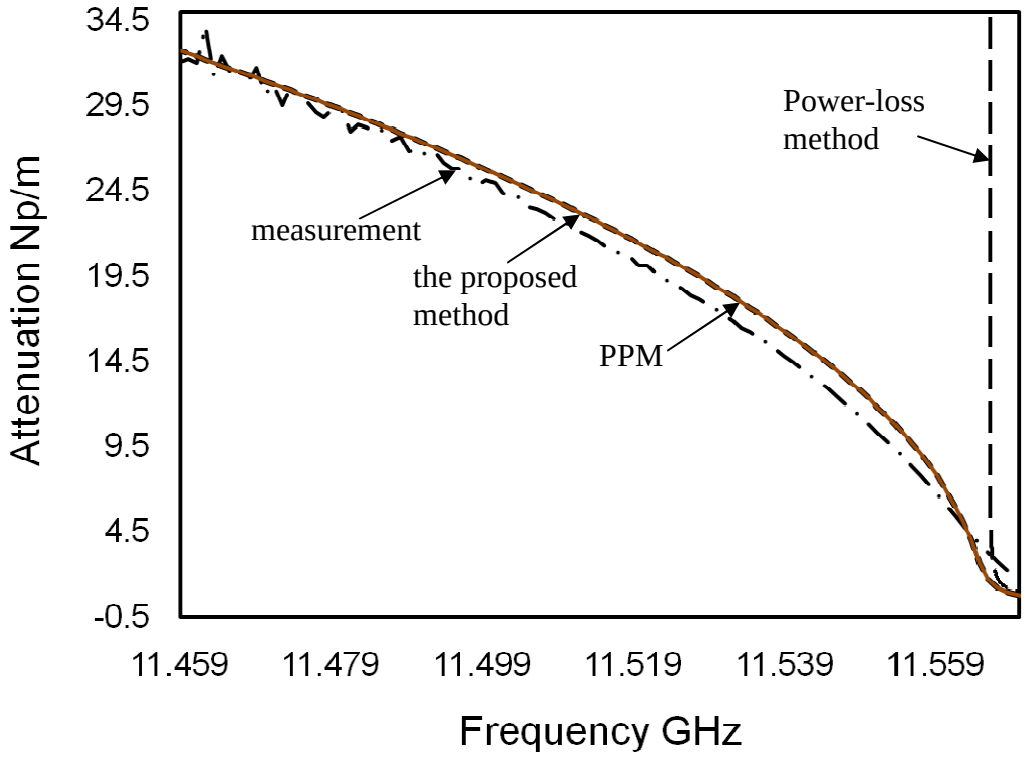

Figure 2.14. Loss of TE_{10} mode in a hollow rectangular waveguide near cutoff. — · — · — · measurement. — — — — power loss method. ——— the proposed method. ▪▪▪▪▪▪▪▪▪▪▪▪▪ perturbation method.

As shown in Table 2.1, the loss between 11.47025 GHz and 11.49950 GHz computed by the two methods agree with measurement to within 5% which is comparable to the error in the measurement.

Figure 2.15 shows the attenuation curve when the frequency is extended to higher values. Here, the loss due to TE_{10} alone could no longer be measured since higher-order modes, such as TE_{11} and TM_{11}, etc., start to propagate. At higher frequencies the loss due to TE_{10} predicted by the three methods, i.e. the proposed method, the power-loss method, and the PPM are in very close agreement. As depicted in Figure 2.16, at frequencies beyond millimeter wavelengths, however, the loss computed by the proposed method appears to be higher than those by the power-loss method and the PPM. The differences can be attributed to the fact that at extremely high frequencies, the field in a lossy waveguide can no longer be approximated to those derived from a perfectly conducting waveguide. At such high frequencies, the wave propagating in the waveguide is a hybrid mode and the presence of the longitudinal electric field E_z can no longer be neglected.

Table 2.1. Attenuation of TE_{10} mode in a lossy rectangular waveguide.

Frequency GHz	**Attenuation Constant Np/m**				
	Experiment	**PPM**	**%Δ**	**Proposed method**	**%Δ**
11.47025	30.17693	30.95772	2.59	30.95782	2.59
11.47138	30.68101	30.77407	0.30	30.77417	0.30
11.47250	29.53345	30.5893	3.58	30.5894	3.58
11.47363	30.51672	30.40339	0.37	30.40349	0.37
11.47475	30.16449	30.21631	0.17	30.21642	0.17
11.47588	29.68032	30.02805	1.17	30.02816	1.17
11.47700	29.09721	29.83859	2.55	29.8387	2.55
11.47813	28.85077	29.6479	2.76	29.648	2.76
11.47925	29.25528	29.45595	0.69	29.45606	0.69
11.48038	29.20923	29.26273	0.18	29.26283	0.18
11.48150	27.99881	29.0682	3.82	29.06831	3.82
11.48263	28.38341	28.87234	1.72	28.87245	1.72
11.48375	28.18551	28.67513	1.74	28.67524	1.74
11.48488	27.91169	28.47653	2.02	28.47664	2.02
11.48600	28.08407	28.27651	0.69	28.27663	0.69
11.48713	27.44495	28.07506	2.30	28.07517	2.30
11.48825	27.67956	27.87212	0.70	27.87224	0.70
11.48938	26.84192	27.66768	3.08	27.66779	3.08
11.49050	26.95767	27.4617	1.87	27.46181	1.87
11.49163	26.60108	27.25414	2.46	27.25425	2.46
11.49275	26.78715	27.04496	0.96	27.04508	0.96
11.49388	26.14928	26.83414	2.62	26.83426	2.62
11.49500	25.83003	26.62162	3.06	26.62174	3.07
11.49613	25.82691	26.40738	2.25	26.4075	2.25
11.49725	25.26994	26.19136	3.65	26.19148	3.65
11.49838	24.82685	25.97353	4.62	25.97365	4.62
11.49950	25.1100	25.75383	2.56	25.75395	2.56

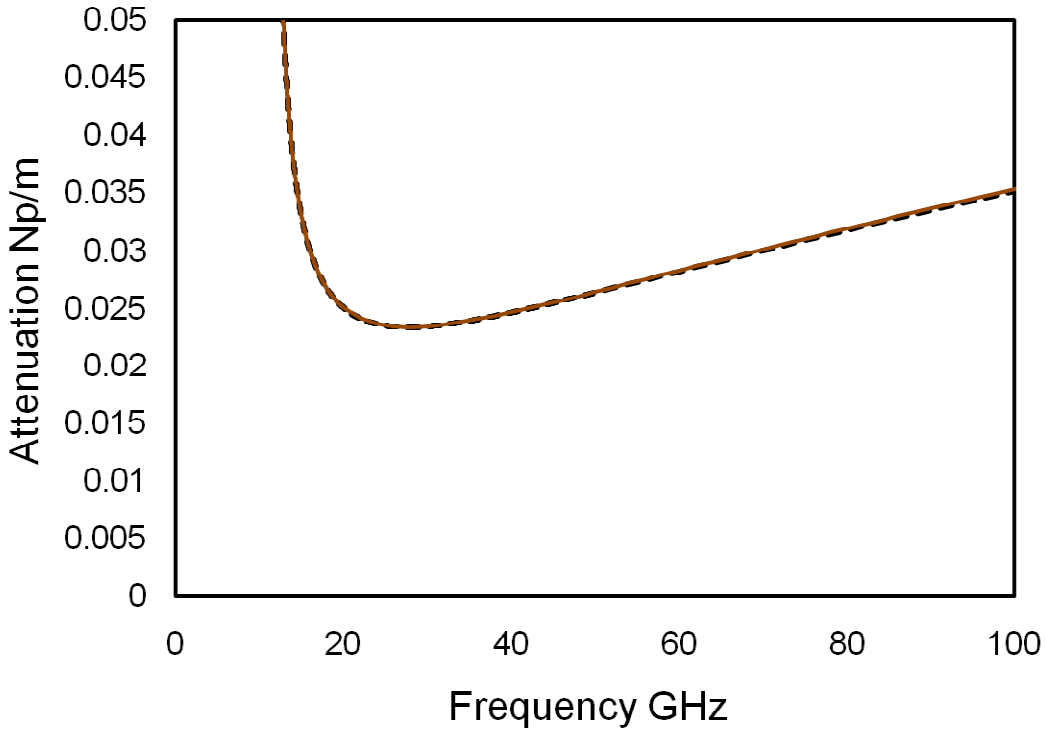

Figure 2.15. Loss of TE_{10} mode in a hollow rectangular waveguide from 0 to 100 GHz. — — — — power loss method. ——— the proposed method. ▪▪▪▪▪▪▪▪▪▪▪▪▪ perturbation method.

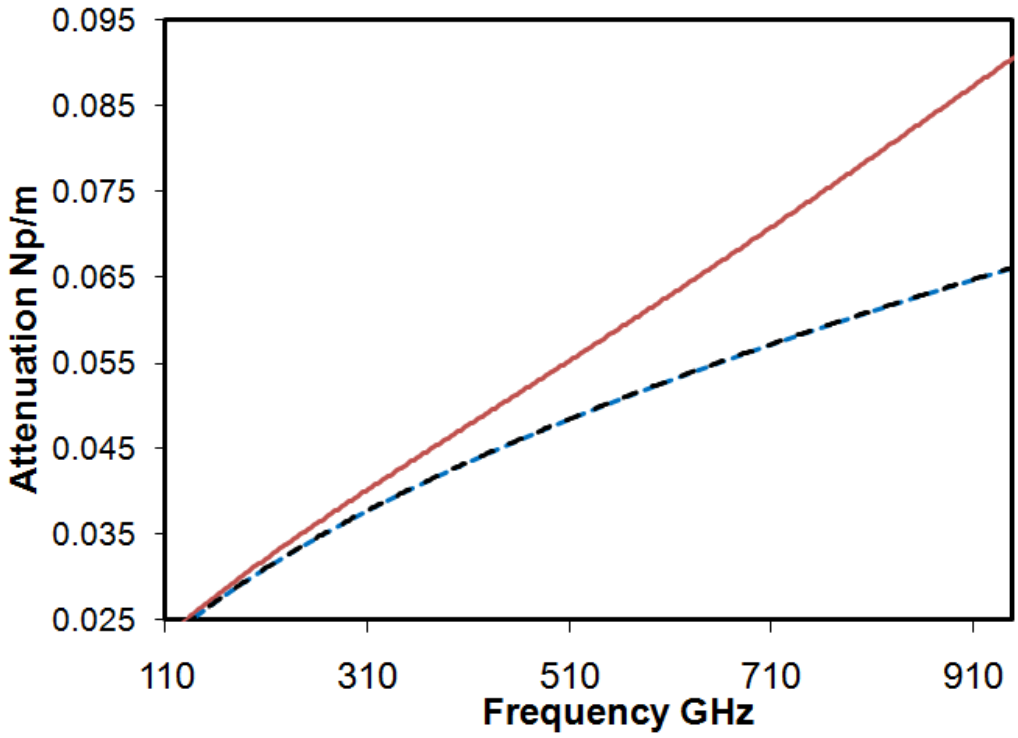

Figure 2.16. Loss of TE_{10} mode in a hollow rectangular waveguide at millimeter waves. — — — — power loss method. ——— the proposed method. ····· perturbation method.

Next, the propagation constants k_z of TE_{11} and TM_{11} degenerate modes, which have identical phase constants β_z in the lossless case, are compared. Here, the power-loss method can only give α_z whereas both the PPM and the proposed method give both β_z and α_z. Figure 2.17 shows that the phase constant β_z for TE_{11} mode computed using the proposed method is in good agreement with that computed using the PPM. For TM_{11} mode however, the results differ slightly. Unlike that of the lossless case, the values of β_z differ slightly for the different modes in a lossy waveguides giving dispersive effects.

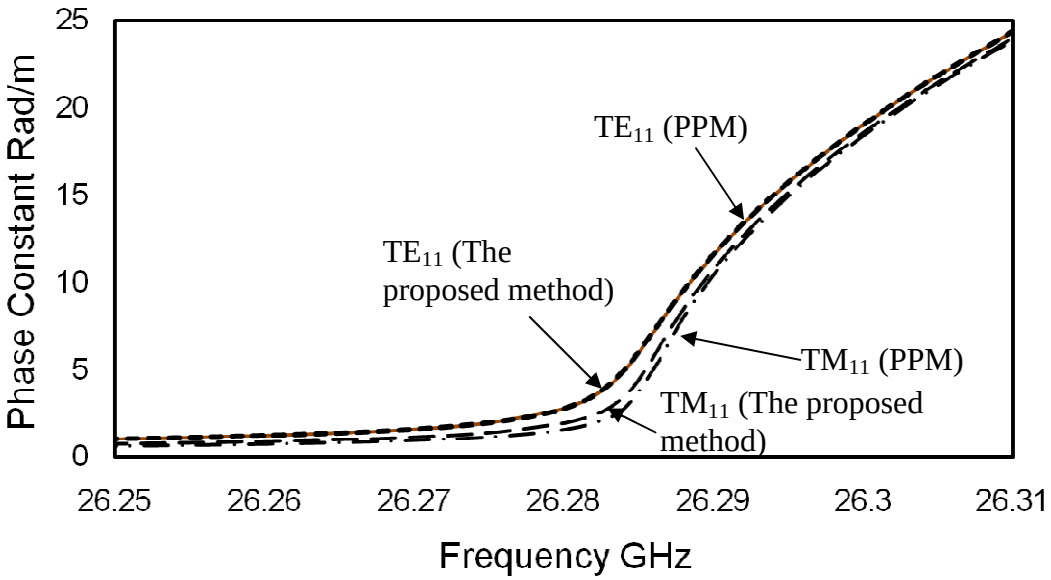

Figure 2.17. Phase constant β_z of TE_{11} and TM_{11} in a rectangular waveguide. β_z of TE_{11} computed using the perturbation method (▪▪▪▪▪▪▪▪▪▪▪▪▪▪) and the proposed method (——————); β_z of TM_{11} computed using the perturbation method (— · — · — ·) and the proposed method (— — —).

The attenuation α_z of the degenerate TE_{11} and TM_{11} modes is illustrated in Figures 2.18 to 2.21, both near cutoff and in the propagating region. In Figures 2.18 and 2.19, α_z computed by the PPM and the proposed method, agree very well near cutoff. However, Figures 2.20 and 2.21 show that when the frequency increases beyond 28.5 GHz for TE_{11} and 27.0 GHz for TM_{11}, the results start to disagree significantly.

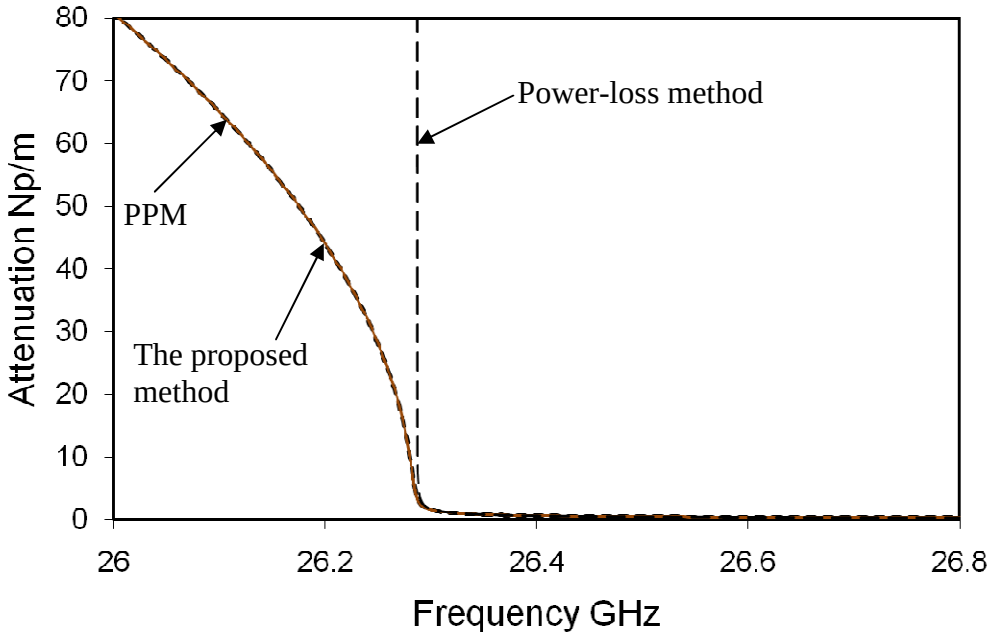

Figure 2.18. Loss of TE_{11} mode in a rectangular waveguide near cutoff. — — — — power loss method. ——— the proposed method. ▪▪▪▪▪▪▪▪▪▪▪▪▪ perturbation method.

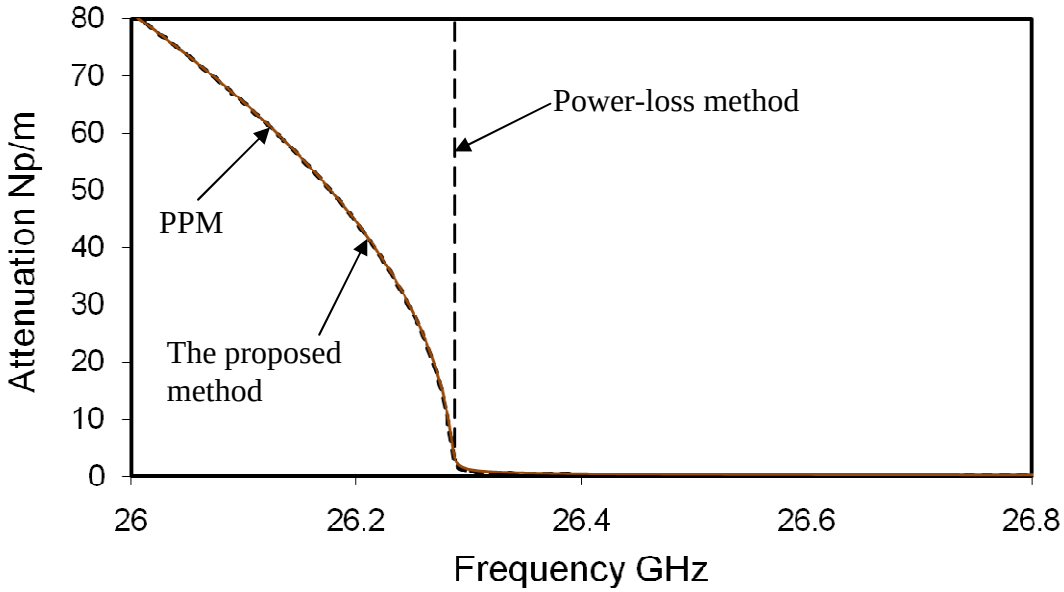

Figure 2.19. Loss of TM_{11} mode in a rectangular waveguide near cutoff. — — — — power loss method. ——— the proposed method. ▪▪▪▪▪▪▪▪▪▪▪▪▪ perturbation method.

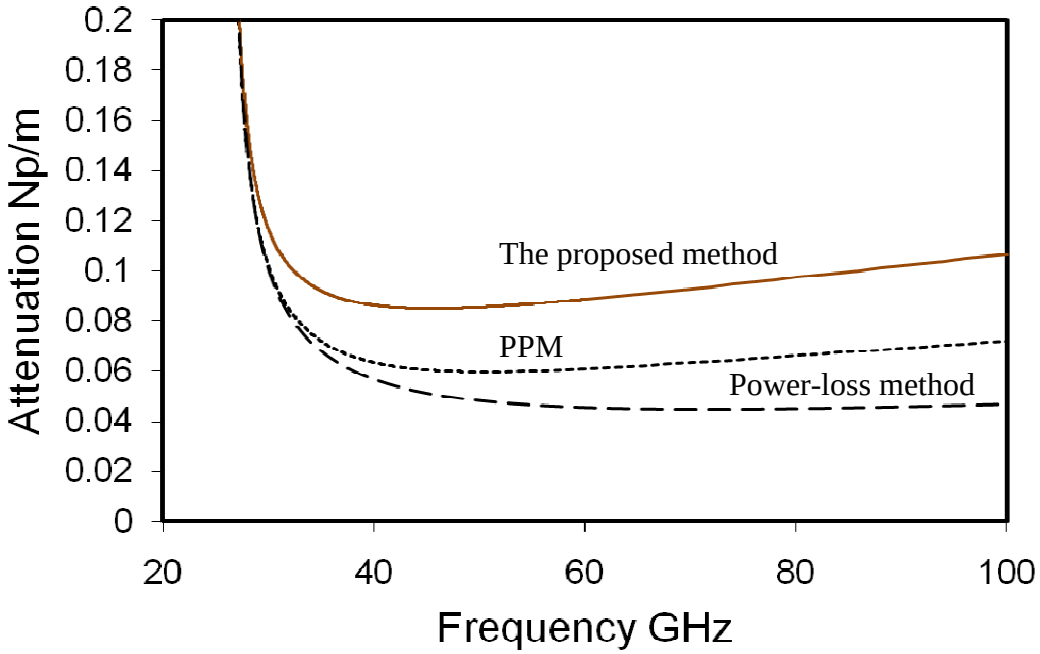

Figure 2.20. Loss of TE_{11} mode in a hollow rectangular waveguide from 20 GHz to 100 GHz. — — — — power loss method. ——— the proposed method. ▪▪▪▪▪▪▪▪▪▪▪▪▪ perturbation method.

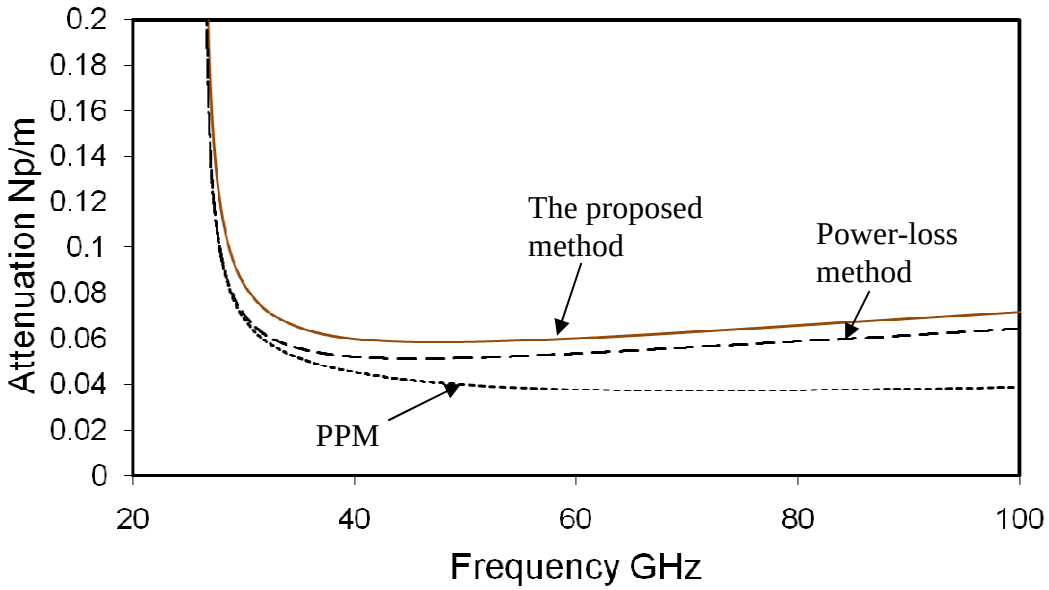

Figure 2.21. Loss of TM_{11} mode in a hollow rectangular waveguide from 20 GHz to 100 GHz. — — — — power loss method. ——— the proposed method. ▪▪▪▪▪▪▪▪▪▪▪▪▪ perturbation method.

According to the findings of Imbriale *et al.* (1998), power losses of a number of modes that propagate simultaneously in a waveguide is not simply additive. The cross product terms between the different modes give rise to additional dissipation, making the total loss greater than the one obtained from the addition of loss in independent propagation of single modes. This is because the product of the average power density, $P_{av} = \frac{1}{2} Re(\vec{E}_1 \times \vec{H}_1 *)$ of the electric field of mode 1 $\vec{E}_1$ and magnetic field of mode 2 $\vec{H}_1$, when integrated along the boundary, is not zero and the current induced by $\vec{H}_1$ will deliver power to mode 1, and vice versa. In this case, there will be coupling of power between multiple propagating modes, which give rise to power loss as a result

of the change in the amplitude distribution of the fields across the area of the waveguide (Imbriale *et al.*, 1998)

$$
\begin{aligned}
P_L = \frac{1}{2}R\Bigg\{ & \sum_{m=1}^{M}\left|A_m^{(TE)}\right|^2 l\oint_c\left(\left|H_{mc}^{(TE)}\right|^2+\left|H_{mz}^{(TE)}\right|^2\right)dc+\sum_{m'=1}^{M'}\left|A_{m'}^{(TM)}\right|^2 l\oint_c\left|H_{m'c}^{(TM)}\right|^2 dc \\
& +\sum_{m=1}^{M}\sum_{\substack{n=1\\ n\neq m}}^{M} A_m^{(TE)}A_n^{(TE)^*}\oint_c\left[H_{mc}^{(TE)}H_{nc}^{(TE)^*}+H_{mz}^{(TE)}H_{nz}^{(TE)^*}\right]dc\int_0^l \exp\left[j(\beta_m^{(TE)}-\beta_n^{(TE)})z\right]dz \\
& +\sum_{m'=1}^{M'}\sum_{n=1}^{M} A_{m'}^{(TM)}A_n^{(TE)^*}\oint_c\left[H_{m'c}^{(TM)}H_{nc}^{(TE)^*}\right]dc\int_0^l \exp\left[j(\beta_{m'}^{(TM)}-\beta_n^{(TE)})z\right]dz \\
& +\sum_{m=1}^{M}\sum_{n'=1}^{M'} A_m^{(TE)}A_{n'}^{(TM)^*}\oint_c\left[H_{mc}^{(TE)}H_{n'c}^{(TM)^*}\right]dc\int_0^l \exp\left[j(\beta_m^{(TE)}-\beta_{n'}^{(TM)})z\right]dz \\
& +\sum_{m'=1}^{M'}\sum_{\substack{n=1\\ n\neq m}}^{M'} A_{m'}^{(TM)}A_{n'}^{(TM)^*}\oint_c\left[H_{m'c}^{(TM)}H_{n'c}^{(TM)^*}\right]dc\int_0^l \exp\left[j(\beta_{m'}^{(TM)}-\beta_{n'}^{(TM)})z\right]dz\Bigg\}
\end{aligned}
\qquad (2.51)
$$

Here, $A^{(TE)}$ and $A^{(TM)}$ are arbitrary amplitude coefficients for the TE and TM modes respectively, *R* the surface resistance, and *c* the contour around the inner surface of the waveguide, which is also normal to the propagating *z* axis. The subscript *c* represents the component of the transverse field tangential to the contour *c*. *M* is the number of different TE propagating modes, and *M'* is the number of different TM propagating modes.

It turns out that mode coupling increases the interaction between the propagating power and the waveguide walls, making the attenuation dependent on the axial distance from the source. Integrating the exponential terms in (2.51), it could be seen that the factor below determines the importance of the coupling term (Imbriale *et al.*, 1998)

$$F = \frac{\exp[\, j(\beta_m^{TE} - \beta_n^{TM})l] - 1}{[\, j(\beta_m^{TE} - \beta_n^{TM})l]}, \tag{2.52}$$

where β_m and β_n are the phase constants of two different modes which could be either TM or TE, while l is the length of the waveguide. As expected, equation (2.52) shows that the cross coupling is significant when the difference between the phase constants of the propagating modes that exist in the waveguide is small. Therefore, the coupling effect between TE_{11} and TM_{11} in a waveguide fabricated from a good conductor is expected to be significant because the phase constants for TE_{11} and TM_{11} are very close as shown in Figure 2.17.

Figures 2.20 and 2.21 depict the attenuation constant for the TE_{11} and the TM_{11} modes at frequencies when both of them can propagate simultaneously. It can clearly be seen that in this region, the computed attenuation using the proposed method is significantly higher than the one computed using the power loss method. This is of course to be expected because in the power loss method, attenuation is obtained excluding coupling losses. Finger and Kerr (2008) has performed an experimental validation on the loss in transmission lines. In their findings, the measurement result was found to be much higher than those computed using the power-loss method. Indeed, such result suggests that the proposed method agree reasonably well with the result obtained by Finger and Kerr (2008). It is interesting to see however that in this range, the attenuation computed by the PPM is even lower

than that obtained by the power loss method, indicating that the PPM under-estimates the loss significantly in degenerate mode propagation.

2.9 Summary

A new technique using fundamental principle for formulation, with no assumption of perfect conductor to compute the propagation constant of waves in a lossy rectangular waveguide has been proposed. The formulation is based on matching the tangential electric and magnetic fields at the boundary of the wall, and allowing the wavenumbers to take complex values. The electromagnetic fields are used in conjunction of the concept of surface impedance to derive transcendental equations, whose roots give values for the wavenumbers in the x and y directions for different TE or TM modes. The wave propagation constant k_z could then be obtained from k_x, k_y, and k_0 using the dispersion relation.

The computed attenuation curves are in good agreement with the PPM and experimental results for the case of the dominant TE_{10} mode. An important consequence of this work is the demonstration that the loss computed for degenerate modes propagating simultaneously is not additive. In other words, the combined loss of two co-existing modes is higher than adding the losses of the two modes propagating independently. This can be explained by the mode coupling effects, which is significant when the phase constants of two propagating modes are different yet very close.

CHAPTER 3

CIRCULAR WAVEGUIDES*

In this chapter, the new proposed method introduced in Chapter 2 is extended to characterize the attenuation of waves in circular waveguides. To validate the result, a comparison was performed with the loss obtained from simulation, experimental measurement, and Stratton's equation. This chapter demonstrates the versatility of the new method, i.e. being able to be applied in waveguides with different geometry – especially in circular and rectangular waveguides.

3.1 Introduction

The efficiency of coupling the radiation from a telescope to a detector element is one of the key factors to determine the performance of a receiver. In direct detection such as those using bolometers (Blundell and Tong, 1991; Baselmans *et al.*, 2004; Cherednichenko *et al.*, 2002), waveguide coupling is accomplished by receiving the radiation signal via a feed horn and channeling the signal via a circular waveguide to a waveguide probe where the detector is located. Similarly, for heterodyne detection such as those using the waveguide Superconductor-Insulator-Superconductor (SIS) mixers (Woody *et al.*, 1985; Ellison and Miller, 1988; Kittara *et al.*, 2004), the signal from the horn is first channeled to a circular waveguide. The structure subsequently undergoes a

*Parts of this chapter were published in "K. H. Yeap, C. Y. Tham, K. C. Yeong, and H. J. Woo, "Wave Propagation in Lossy and Superconducting Circular Waveguides", *Radioengineeringl*, Vol. 19(2), June 2010, pp. 320 – 325."

circular-to-rectangular waveguide transition before allowing the waves to be coupled to the detectors via the microstrip probe. A typical bolometer design is shown in Figure 3.1 (Blundell and Tong, 1992); whereas waveguide mixer designs are shown in Figures 1.2 and 3.2 (Wengler, 1992). It is apparent that, in both direct and heterodyne detections, circular waveguides are required in the coupling of waves from the horn. Hence, the prediction and reduction of

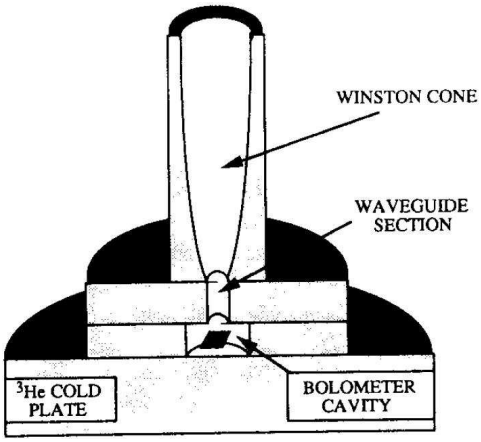

Figure 3.1. A bolometer receiver (Blundell and Tong, 1992).

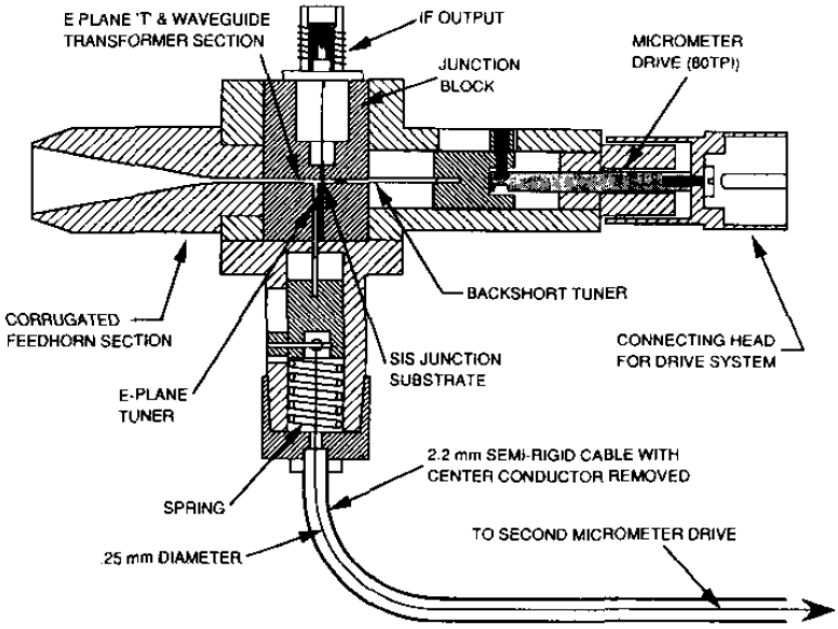

Figure 3.2. Caltech two-tuner waveguide design (Wengler, 1992) which has been implemented for 230, 345, and 492 GHz band mixers.

loss to its minimal at the circular waveguide is of considerable importance, particularly for the detection of THz signals which is extremely weak.

Developing a standard approach capable of characterizing the propagation of waves in both rectangular and circular waveguides (or at best in waveguides with any arbitrary shapes) is certainly a great convenience, since there is no need to employ different methods in analyzing waveguides with different geometries. It is worthwhile noting that circular-to-rectangular waveguide transitions have been widely implemented, not only in the design of heterodyne receivers, but also in the design of waveguide polarizers (Cresci *et al.*, 2002) and Ortho-Mode Transducers (OMT) (Chattopadhyay *et al.*, 1998). Hence, in this chapter, the proposed new method implemented in the case of rectangular waveguides (as illustrated in Chapter 2) is extended to compute the propagation constant of waves in circular waveguides.

3.2 Fields in Circular Cylindrical Coordinates

For waves propagating in a circular waveguide, such as that shown in Figure 3.3, Helmholtz's equation in (2.3) can be expressed in cylindrical coordinates to give

$$\frac{1}{r}\frac{\partial}{\partial r}\left(r\frac{\partial \psi_z}{\partial r}\right)+\frac{1}{r^2}\frac{\partial^2 \psi_z}{\partial \phi^2}+(k^2-k_z{}^2)\psi_z=0\,. \tag{3.1}$$

Applying the method of separation of variables, ψ_z can be expressed as

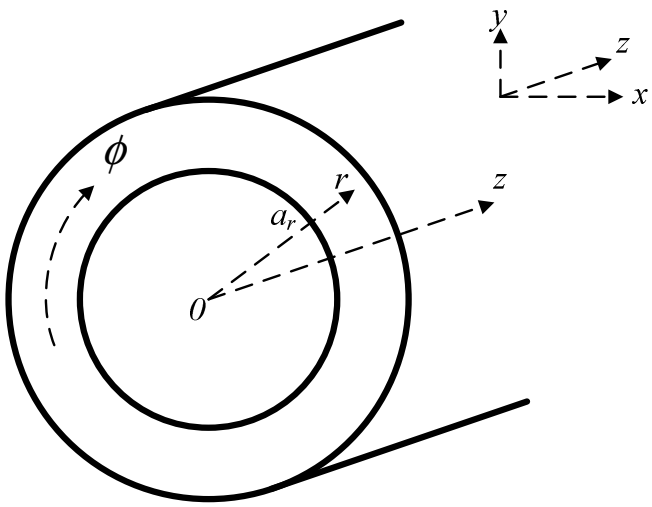

Figure 3.3. The cross section of a circular waveguide.

$$\psi_z = R(r)\Phi(\phi). \tag{3.2}$$

Equation (3.2) can be separated into two sets of second order linearly independent differential equations, as shown below (Pozar, 2005; Marcuvitz, 1986)

$$\frac{\partial^2 R(r)}{\partial r^2} + \frac{1}{r}\frac{\partial R(r)}{\partial r} + (h^2 - \frac{N}{r^2})R(r) = 0, \tag{3.3}$$

$$\frac{\partial^2 \Phi(\phi)}{\partial \phi^2} + N^2\Phi(\phi) = 0, \tag{3.4}$$

where N is a separation constant and (3.3) is known as Bessel's differential equation.

Solving (3.3), the following solutions can be obtained,

$$R(r) = C_n J_n(hr)\,, \tag{3.5}$$

and

$$R(r) = D_n H_n(hr)\,, \tag{3.6}$$

where C_n and D_n are arbitrary constants, $J_n(hr)$ is known as the Bessel function of the first kind, and $H_n(hr)$ is known as the Hankel function of the first kind.

The fields confined within the waveguide have to be finite at $r = 0$. Hence, (3.5) is applied to define the fields propagating in the waveguide. For the case of dielectric or lossy conducting walls, (3.6) is used to represent the elementary field beyond the wall.

Since all field components are periodic with respect to ϕ, the only admissible solution for (3.4) is either $\cos(n\phi)$ or $\sin(n\phi)$ or a linear combination of both.

Thus, the longitudinal electric field (E_z) and magnetic field (H_z) within the waveguide can be, customarily, expressed as

$$E_z = C_n J_n(hr)\cos(n\phi)\,, \tag{3.7}$$

$$H_z = C_n' J_n(hr)\sin(n\phi)\,, \tag{3.8}$$

where C_n and C_n' denote the coefficients of the fields.

The transverse field components can be derived by substituting the longitudinal field components into Maxwell's source free curl equations in (2.8) and (2.9). Expressing the transverse field components in term of the longitudinal field components E_z and H_z, the following can be obtained (Pozar, 2005)

$$H_r = -\frac{1}{h^2}\left(jk_z \frac{dH_z}{dr} - \frac{j\omega\varepsilon}{r}\frac{dE_z}{d\phi} \right), \tag{3.9}$$

$$H_\phi = -\frac{1}{h^2}\left(\frac{jk_z}{r}\frac{dH_z}{d\phi} + j\omega\varepsilon \frac{dE_z}{dr} \right), \tag{3.10}$$

$$E_r = -\frac{1}{h^2}\left(jk_z \frac{dE_z}{dr} + \frac{j\omega\mu}{r}\frac{dH_z}{d\phi} \right), \tag{3.11}$$

$$E_\phi = -\frac{1}{h^2}\left(\frac{jk_z}{r}\frac{dE_z}{d\phi} - j\omega\mu \frac{dH_z}{dr} \right). \tag{3.12}$$

3.3 A Review of Stratton's Approach

In Stratton's formulation, the fields at the wall surface are made continuous into the wall material. Since the fields beyond the radius a_r of the inner core, i.e. $r > a_r$, must be evanescent, (3.6) is employed to derive the field expression within the wall material.

Equating the tangential fields at the boundary of the wall (i.e. $r = a_r$) and letting the determinants of the coefficients equal zero lead to the following transcendental equation for circular waveguides (Stratton, 1941)

$$\left[\frac{\mu_0}{u}\frac{J_n(u)'}{J_n(u)} - \frac{\mu_c}{v}\frac{H_n(v)'}{H_n(v)}\right]\left[\frac{\omega^2\varepsilon_0}{u}\frac{J_n(u)'}{J_n(u)} - \frac{\omega^2\varepsilon_c}{v}\frac{H_n(v)'}{H_n(v)}\right] = k_z{}^2 n^2\left[\frac{1}{u^2} - \frac{1}{v^2}\right]^2, \tag{3.13a}$$

where $u = h_0 a_r$, $v = h_c a_r$, $h_c = \sqrt{k_c{}^2 - k_z{}^2}$, and k_c is the wavenumber in the wall material.

Equation (3.13a) can be solved numerically for the propagation constant k_z of TE_{np} modes. Here, the n and p subscripts denote the n-th order and p-th zero of $J_n(hr)$, respectively. By convention, the n subscript always represents the number of half-wave field variations in the ϕ-direction; whereas, the p subscript represents the number of half-wave field variations in the r-direction (Cheng, 1989).

Since TE and TM modes are determined by the roots of $\frac{J_n(u)'}{J_n(u)} = 0$ and $\frac{J_n(u)}{J_n(u)'} = 0$, respectively (Stratton, 1941), an alternate form of the equation is required for TM_{np} modes (Yassin *et al.*, 2003)

$$\left[\frac{J_n(u)}{J_n(u)'}\right]^2\left[\frac{H_n(v)'}{H_n(v)}\right]^2\frac{k_c{}^2}{v^2}+\frac{k_0{}^2}{u^2}-\frac{1}{uv}\left[\frac{J_n(u)}{J_n(u)'}\right]\left[\frac{H_n(v)'}{H_n(v)}\right]\left[\frac{\mu_0}{\mu_c}k_c{}^2+\frac{\mu_c}{\mu_0}k_0{}^2\right]$$
$$=\left[\frac{J_n(u)}{J_n(u)'}\right]^2 k_z{}^2 n^2\left[\frac{1}{u^2}-\frac{1}{v^2}\right]^2 \quad \text{(3.13b)}$$

3.4 The Proposed Method

It is necessary to develop an approach which is able to account for the mode-coupling effect in waveguides; while at the same time, versatile enough to solve for the propagation constants in waveguides with different geometry (for eg. circular and rectangular waveguides). In this section, the new boundary-matching method introduced in Chapter 2 used in solving for the propagation constant in rectangular waveguides, shall be extended to the case of circular waveguides. The tangential fields in a circular waveguide, i.e. E_ϕ and H_ϕ, are first derived by substituting the longitudinal fields in (3.7) and (3.8) into (3.10) and (3.12), giving

$$E_\phi=\frac{1}{h^2}\left[\frac{jnk_z}{r}C_nJ_n(hr)\sin n\phi+j\omega\mu_0 hC_n{}'J_n(hr)'\cos n\phi\right], \quad \text{(3.14)}$$

$$H_\phi=-\frac{1}{h^2}\left[\frac{jnk_z}{r}C_n{}'J_n(hr)\cos n\phi+j\omega\varepsilon_0 hC_nJ_n(hr)'\cos n\phi\right]. \quad \text{(3.15)}$$

From (2.38), the surface impedance Z_s at the boundary of the wall ($r = a_r$) can be expressed as $Z_s = \frac{E_\phi}{H_z} = -\frac{E_z}{H_\phi} = \sqrt{\frac{\mu_c}{\varepsilon_c}}$. Substituting (3.7), (3.8), (3.14), and (3.15) into (2.38), the following equations are obtained

$$\left[\frac{jnk_z}{h^2 a_r}\right]C_n + \left[\frac{j\omega\mu_0 J_n(u)'}{hJ_n(u)} - \sqrt{\frac{\mu_c}{\varepsilon_c}}\right]C_n' = 0, \tag{3.16a}$$

$$\left[\frac{j\omega\varepsilon_0 J_n(u)'}{hJ_n(u)} - \sqrt{\frac{\varepsilon_c}{\mu_c}}\right]C_n + \left[\frac{jnk_z}{h^2 a_r}\right]C_n' = 0. \tag{3.16b}$$

Solving the determinants of the coefficients C_n and C_n' in (3.16) results in the following transcendental equation

$$\left[jh^2\sqrt{\frac{\mu_c}{\varepsilon_c}} + \omega\mu_0 h\frac{J_n(u)'}{J_n(u)}\right]\left[jh^2\sqrt{\frac{\varepsilon_c}{\mu_c}} + \omega\varepsilon_0 h\frac{J_n(u)'}{J_n(u)}\right] = \left[\frac{nk_z}{a_r}\right]^2. \tag{3.17a}$$

Like Stratton's equation, (3.17a) is only applicable in solving for k_z of TE modes. To solve for TM modes, an alternate form must be taken, as shown below

$$\left[jh^2\sqrt{\frac{\mu_c}{\varepsilon_c}}\frac{J_n(u)}{J_n(u)'} + \omega\mu_0 h\right]\left[jh^2\sqrt{\frac{\varepsilon_c}{\mu_c}}\frac{J_n(u)}{J_n(u)'} + \omega\varepsilon_0 h\right] = \left[\frac{nk_z}{a_r}\frac{J_n(u)}{J_n(u)'}\right]^2 \tag{3.17b}$$

.

3.5 HFSS Simulation

In order to obtain a preliminary verification on the new proposed equation, the loss computed using the new formulation is compared with that using the Finite Element Method (FEM). Like the case of the rectangular waveguide, HFSS is implemented to simulate the result of the Finite Element Method.

Figure 3.4 depicts the structure of a copper circular waveguide plotted in the HFSS. The radius and length of the waveguide are 5.8533 mm and 20 cm, respectively. The attenuation constant of the dominant TE_{11} mode is simulated and compared with that obtained from (3.17a). Figures 3.5 and 3.6 show the electric and magnetic fields in the circular waveguide, respectively; while Figures 3.7 and 3.8 show comparison of loss at the vicinity of cutoff. It is indeed surprising to find from Figure 3.7, that the simulation result differs considerably from the calculation result. The cutoff frequency f_c found from the simulation result is much higher; and in fact, the loss from the simulation is also much higher than that from the calculation result. Further attempt in the simulation shows that the loss as well as the cutoff frequency, decrease as the radius a_r of the waveguide increases. As shown in Figure 3.8, the simulation loss found in a circular waveguide with radius a_r = 5.9270 mm turns out to be much closer with the calculation result with a_r = 5.8533 mm.

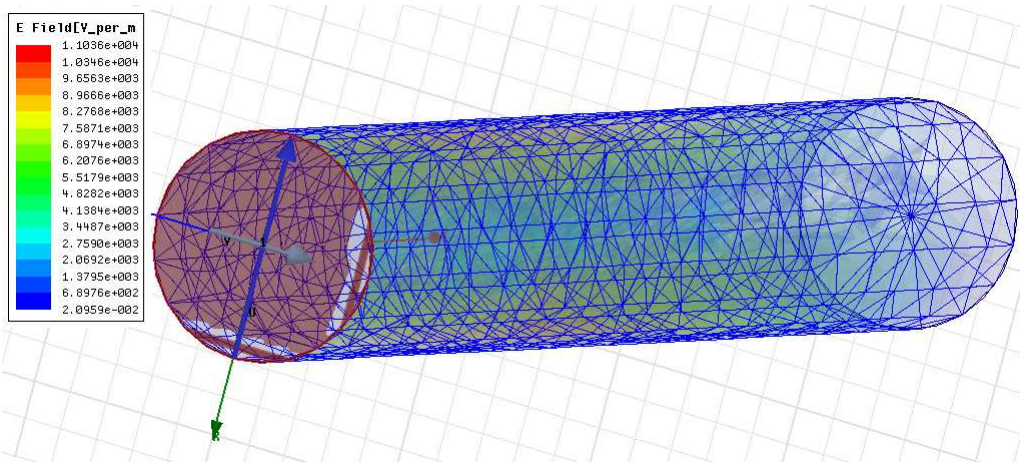

Figure 3.4. The mesh structure of a circular waveguide in HFSS.

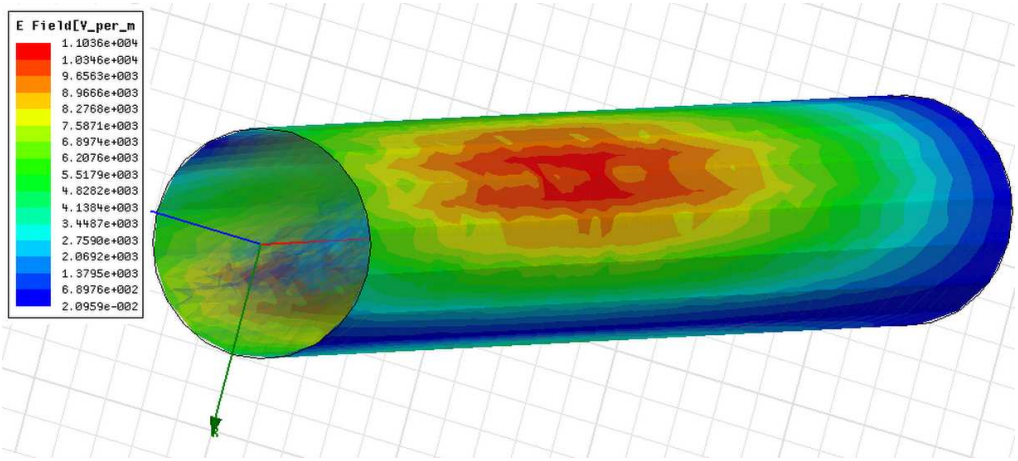

Figure 3.5. Electric field of a TE_{11} mode in a circular waveguide.

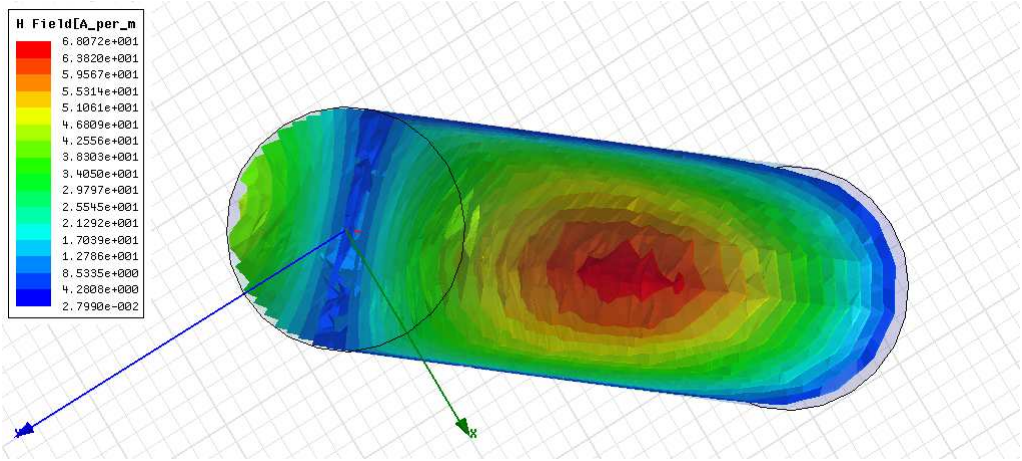

Figure 3.6. Magnetic field of a TE_{11} mode in a circular waveguide.

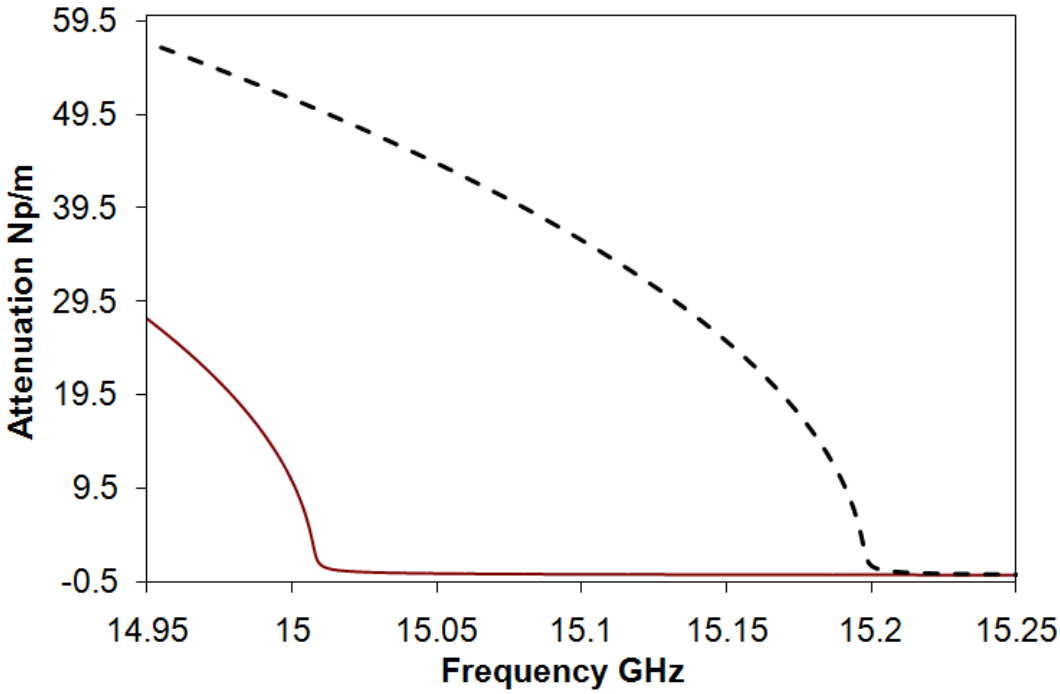

Figure 3.7. Attenuation of TE_{11} wave in a copper circular waveguide with radius a_r = 5.8533 mm. — — — — simulation result. ———— the proposed method.

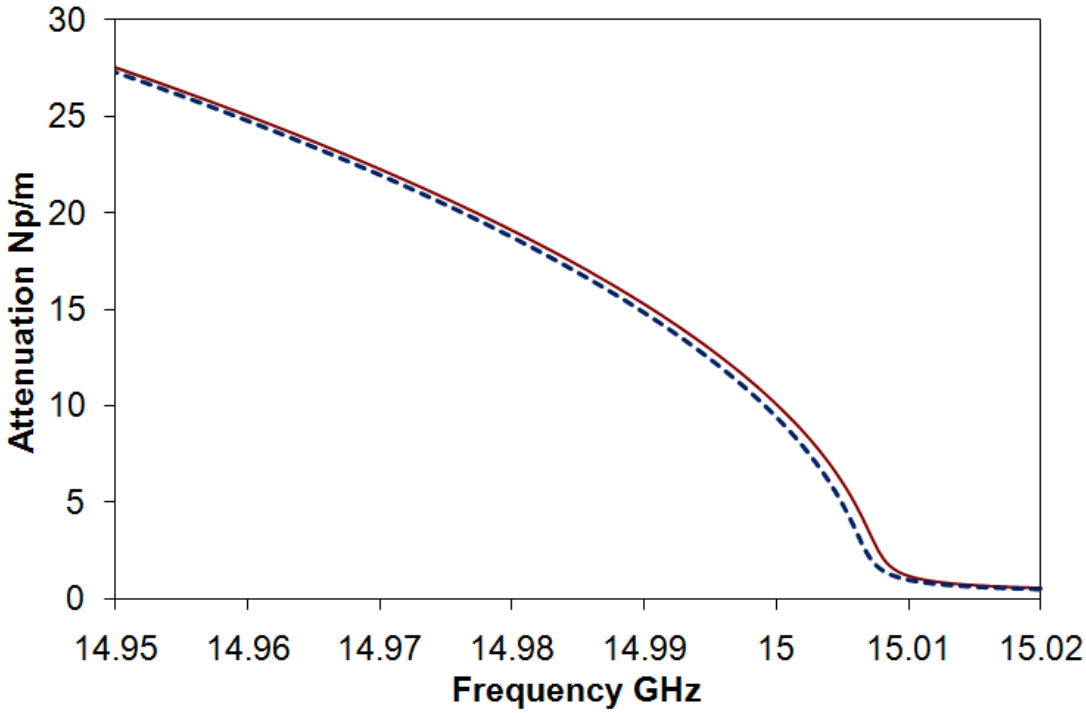

Figure 3.8. Comparison of loss in a copper circular waveguide.

- - - - - - - simulation result (radius a_r = 5.927 mm).

——— the proposed method (radius a_r = 5.8533 mm).

3.6 Experimental Setup

In order to further validate the new formulation, an experiment similar to that used to measure the scattering matrix of a rectangular waveguide was set up. As shown in Figure 3.9, some of the components used in the measurement are circular waveguides, a pair of tapers, chokes, and circular-to-rectangular waveguide transitions. Figure 3.10 depicts the complete setup of the experiment where a 20 cm hollow circular waveguide made of brass with radius a_r = 5.8533 mm is connected to the VNA. The S_{21} parameter of the dominant TE_{11} mode was measured from the VNA.

(a) (b) (c) (d)

Figure 3.9. (a) Hollow circular waveguides made of brass, (b) a taper, (c) a circular choke, and (d) a circular-to-rectangular waveguide transition.

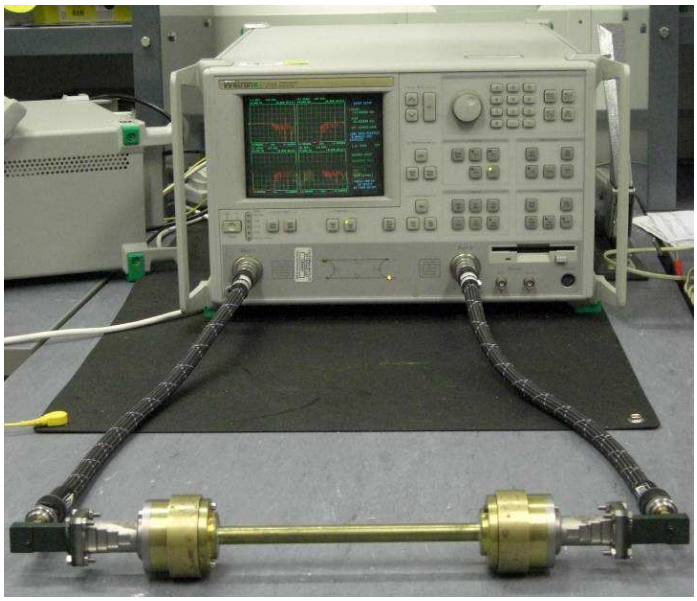

Figure 3.10. A 20 cm hollow circular waveguide connected to the VNA via tapers, chokes, circular-to-rectangular waveguide transitions, and adapters.

3.7 Results and Discussion

A comparison is performed among the attenuation computed by the proposed method, Stratton's equation, and the measured S_{21} parameter using a hollow circular waveguide made of brass, with radius a_r = 5.8533 mm. The geometrical dimensions and material properties of the circular waveguide are illustrated in Figure 3.11. As can be clearly observed from Figure 3.12, at frequencies below cutoff, both Stratton's and the new method tally very closely with the experimental result.

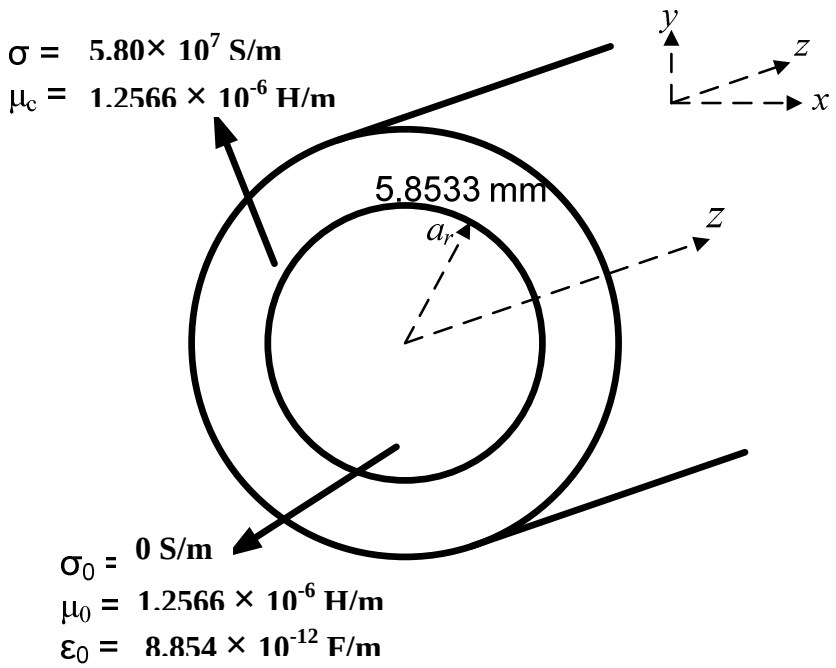

Figure 3.11. Cross section of a hollow circular waveguide with radius a_r = 5.8533 mm.

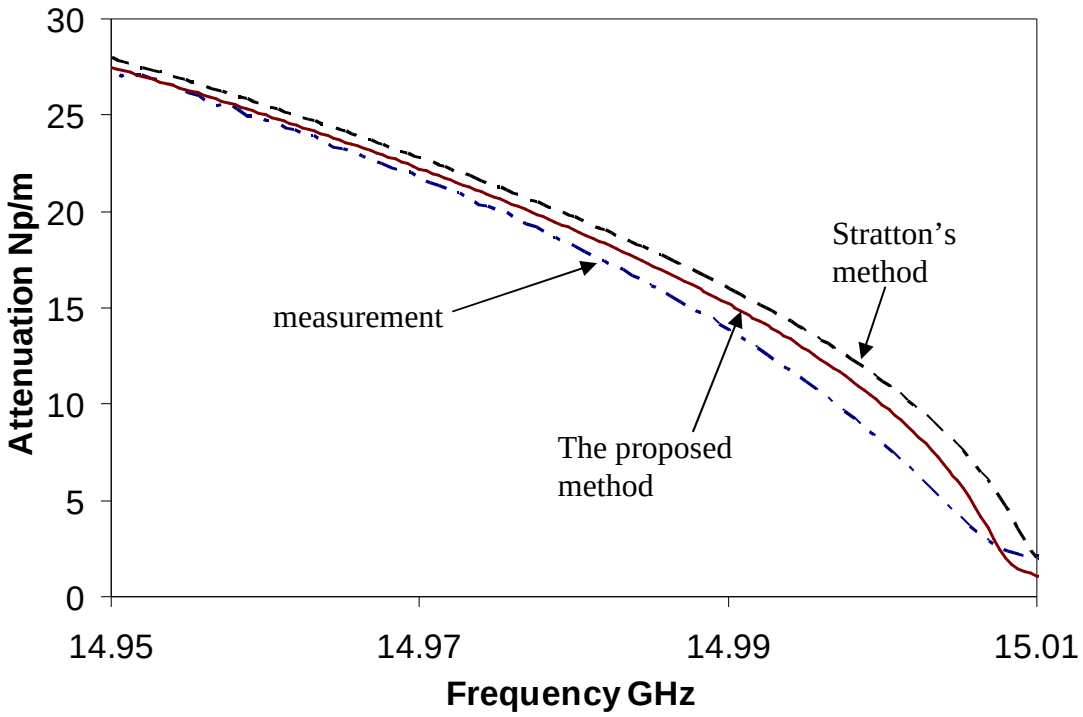

Figure 3.12. Loss of TE_{11} mode in a hollow circular waveguide with radius a_r = 5.8533 mm, near cutoff. measurement. Stratton's method. the proposed method.

To show that the characteristic equation is applicable to circular waveguides with different radius and material properties, the attenuation constants for the propagation of TE_{11} and TM_{11} modes in a copper circular waveguide with radius a_r = 8.1 mm are computed. The range of frequencies f is extended to the millimeter wave regime at f = 120 GHz. As shown in Figures 3.13 and 3.14, respectively, the losses predicted by the proposed method are in high exactness with Stratton's method, thus, verifying the validity of the new method.

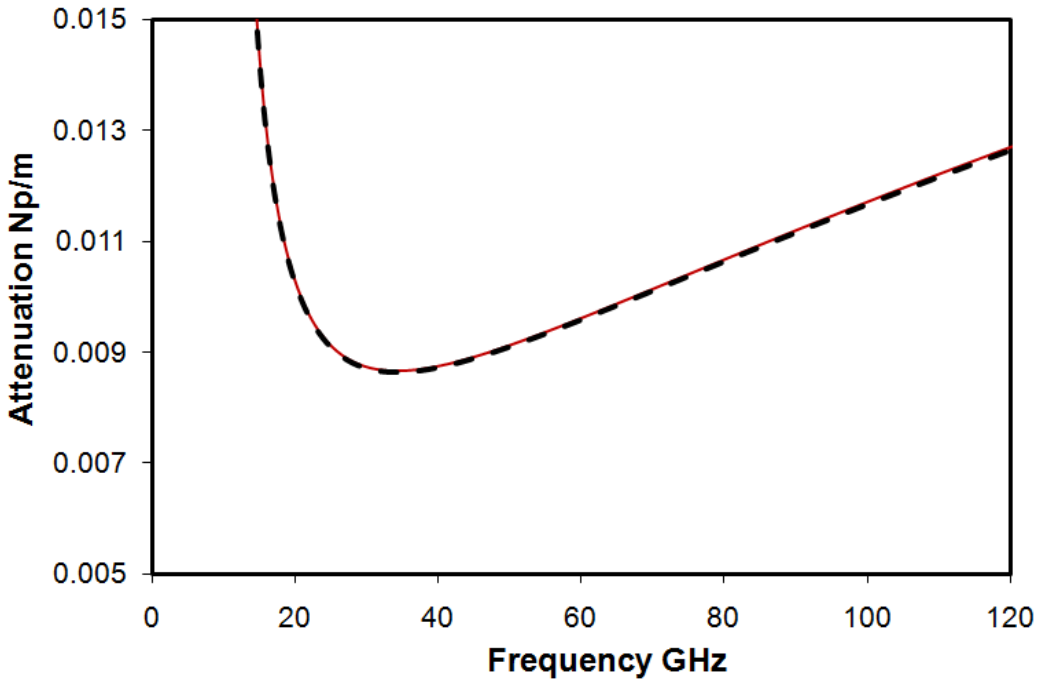

Figure 3.13. Loss of TE_{11} mode in a hollow circular waveguide with a_r = 8.1 mm, at millimeter wave frequencies. — — — — Stratton's method. ——— the proposed method.

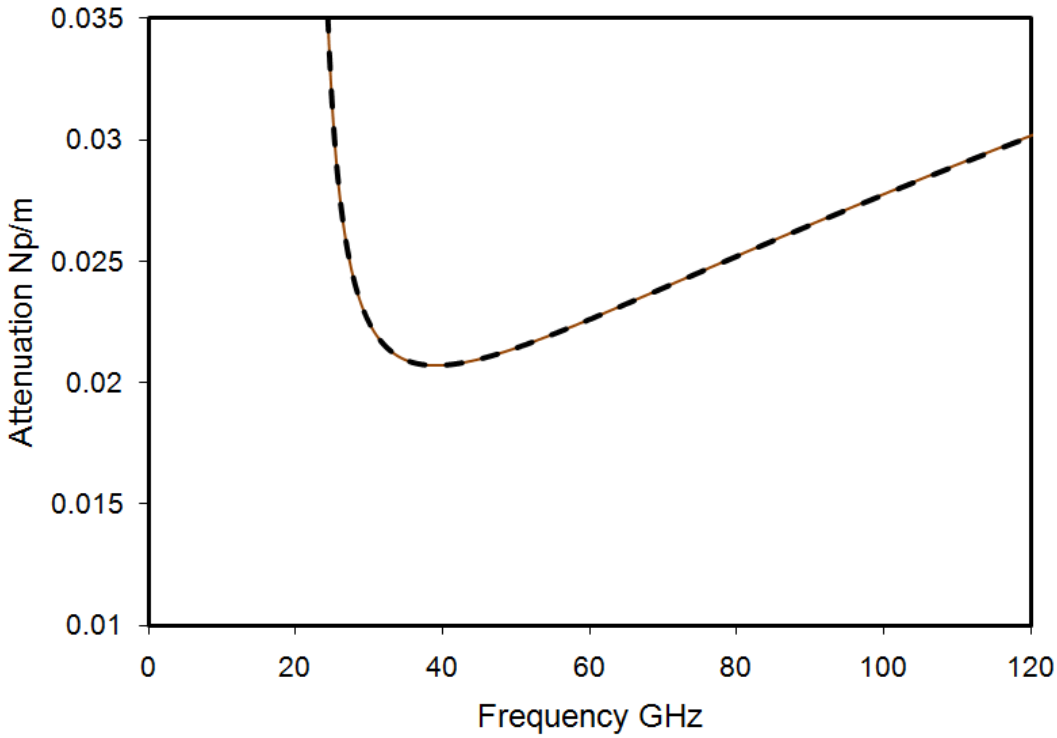

Figure 3.14. Loss of TM_{11} mode in a hollow circular waveguide with a_r = 8.1 mm, at millimeter wave frequencies. — — — — Stratton's method. ——— the proposed method.

3.8 Summary

This chapter demonstrates the versatility of the new boundary-matching method introduced in Chapter 2. Besides rectangular waveguides, the method is shown to be applicable in computing the loss of wave in circular waveguides as well. A set of transcendental equation to solve for the loss in circular waveguides can be formulated by matching the tangential fields with the surface impedance of the wall, expressed in terms of the electrical properties of the wall material.

Comparison shows that the losses predicted by the proposed method are in good agreement with the experimental measurements, as well as Stratton's method. However, unlike Stratton's method which is only restricted to the case of circular waveguides, the new method has the flexibility of being able to be applied to both rectangular and circular waveguides. Having a standard and accurate approach certainly provides much convenience, especially when the propagation constant in waveguides with more than one kind of geometry is required to be computed. As shall be seen in later chapters, with modification made on the proposed method, it can also be applied in calculating the propagation constant of microstrip transmission lines.

CHAPTER 4

SUPERCONDUCTING WAVEGUIDES*

In this chapter, the characteristics of the propagation of waves in superconducting waveguides are investigated. To compute the propagation constant, the complex conductivity of the superconductor is incorporated into the equations, derived in Chapters 2 and 3. An important outcome from this analysis is that superconducting waveguides are shown to behave like a lossless waveguide, exhibiting lossless behaviour at frequencies above cutoff. Above the gap frequency, however, the waveguide loses its superconductivity, giving loss higher than those operating at room temperature.

4.1 Introduction

A waveguide mounted superconductor-insulator-superconductor (SIS) heterodyne receiver is commonly used to detect THz signals in radio astronomy (Kooi *et al.*, 1994; Yassin *et al.*, 1997; Yassin *et al.*, 2000). Due to its high gap frequency f_g of about 700 GHz at 4.2 K, Niobium (Nb) has generally been employed as the superconducting material for the detection of millimeter and submillimeter waves. On the whole, the emission strength of signals in the millimeter and submillimeter bands for astronomical objects is at extremely low orders of magnitude (Phillips and Keene, 1992). Although most waveguides implemented in SIS receivers are made of copper, attenuation

*Parts of this chapter were published in "K. H. Yeap, C. Y. Tham, K. C. Yeong, and H. J. Woo, "Wave Propagation in Lossy and Superconducting Circular Waveguides", *Radioengineeringl*, Vol. 19(2), June 2010, pp. 320 – 325."

level exhibited in standard metallic waveguides such as copper may actually degrade the detection of signals at such weak intensity (Winters and Rose, 1991). Superconducting waveguides which feature low transmission losses and dispersion level below the gap frequency f_g can thus be considered to be implemented in the SIS receiver system.

A perfect conductor exhibits lossless condition, where the tangential electric field E_t and the normal derivative of the tangential magnetic field $\frac{\partial H_t}{\partial a_n}$ at the boundary of the wall are zero. In contrast with a perfect conductor, field penetration occurs at the superconducting walls. In order to account for the field penetration, an alternative boundary condition based on the penetration depth of the Meissner effect has been suggested to study the wave properties of superconducting rectangular (Wang *et al.*, 1994; Yalamanchili *et al.*, 1995; Ma, 1998), circular (Ma, 1995), and parallel-plate (Ma, 1999) waveguides. In the work of these authors, the boundary condition for the longitudinal magnetic field H_z of a TE mode is given by,

$$\frac{\partial H_z}{\partial a_n} - \frac{1}{\lambda_L} H_z = 0, \tag{4.1}$$

where λ_L known as the London penetration depth, is a measure of the distance of magnetic field penetration into the superconductor. An important implication of this theoretical study is that the dominant mode for a rectangular waveguide is found to have switched from TE_{10} to TE_{11}; while that for a circular waveguide has switched from TE_{11} to TE_{01}. The formulation

developed based on (4.1) predicts that the cutoff frequencies f_c for both TE_{10} and TE_{11} of rectangular and circular waveguides, respectively, increase when the temperature T drops below the critical temperature T_c, therefore resulting in the change of dominant modes in superconducting waveguides. Yassin *et al.* (2001) has performed an experimental validation on the above theory using a superconducting circular waveguide. The experimental result, however, shows that the work reported in Wang *et al.* (1994), Yalamanchili *et al.* (1995), Ma (1998), Ma (1995), and Ma (1999) turned out to be invalid. The mode order in a superconducting waveguide remains the same as those found in a perfectly conducting waveguide.

Yassin *et al.* (2003) had performed a theoretical analysis on superconducting circular waveguides based on incorporating the complex conductivity of a superconductor into Stratton's equation (Stratton, 1941). The complex conductivity was found by solving Mattis-Bardeen's equation (Mattis and Bardeen, 1958), derived from BCS theory. Winters and Rose (1991) had performed a study on the attenuation in superconducting rectangular waveguides. As mentioned in Chapters 1, 2, and 3, Stratton's equation fails to be applied in the case of rectangular waveguides. The method proposed by Winter and Rose (1991) was, therefore, based on the approximate power-loss method and the phenomenological two-fluid model. Since the power-loss method assumes lossless field's expression in the waveguide, it fails to account for the penetration depth in a superconductor. Moreover, the two-fluid model does not account for the existence of the gap energy in its formulation and therefore is not able to indicate clearly the transition from

superconducting to normal states. As concluded by Kautz (1978), due to its ability in describing the relationship of quasiparticles and Cooper-pairs with the energy gap, Mattis-Bardeen's equations were found to be more realistic to be applied in the case of superconductors.

In this chapter, a new approach to investigate the propagation of waves in both superconducting circular and rectangular waveguides is presented. In the analysis, the complex conductivity of a superconductor based on Mattis-Bardeen's equation is incorporated into the transcendental equations formulated for rectangular and circular waveguides in Chapters 2 and 3, respectively. The new method introduced in the previous chapters allows the penetration of fields into the wall material; whereas, Mattis-Bardeen's equation takes into account the existence of the energy gap. Hence, the incorporation of the two in this chapter provides a more realistic study of superconductivity effect in waveguides – in particular, rectangular waveguides. In the results and discussion section, a comparison between the loss in superconducting and normal waveguides is made. It is worthwhile noting that the results obtained using the new proposed method actually show that the cutoff frequencies f_c of the dominant modes remain unchanged when T drops below T_c. This agrees with the experimental result of Yassin *et al.* (2001), further confirming the validity of the new method and therefore disproving the theoretical findings in Wang *et al.* (1994), Yalamanchili *et al.* (1995), Ma (1998), Ma (1995), and Ma (1999).

4.2 Properties of Superconductors

Superconductivity denotes a remarkable state transition of a material which is characterized by the disappearance of electrical resistance and the complete expulsion of magnetic flux. The temperature at which the superconducting state transition occurs is known as the critical temperature T_c. A superconductor exhibits zero DC resistivity and diamagnetism at temperatures below T_c. At temperatures above the critical temperature a superconductor behaves as a normal metal.

The understanding of superconductivity was advanced in 1957 by John Bardeen, Leon Cooper, and John Schrieffer, through their microscopic theory of superconductivity, known as the Bardeen–Cooper–Schrieffer (BCS) theory (Bardeen *et al.*, 1957). To explain the phenomenon of superconductivity in a simple manner, one can imagine a negatively charged electron passing by positively charged ions in the lattice of the superconductor. Due to the attraction of the charges, the positively charged atoms distort toward the electron. This in turn causes phonons or packets of sound waves to be emitted which forms a trough of positive charges around the electrons. As depicted in Figure 4.1, before the electron passes by and before the lattice springs back to its normal position, a second electron is drawn into the trough. The forces exerted by the phonons overcome the electrons' natural repulsion, allowing the electrons to pair up. The coupled electrons are known as Cooper pairs (Cooper, 1956).

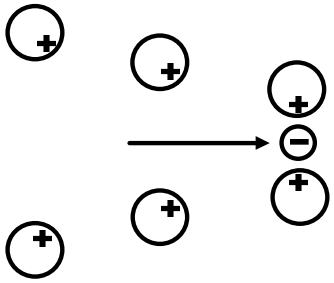

Figure 4.1. A negatively charged electron passes between positively charged atoms in the lattice causes the atoms to be attracted inward.

4.3 The Semiconductor Picture of the Superconductor

The condensation of electrons out of a continuum of allowed energy values into Cooper pairs at a single energy level also gives rise to an energy gap (Δ) at the Fermi surface. This energy gap is orders of magnitude less than the Fermi energy, typically about one millielectron volt, compared to Fermi energies of several electrons volts. The energy gap Δ is the average energy per electron of a Cooper pair, relative to the continuum. The binding energy of a Cooper pair is thus 2Δ, this being the minimum energy required to break the pair. The situation in a superconductor can be thought of as analogous to a semiconductor, with both having an energy gap at the Fermi surface. When a superconductor is at finite temperatures below the critical temperature, T_c, thermal energy and incident radiation can break Cooper pairs. The electrons from the broken pairs are known as excited quasiparticles, which behave as normal electrons with well specified momenta. Since the binding energy between paired electrons is 2Δ, absorption of incident radiation is possible for

field frequencies of $f > \frac{\Delta}{(\pi\hbar)}$, where $\hbar$ is the reduced Planck's constant. Frequency $f_g = \frac{\Delta}{(\pi\hbar)}$ is thus referred to as the gap frequency of a superconductor.

A comparison between the normal electron and quasiparticle density of states is depicted in Figure 4.2 (Wengler, 1992). In the superconductor, the electronic states in the immediate neighbourhood of the Fermi energy E_F have their energy pushed away from E_F. The result is a range of energies from $E_F - \Delta$ to $E_F + \Delta$ in which there are no quasiparticle states. Immediately above and below are more states than in the normal metal. These are the states that would have been in the gap if the superconductor were a normal metal. In the ground-state superconductor shown, there is an empty continuum of states available above the gap which is analogous to the conduction band in an

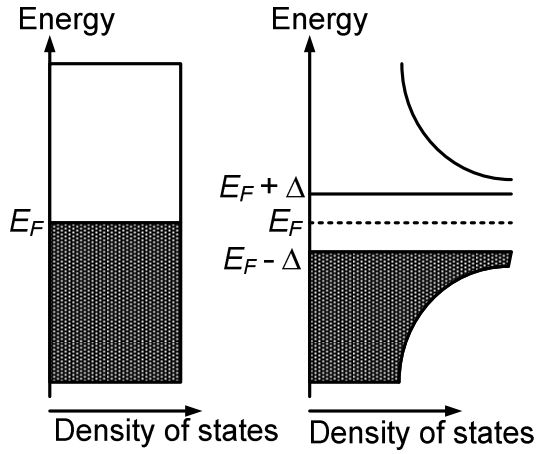

(a) (b)

Figure 4.2. (a) The electronic density of states in a normal metal at 0 K and (b) the quasiparticle density of states in a superconductor cooled to 0 K (Wengler, 1992).

intrinsic semiconductor. Below the gap is a filled valence like band. This density of states description of a superconductor which shows the presence of an energy gap reminiscent to that of an intrinsic semiconductor, and is thus called the semiconductor picture of the superconductor.

4.4 The Complex Conductivity

The equations for the complex conductivity, i.e. $\sigma_1 - j\sigma_2$, of a superconductor have been developed by Mattis and Bardeen from the microscopic analysis of BCS superconductor weak coupling theory, as shown below (Mattis and Bardeen, 1958)

$$\frac{\sigma_1}{\sigma_n} = \frac{2}{\hbar\omega}\int_{\Delta}^{\infty}\left[f(E) - f(E+\hbar\omega)\right]\frac{E^2+\Delta^2+\hbar\omega E}{(E^2-\Delta^2)^{1/2}\left[(E+\hbar\omega)^2-\Delta^2\right]^{1/2}}dE + \frac{1}{\hbar\omega}\int_{\Delta-\hbar\omega}^{-\Delta}\left[1-2f(E+\hbar\omega)\right]\frac{E^2+\Delta^2+\hbar\omega E}{(E^2-\Delta^2)^{1/2}\left[(E+\hbar\omega)^2-\Delta^2\right]^{1/2}}dE, \quad (4.2a)$$

$$\frac{\sigma_2}{\sigma_n} = \frac{1}{\hbar\omega}\int_{\Delta-\hbar\omega,-\Delta}^{\Delta}\left[1-2f(E+\hbar\omega)\right]\frac{E^2+\Delta^2+\hbar\omega E}{(\Delta^2-E^2)^{1/2}\left[(E+\hbar\omega)^2-\Delta^2\right]^{1/2}}dE, \quad (4.2b)$$

where σ_n is the normal conductivity and $\Delta = \Delta(T)$ the energy-gap parameter. The function,

$$f(E) = \frac{1}{1+\exp(E/kT)}, \quad (4.3)$$

gives the Fermi-Dirac statistics and k is the Boltzmann's constant. The first integral in (4.2a) describes the effect of the thermally excited quasiparticles. The second integral denotes the generation of quasiparticles by fields with frequencies f corresponding to energies above the gap energy. Thus, the second integral is zero for $\hbar\omega < 2\Delta$. Since σ_2 indicates the contribution due to the Cooper pairs, the lower integration limit in (4.2b) becomes $-\Delta$ when $\hbar\omega > 2\Delta$. Δ depends on temperature and is obtained from the relation (Kautz, 1978)

$$\ln\left(\tilde{\Delta}\right) = -2\int_0^{\infty}\left(E^2+\tilde{\Delta}^2\right)^{-1/2}\left\{1+\exp\left[\left(\pi/\gamma_E\,\tilde{T}\right)\left(E^2+\tilde{\Delta}^2\right)^{1/2}\right]\right\}^{-1} dE\,. \qquad (4.5)$$

where $\tilde{\Delta} = \dfrac{\Delta(T)}{\Delta(0)}$, $\tilde{T} = \dfrac{T}{T_c}$, and $\gamma_E = 1.781$ is the Euler's constant.

4.5 Characteristic Equations for Superconducting Waveguides

Substituting the complex conductivity of the superconductor in (4.2) into (2.43) for rectangular waveguides and (3.17) for circular waveguides the following characteristic equations can be obtained

For superconducting rectangular waveguides:

$$\left[\frac{j\omega\mu_0 k_y \tan\left(k_y b+\phi_y\right)}{h^2}+\sqrt{\frac{\mu\omega(\omega\varepsilon-\sigma_2+j\sigma_1)}{(\omega\varepsilon-\sigma_2)^2+\sigma_1}}\right]\left[\frac{j\omega\varepsilon_0 k_y \cot\left(k_y b+\phi_y\right)}{h^2}-\sqrt{\frac{\omega\varepsilon-(\sigma_2+j\sigma_1)}{\omega\mu}}\right]=\left[\frac{k_z k_x}{h^2}\right]^2, \qquad (4.6a)$$

$$\left[\frac{j\omega\mu_0 k_x \tan(k_x a+\phi_x)}{h^2}+\sqrt{\frac{\mu\omega(\omega\varepsilon-\sigma_2+j\sigma_1)}{(\omega\varepsilon-\sigma_2)^2+\sigma_1}}\right]\left[\frac{j\omega\varepsilon_0 k_x \cot(k_x a+\phi_x)}{h^2}-\sqrt{\frac{\omega\varepsilon-(\sigma_2+j\sigma_1)}{\omega\mu}}\right]=\left[\frac{k_z k_y}{h^2}\right]^2 \quad , \tag{4.6b}$$

and for superconducting circular waveguides:

$$\left[jh^2\sqrt{\frac{\mu\omega(\omega\varepsilon-\sigma_2+j\sigma_1)}{(\omega\varepsilon-\sigma_2)^2+\sigma_1}}+\omega\mu_0 h\frac{J_n'(ha)}{J_n(ha)}\right]\left[jh^2\sqrt{\frac{\omega\varepsilon-(\sigma_2+j\sigma_1)}{\omega\mu}}+\omega\varepsilon_0 h\frac{J_n'(ha)}{J_n(ha)}\right]=\left[\frac{nk_z}{a}\right]^2 \quad . \tag{4.7}$$

4.6 Results and Discussion

To investigate the attenuation of the dominant modes for waves propagating in superconducting waveguides, the transcendental equations in (4.6) and (4.7) are numerically solved using a root-searching algorithm from NAG. The attenuation constant of a Nb rectangular waveguide with dimensions 2.29 × 1.02 cm^2 and Nb circular waveguide with radius a = 8.1 mm, below and above the critical temperature T_c of 9.2 K is computed and plotted in Figure 4.3 and Figure 4.4, respectively. As can be clearly seen, at frequencies f below the gap frequency f_g, the superconducting waveguides operating at T = 4.2 K behave exactly like a perfectly conducting waveguide. The attenuation diverges to infinity at cutoff frequency f_c. Above cutoff, the superconducting waveguides exhibit lossless attenuation. To explain this phenomenon, the complex conductivity of the superconducting Nb at 4.2 K

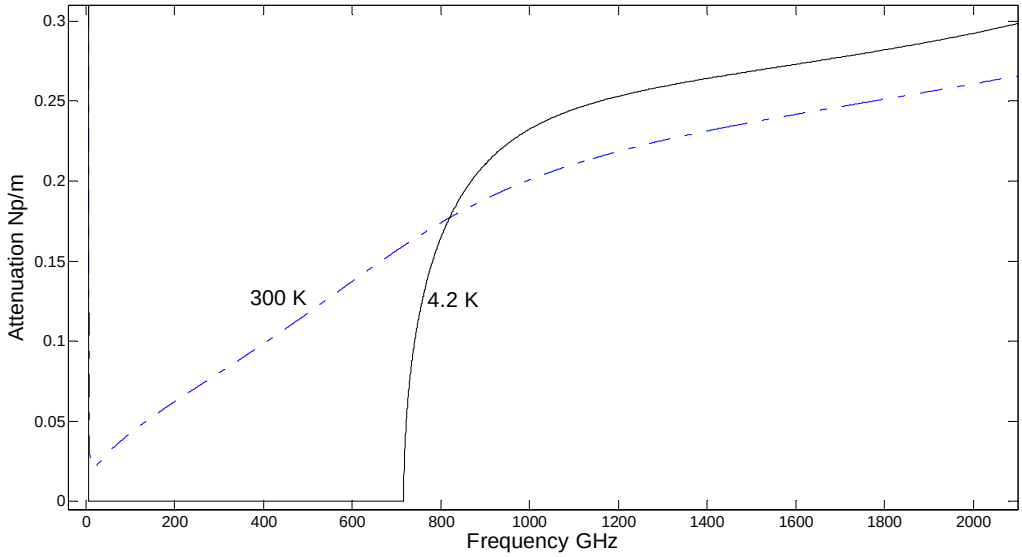

Figure 4.3. Attenuation for TE_{10} mode in a Nb rectangular waveguide at T = 4.2 K and room temperature (300 K).

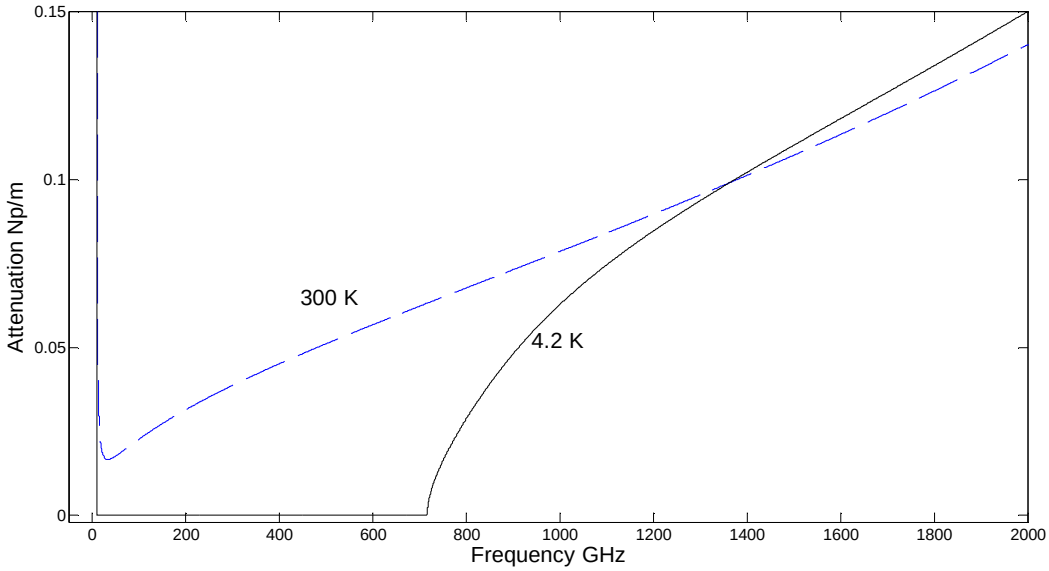

Figure 4.4. Attenuation for TE_{11} mode in a Nb circular waveguide at T = 4.2 K and room temperature (300 K).

has been computed using Mattis-Bardeen equation in (4.2). As can be observed in Figure 4.5, σ_1 which indicates the effect of the quasiparticles, is negligible at frequencies below f_g, explaining the lossless result below f_g in Figures 4.3 and 4.4. Above f_g of approximately 716.45 GHz, σ_2 decreases gradually toward zero, while σ_1 approaches the value of σ_n, implying that Cooper-pair breaking takes place above f_g. With the increase of quasiparticles, the random collision of quasiparticles with the lattice structure can thus be expected to become more frequent, resulting in higher conduction loss at frequencies above f_g.

The attenuation for the superconducting waveguides above f_g eventually surpass the attenuation of the waveguide operating at room temperature. Conduction loss in a waveguide is directly proportional to the surface resistance R_s and the square of the current induced by the magnetic

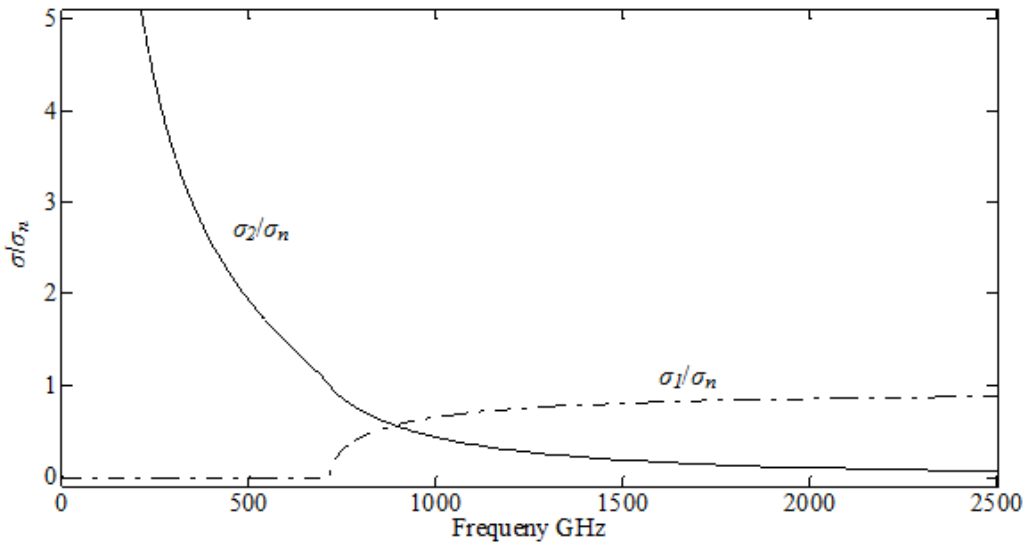

Figure 4.5. The normalized complex conductivity of niobium at 4.2 K, computed using Mattis and Bardeen equation.

field penetration in the wall. Hence, to understand such phenomenon, the skin depth and surface resistance of the superconducting Nb are plotted as a function of frequency. The skin depth δ of the field is given as (Duzer and Turner, 1981)

$$\delta = \sqrt{\frac{2}{\omega \mu_{nb} \sigma_{nb}}}. \tag{4.8}$$

where μ_{nb} and σ_{nb} are permeability and complex conductivity of Nb, respectively.

Figures 4.6 and 4.7 show the skin depth δ of Nb at different range of frequency. For frequencies below the gap frequency f_g, the skin depth of the superconducting Nb is of the order of 10^{-8} m, which is much smaller than that in the normal state. As the frequency increases above the gap frequency f_g, δ

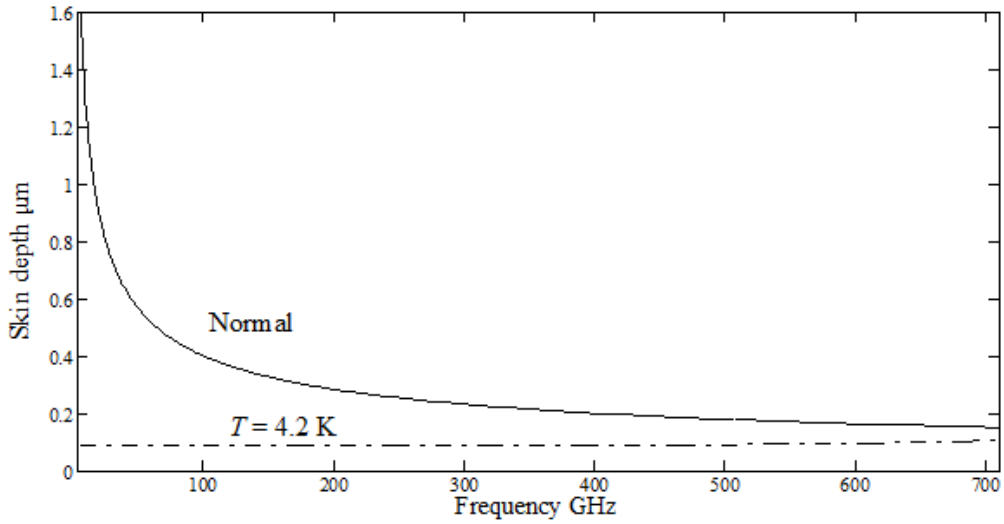

Figure 4.6. Comparison between the skin depth of Nb in superconducting and normal state, with f below f_g.

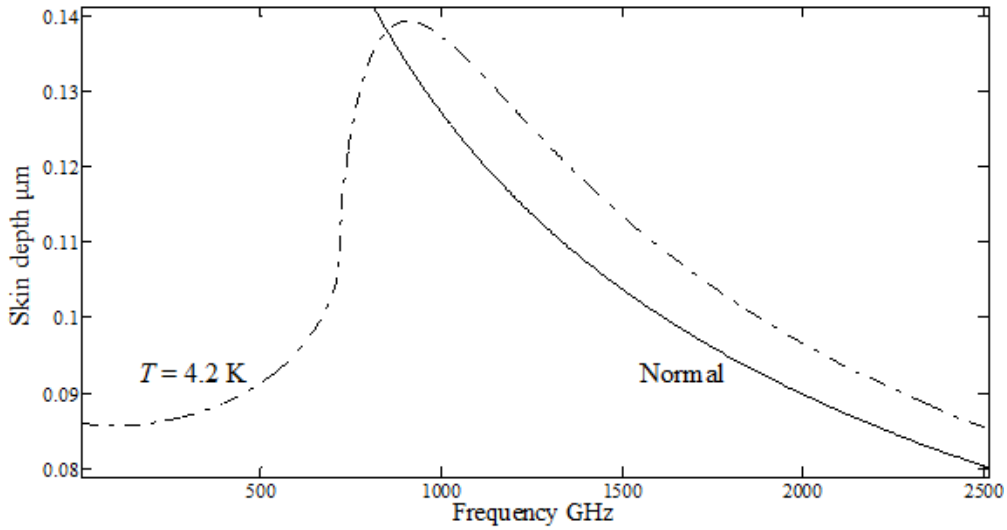

Figure 4.7. Comparison between the skin depth of Nb in superconducting and normal state, from 0 to 2500 GHz.

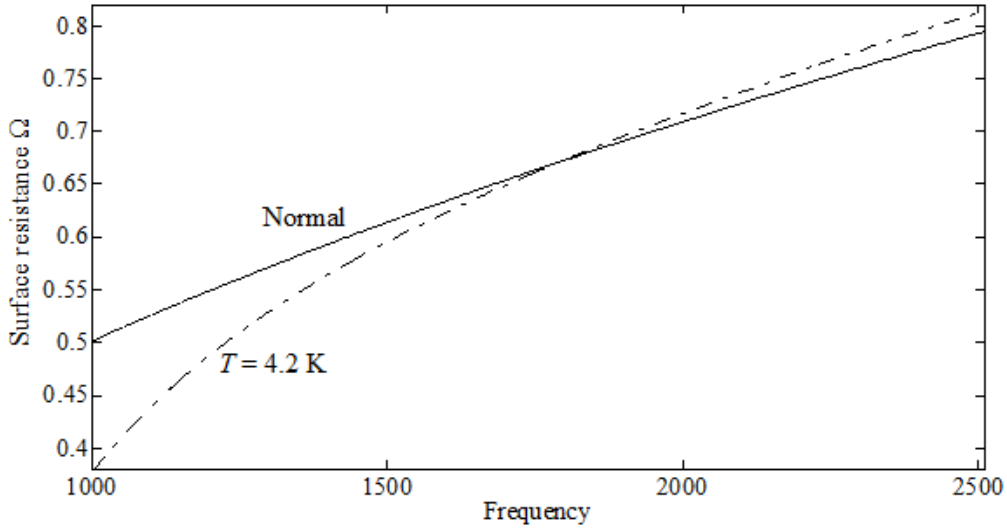

Figure 4.8. The surface resistance of Nb in both normal and superconducting state.

for the superconducting Nb turns out to be much higher than the normal state, as can be observed from Figure 4.7.

The surface resistance R_s of the waveguide can be computed by substituting the values of the complex conductivity into the real part of Z_s in (2.38). As shown in Figure 4.8, R_s for the superconducting Nb at 4.2 K increases at a higher rate than that at room temperature. As the frequency increases above approximately 1.75 THz, R_s at 4.2 K eventually surpasses that at room temperature. Duzer and Turner (1981) have derived the surface resistance of a superconductor using the macroscopic two-fluid model (Duzer and Turner, 1981; London, 1961), as given in (4.9) below

$$R_s = \frac{\omega^2 \mu^2 \lambda_L{}^3 n_n \sigma_n}{2}, \tag{4.9}$$

where n_n is the number density of the quasiparticles. As compared to the value of R_s for normal conductors which could be simplified from (2.38) and (2.39) as $\sqrt{\frac{\omega\mu_{nb}}{2\sigma_{nb}}}$, it can be observed that the surface resistance R_s for superconductors increase as the square of the frequency, while R_s for normal conductors only increases proportional to the square root. It is apparent that both the Mattis-Bardeen's equation and the two-fluid model show that R_s in the superconducting state increases faster and will eventually exceed that in the normal state when the frequency increases to a certain extent. The higher loss for superconducting waveguide observed in Figures 4.3 and 4.4 can thus be attributed to the higher surface resistance and greater penetration depth for

frequencies above the gap frequency. It is interesting to see from Yassin *et al.* (2003), however, that the attenuation computed using Stratton's equation for superconducting circular waveguides was below that at room temperature, implying that Stratton's approach underestimates the loss of superconducting waveguides at THz frequencies.

4.7 Summary

A new analysis on wave propagation in superconducting circular and rectangular waveguides is presented. The complex conductivity is calculated using Mattis-Bardeen's equation, developed from BCS theory. The attenuation constants are computed by substituting the values of the complex conductivity into the transcendental equations formulated in Chapters 2 and 3.

The results show that superconducting waveguides behave exactly like lossless waveguides, where the loss diverges to infinity at $f = f_c$ and the waveguides become lossless at f above f_c but below the gap frequency f_g. An important implication of this study is that, the loss above the gap frequency f_g is observed to be higher than that in normal conducting waveguides. Such phenomenon can be attributed to the higher surface resistance and field penetration in the superconductor at frequencies above f_g.

CHAPTER 5

MICROSTRIP TRANSMISSION LINES*

In this chapter, a full-wave analysis on normal and superconducting microstrip transmission lines is presented. A set of transcendental equation is derived based on a similar boundary matching approach implemented in previous chapters. Unlike quasi-static methods which assume the propagation of TEM mode, the new method considers hybrid mode propagation, therefore giving higher accuracy when computing the loss of waves at wavelengths comparable with the dimensional cross section of the strip – for eg. at THz frequencies.

5.1 Introduction

Microstrip lines constitute the basic building blocks of microwave integrated circuits (MIC). Microstrip sections are commonly used in passive and active hybrid and monolithic integrated circuits. Examples of passive circuits include filters (Hsu *et al.*, 2005; Ahn *et al.*, 2001; Hong and Lancaster, 1997), directional couplers (Brenner, 1967a; Brenner, 1967b; Caloz and Itoh, 2004), capacitors (Alley, 1970), and inductors (Sadhir *et al.*, 1994); whereas, active circuits include amplifiers, oscillators (Pozar, 2005; Gupta *et al.*, 1996), and mixers (Endo *et al.*, 2009; Serizawa *et al.*, 2008). Another important application of microstrip lines is in superconducting MICs. Superconducting

*Parts of this chapter were published in " K. H. Yeap, C. Y. Tham, K. C. Yeong, and E. H. Lim, "Full Wave Analysis of Normal and Superconducting Microstrip Transmission Lines", *Frequenz*, Vol. 64, April 2010, pp. 56 – 66."

microstrip lines feature almost lossless transmission and dispersion level. Signals at millimeter and submillimeter wavelengths quite often are from distant sources, resulting in the signals at extremely low orders of magnitude. Thus, to detect such weak signals, superconducting microstrip lines are commonly integrated with Nb superconductor-insulator-superconductor SIS tunnel junctions to build heterodyne receivers with near quantum-limited noise performance (Carter *et al.*, 2004; Yassin and Withington, 1996a; Withington and Yassin, 1997; Withington *et al.*, 1999).

The behaviour of normal and superconducting microstrip transmission lines have been investigated by a number of authors. Due to its simplicity and analytical solution, quasi-static approaches have been widely used in analyzing the propagation constant of waves in microstrip structures. Quasi-static approaches such as the method of conformal transformations (Wheeler, 1964; Wheeler, 1965; Wheeler, 1977; Yassin and Withington, 1995; Yassin and Withington, 1996a; Withington and Yassin, 1996; Hammerstad and Jansen, 1980; Schneider, 1969; Assadourian and Rimai, 1952), variational method (Yamashita and Mittra, 1968; Yamashita, 1968), the relaxation method (Green, 1965; Stinehelfer, 1968; Schneider, 1965), and the transmission line model (Yassin and Withington, 1995; Yassin and Withington, 1996a; Withington and Yassin, 1996; Matick, 1969; Kautz, 1978), assume pure TEM mode of propagation. As experimentally validated by Grunberger *et al.* (1970) and Grunberger and Meinke (1971), the assumption of TEM mode for the propagation of the dominant mode is adequate only at low frequencies *f* where the strip width and substrate thickness is much lower

than the wavelength in the dielectric material. At higher frequencies, however, deviation from the ideal conception of TEM wave is observed. In reality, the nature of wave propagation is a hybrid mode, where both longitudinal electric E_z and magnetic H_z fields exist, respectively. Thus, hybrid mode considers the superposition of both TE and TM modes. As the frequency increases, the fields tend to concentrate in the dielectric substrate, resulting in dispersive effect in the phase velocity.

A more exact but complex approach is the full-wave analysis (Gupta *et al.*, 1996). Full-wave analysis allows the co-existence of longitudinal fields, thus accounting for the dispersive nature of the microstrip lines. Investigations on microstrip lines based on full-wave analysis have been reported in Mittra and Itoh (1971), Itoh and Mittra (1973), Itoh and Mittra (1974), Syahkal and Davies (1979), Kowalski and Pregla (1971), and Zysman and Varon (1969). Although these techniques produce accurate hybrid mode results, they feature certain limitations due to the assumptions made during formulation. For example, the spectral domain approach (SDA) introduced in Mittra and Itoh (1971), Itoh and Mittra (1973), and Itoh and Mittra (1974) assumes that the strip thickness to be infinitesimal, and is, thus, accurate only in cases where the strip thickness t_s, is much smaller than the dielectric height b, i.e. $t_s << b$. Also, the methods introduced by Kowalski and Pregla (1971) and Zysman and Varon (1969) have assumed that the strip to be made of perfect conductor.

In this chapter, a novel full-wave analysis approach which considers the dispersive nature of the microstrip structures is presented. The new

formulation takes into account the finite thickness and width of the strip and also the imperfect conductivity of the strip and groundplane. In the new method, the solution for the propagation constant is found by solving the transcendental equation derived from matching the tangential fields at both regions of the dielectric-air interface and the tangential fields with the surface impedance at the dielectric-conductor interface. The new method can be implemented in superconducting microstrip structures as well, by applying the complex conductivity of a BCS weak coupling superconductor (Mattis and Bardeen, 1958) into the equation. Since single mode operation on microstrip lines is of the most practical importance, detail analysis of the fundamental HE_0 mode will be shown in the subsequent sections. It is to be noted, however, that this technique is not only restricted to the lowest order mode and can actually be applied to all modes in the microstrip lines. The attenuation constants for normal and superconducting microstrip transmission lines are computed and compared with those obtained from the quasi-static methods. Hence, for convenience purpose, some of the available quasi-static methods shall be discussed briefly, prior to discussion on the new method of full-wave analysis. In the subsequent sections, the new method will also be demonstrated to give more realistic values especially for superconducting microstrip lines operating in the millimeter and submillimeter regimes, where the wavelengths are comparable with the dimensions of the microstrip structures.

5.2 Methods to Compute Microstrip Loss

Four separate mechanisms can be identified for power losses and parasitic effects associated with microstrip lines (Edwards, 1981)

(i) Conductor losses

(ii) Dielectric losses

(iii) Radiation losses

(iv) Losses due to surface-wave propagation

The first two losses are dissipative effects, while the last two are essentially parasitic phenomena. Hence, losses due to radiation and surface-wave propagation can actually be suppressed so long as the microstrip structure is carefully and properly designed. In most conventional microstrip circuit designs with a high substrate dielectric constant, conductor losses in the strip and groundplane dominate over the other three losses. In the following sections, a brief review on the conventional quasi-static methods used to calculate loss in microstrip lines shall be presented. Since conductor loss is significantly higher, when calculating the loss using the quasi-static methods, the total loss in the microstrip is assumed to constitute of only conductor loss.

5.2.1 Formulations based on the Incremental Inductance Rule

To formulate the attenuation constant α, Pucel *et al.* (1968a) and Pucel *et al.* (1968b) have used a technique based on the "incremental inductance

rule" (Wheeler, 1942). This rule expresses the series surface resistance R_s per unit length in terms of that part of the total inductance per unit length which is attributable to the skin effect, i.e. the inductance L_i produced by the magnetic field within the conductors. Solving for the external inductance using Wheeler's quasi-static approach (Wheeler, 1964; Wheeler, 1965; Wheeler, 1977), the total resistance per unit length can thus be found. The attenuation constant of an air-filled microstrip line can be obtained by substituting the total resistance into the power-loss method (Seida, 2003; Collin, 1991; Cheng, 1989). Here, only the final relations for the attenuation constant is presented (Pucel *et al.*, 1968b)

For $\frac{w}{b} \leq 1/(2\pi)$:

$$\frac{\alpha Z_0 b}{R_S} = \frac{8.68}{2\pi}\left[1-\left(\frac{w'}{4b}\right)^2\right]\left[1+\frac{b}{w'}+\frac{b}{\pi w'}\left(\ln\frac{4\pi w}{t_s}+\frac{t_s}{w}\right)\right] . \qquad (5.1a)$$

For $1/(2\pi) < \frac{w}{b} \leq 2$:

$$\frac{\alpha Z_0 b}{R_S} = \frac{8.68}{2\pi}\left[1-\left(\frac{w'}{4b}\right)^2\right]\left[1+\frac{b}{w'}+\frac{b}{\pi w'}\left(\ln\frac{2b}{t_s}-\frac{t_s}{b}\right)\right] . \qquad (5.1b)$$

For $2 \leq \frac{w}{b}$:

$$\frac{\alpha Z_0 b}{R_S} = \frac{8.68}{\left\{\frac{w'}{b} + \frac{2}{\pi}\ln\left[2\pi e\left(\frac{w'}{2b} + 0.94\right)\right]\right\}^2}\left[\frac{w'}{b} + \frac{w'/(\pi b)}{\left(\frac{w'}{2b} + 0.94\right)}\right] \times \left[1 + \frac{b}{w'} + \frac{b}{\pi w'}\left(\ln\frac{2b}{t_s} - \frac{t_s}{h}\right)\right] . \quad (5.1c)$$

where Z_0 is the characteristic impedance of an air-filled parallel-plate transmission line, $w' = w + \Delta w$, and Δw is known as the edge correction factor (Wheeler, 1977). The quantity Δw can be found by comparison of the conformal mapping result of a microstrip line with strip thickness $t_s \neq 0$ and $t_s = 0$. Hammerstad and Jensen (1980) have improved the formulation for Δw developed by Wheeler (1977). Hence, the more accurate formulation in Hammerstad and Jansen (1980) has been applied here.

According to Wheeler (1964), a homogeneous medium can be introduced to replace the air and dielectric substrate of the dielectric-filled microstrip line. The dielectric constant of the medium is represented as ε_{eff} and is known as the "effective dielectric constant". Hence, in order to calculate the attenuation of an actual microstrip line with substrate carrier, the attenuation constants of the air-filled line in (5.1) is to be multiplied with $\sqrt{\varepsilon_{eff}}$. A number of authors have developed different equations to describe the value of ε_{eff}, for eg. Wheeler (1964), Wheeler (1965), Wheeler (1977), Hammerstad and Jansen (1980), and Schneider (1969). Since Hammerstad and Jansen

(1980) claimed that the accuracy of their formulation to be better than 0.01 % for $\frac{w}{b} \leq 1$ and 0.03 % for $\frac{w}{b} \geq 1000$ compare to the others which claimed to have a higher relative error, their formulation for the effective dielectric constant ε_{eff} has been substituted into (5.1) to calculate for the loss of a practical dielectric-filled microstrip line.

Schneider *et al.* (1969) has derived the characteristic impedance of a single-dielectric filled microstrip structure using the elliptic function-based exact solution. Applying a similar method as Pucel *et al.* (1968a), i.e. using Wheeler's incremental inductance rule and substituting the equations of the characteristic impedance into their equation, Schneider *et al.* (1969) obtained a simpler expression for the attenuation constant

For $\frac{w}{b} \leq 1$:

$$\alpha = \frac{10R_S}{\pi \ln 10} \frac{\left(\frac{8b}{w} - \frac{w}{4b}\right)\left(1 + \frac{b}{w} + \frac{b}{w}\frac{\partial w}{\partial t_s}\right)}{bZ_0(\varepsilon_r = 1)\exp\left(\frac{Z_0(\varepsilon_r = 1)}{60}\right)}, \qquad (5.2a)$$

For $\frac{w}{b} \geq 1$:

$$\alpha = \frac{R_S Z_0(\varepsilon_r = 1)}{720\pi^2 b \ln 10}\left[1 + \frac{0.44b^2}{w^2} + \frac{6b^2}{w^2}\left(1 - \frac{b}{w}\right)^5\right]\left(1 + \frac{w}{b} + \frac{\partial w}{\partial t_s}\right). \qquad (5.2b)$$

The formula published by Hammerstad and Bekkadal (1975) is identical with (5.2) although it is modified in writing. According to the theoretical derivation shown in Hammerstad and Bekkadal (1975), the term $\exp\left(\frac{Z_0}{60}\right)$ in (5.2) can be expressed by $\frac{8b}{w}+\frac{w}{4b}$. The relation after Hammerstad and Bekkadal (1975) reads

For $\frac{w}{b} \le 1$:

$$\alpha = \frac{10R_S}{\pi b Z_0(\varepsilon_r = 1)\ln 10}\frac{32-(w/b)^2}{32+(w/b)^2}\left[1+\frac{b}{w}\left(1+\frac{\partial w}{\partial t_s}\right)\right], \qquad (5.\ 3a)$$

For $\frac{w}{b} \ge 1$:

$$\alpha = \frac{20R_S Z_0 \varepsilon_0(\varepsilon_r = 1)}{\mu_0 \ln 10}\left\{\frac{w}{b}+\frac{6b}{w}\left[\left(1-\frac{b}{w}\right)^5+0.08\right]\right\}\left[1+\frac{b}{w}\left(1+\frac{\partial w}{\partial t_s}\right)\right] \quad . \qquad (5.3b)$$

It is to be noted that the formulations developed by Pucel *et al.* (1968b), Schneider *et al.* (1969), and Hammerstad and Bekkadal (1975) are all based on the incremental inductance rule (Wheeler, 1942). Since the external inductance applied in this rule is derived using a quasi-static conformal mapping approach, the accuracy of equations (5.1) to (5.3) is therefore

restricted to the range of frequencies where the propagation of wave resembles closely to that of TEM wave.

5.2.2 Formulations based on the Transmission Line Model

Matick (1969) has adopted a simpler and straightforward approach in deriving the propagation constant k_z of a microstrip line. In analyzing a microstrip line, Matick has assumed that the width of the strip w to approach infinity, such that fringing fields at the edges of the strip can be neglected. Solving for the series impedance Z and shunt admittance Y of the microstrip line and substituting them into the approximate propagation constant equation derived from a sinusoidal voltage on a transmission line (Cheng, 1989)

$$k_z = -j\sqrt{ZY} \quad , \tag{5.4}$$

the attenuation constant α and phase constant β can be found respectively as (Matick, 1969; Kautz, 1978)

$$\alpha = -k_0\sqrt{\varepsilon_r}\ \mathrm{Im}\left[1 - j\frac{Z_{ss} + Z_{sg}}{\omega b \mu_0}\right]^{0.5} \quad , \tag{5.5a}$$

$$\beta = k_0\sqrt{\varepsilon_r}\ \mathrm{Re}\left[1 - j\frac{Z_{ss} + Z_{sg}}{\omega b \mu_0}\right]^{0.5} \quad . \tag{5.5b}$$

where Z_{ss} and Z_{sg} are the surface impedance of the strip and groundplane, respectively, and are given as (Kautz, 1978)

$$Z_{ss} = \sqrt{\frac{j\omega\mu_0}{\sigma_s}} \coth\left[\left(\sqrt{j\omega\mu_0\sigma_s}\right)t_s\right], \tag{5.6a}$$

$$Z_{sg} = \sqrt{\frac{j\omega\mu_0}{\sigma_g}} \coth\left[\left(\sqrt{j\omega\mu_0\sigma_g}\right)t_g\right]. \tag{5.6b}$$

Here, σ_s and σ_g are the conductivities and t_s and t_g the thicknesses of the strip and groundplane, respectively.

Clearly, the loss computed in Matick's model is exactly the same as that of a TEM wave propagating in a parallel-plate capacitor with no fringing field. In order to account for the fringing loss and dispersion of a practical microstrip line, Yassin and Withington (1995) has introduced a penetration factor χ into Matick's formulation. According to Yassin and Withington (1995), χ takes into account the increase in the attenuation constant due to the actual distribution of the current not being uniform and the characteristic impedance being lowered by the fringing field. By incorporating χ into Matick's equation and substituting the dielectric constant ε_r of the substrate with the effective dielectric constant ε_{eff}, the attenuation constant α and phase constant β read

$$\alpha = -k_0\sqrt{\varepsilon_{eff}}\ \mathrm{Im}\left[1 - j\frac{\left(Z_{ss} + Z_{sg}\right)\chi}{\omega b\mu_0}\right]^{0.5}, \tag{5.7a}$$

$$\beta = k_0\sqrt{\varepsilon_{eff}}\ \mathrm{Re}\left[1 - j\frac{\left(Z_{ss} + Z_{sg}\right)\chi}{\omega b\mu_0}\right]^{0.5}. \tag{5.7b}$$

According to Yassin and Withington (1995), the penetration factor χ is derived using the conformal mapping technique of Assadourian and Rimai (1952) to compute the power loss in microstrip lines.

It is to be further noted that the introduction of the penetration factor χ and the effective dielectric constant ε_{eff} into the transmission line model are not derived from fundamental principles. They are based on mere empirical assumption. Moreover, χ is obtained from the conformal transformation, valid only when TEM wave is assumed. Hence, Yassin-Withington's equation, though claimed to have accounted for the fringing field's effect, could only be taken as a better approximate method, improved from Matick's.

5.3 The Proposed Method

It can be clearly seen that, in order to derive the attenuation expressions using the quasi-static methods discussed in the previous section, the propagation of wave must be assumed to be in TEM mode. Strictly speaking, however, since fringing loss exists at the edges of the strip, fields penetration occurs in the lossy conductor material, and the wave velocity in the dielectric substrate is different from that in free space, it is not possible to support a pure TEM mode in the structure. In fact, not even pure TE or TM modes can exist in a microstrip structure. A practical microstrip line can only support hybrid mode. This can be seen rather easily by considering a microstrip line being encapsulated in a rectangular waveguide, as shown in Figure 5.1. If the center strip is removed from the waveguide, it reduces to a

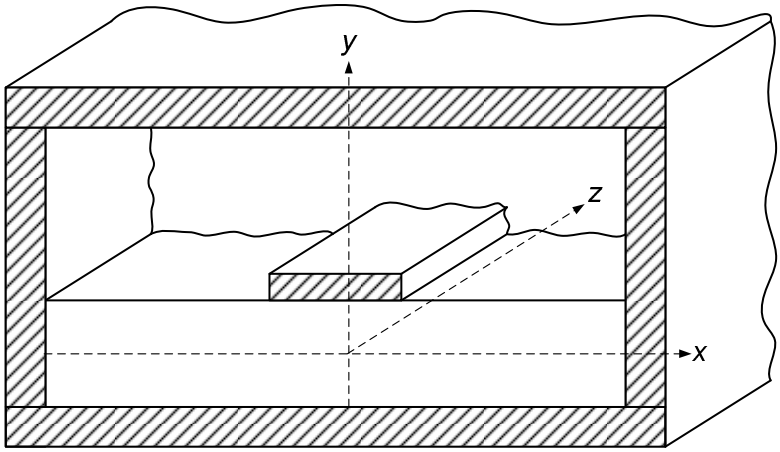

Figure 5.1. Cross section of a microstrip line encapsulated in a shielded case.

partially filled guide that can support longitudinal section electric (LSE) or longitudinal section magnetic (LSM) types of mode (Balanis, 1989), but not a pure TE or TM mode. The insertion of the center strip in the waveguide causes currents to flow in the *x*- and *z*-directions on the strip. The strip thus serves to couple the LSE and LSM modes so that the final mode configuration is hybrid in nature (Itoh and Mittra, 1972).

Hence, in this section, a new full-wave analysis which takes into account the coexistence of hybrid modes in a microstrip line shall be introduced. To analyze a microstrip line using full-wave method, it is a common practice to assume the microstrip line to be encapsulated in a metallic box (Mittra and Itoh, 1971; Itoh and Mittra, 1973; Itoh and Mittra, 1974; Syahkal and Davies, 1979; Kowalski and Pregla, 1971; Zysman and Varon, 1969) such as a rectangular waveguide shown in Figure 5.1. The shielded form of the microstrip transmission line makes the theoretical treatment less difficult since the field region is confined within the metallic box. However,

care must be taken when defining the dimension of the metallic box. The enclosure dimension must be made much larger than the strip width *w* and substrate height *b* so that the presence of walls does not affect the microstrip line characteristics. Besides, it can also be seen that by letting the distance between the walls and the microstrip line approaches infinity, the structure reduces back to an open microstrip.

The new method is inspired from the approach introduced by Kowalski and Pregla (1971) and Zysman and Varon (1969), whereby a solution to solve for the phase constant is obtained by matching the fields at the air-substrate interface. However, unlike Kowalski and Pregla (1971) and Zysman and Varon (1969) which assume the strip to be made of perfect conductor, the formulation developed by Kerr (1999) which describes the surface impedance of a conductor with finite thickness is incorporated into the new method. Taking a similar approach as that used in Chapters 2 and 3, i.e. matching the fields and the surface impedance at the boundary of two different media, a set of characteristic equation can be found, solving which gives the propagation constant of a lossy microstrip line. It is worthwhile noting that, instead of fully encapsulated in a metallic box as assumed by others (Mittra and Itoh, 1971; Itoh and Mittra, 1973; Itoh and Mittra, 1974; Syahkal and Davies, 1979; Kowalski and Pregla, 1971; Zysman and Varon, 1969), the microstrip line analyzed using the new method is only assumed to be partially enclosed at both sides. This reduces the number of boundary conditions to be satisfied and therefore, simplifying the process of derivation.

5.3.1 Fields in the Dielectric Substrate

The microstrip configuration analyzed using the new method is partially enclosed as indicated in Figure 5.2. The structure is assumed to be infinite in length in the x and z directions. The sidewalls at $x = \pm\frac{a}{2}$ are perfectly conducting and the width a approaches infinity so that the walls do not perturb the field lines localized around the strip conductor. The fundamental HE_0 mode is an even mode, which has the property that the electrical field distribution is symmetrical with respect to the y-z plane at $x = 0$. Thus, the mathematical problem can be simplified by treating only one half of the microstrip structure. In this case, only the right half of the structure in Figure 5.2 is considered. The symmetry plane at $x = 0$ represents a magnetic wall or an ideal electrical open. On a magnetic wall, the tangential magnetic field vanishes and the electric field is purely tangential (Kowalski and Pregla, 1971). In other words, at $x = 0$, both the resultant tangential magnetic field H_t and the normal derivative of the tangential electric field $\partial E_t / \partial a_n$ are zero.

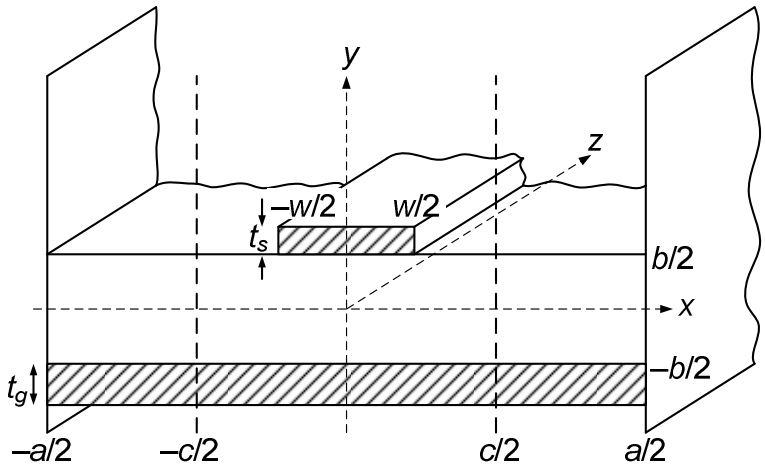

Figure 5.2. Cross section of a microstrip line, with perfectly conducting walls enclosed at both ends.

As illustrated in (2.30) in chapter 2, the boundary condition in a lossless microstrip line, requires that the tangential component of the electric field E_t and normal derivative of the tangential magnetic field $\frac{\partial H_t}{\partial a_n}$ to vanish at the dielectric-conductor interface. Here, a_n is the normal direction to the conductor material. Nevertheless, due to the finite conductivity of the strip and groundplane material, both E_t and $\frac{\partial H_t}{\partial a_n}$ do not decay to zero at the boundary (see equation (2.31)). To account for the different fields at the boundary of the strip and groundplane with different surface impedance, a phase parameter ϕ_y is introduced. Like χ in Yassin-Withington's equation (Yassin and Withington, 1995; Yassin and Withington, 1996; Withington and Yassin, 1996), ϕ_y describes the penetration of fields into the lossy conductor. Hence, for convenience purpose it shall also be referred to as the fields' penetration factor. Applying the boundary conditions at the magnetic wall and dielectric-conductor interface, the longitudinal fields E_z and H_z can be derived by solving Helmholtz homogeneous equation in Cartesian coordinate. It is to be noted that, the introduction of ϕ_y in the solution complies with Maxwell's equations, therefore, abide by the fundamental principles. Using the method of separation of variables (Cheng, 1989), the following set of field equations can be obtained in the dielectric substrate

$$E_{zd} = E_d \cos(k_{xd} x)\sin(k_{yd} y + \phi_y), \tag{5.8}$$

$$H_{zd} = H_d \sin(k_{xd} x)\cos(k_{yd} y + \phi_y), \tag{5.9}$$

where E_d and H_d are the constant amplitudes of the fields; while $k_{xd} = \frac{\pi}{a}$ and k_{yd} are the transverse wavenumbers in the x and y directions, respectively. The subscript d denotes electromagnetic fields in the dielectric substrate. The usual wave factor in the form of $\exp[j(\omega t - k_z z)]$ is omitted, as one deals with the time harmonic excitations.

For a microstrip structure having an equivalent surface impedance at the strip and groundplane, the skin depth and, thus, E_t and $\frac{\partial H_t}{\partial a_n}$ at the dielectric-conductor boundary at $y = \pm\frac{b}{2}$ must be the same. In this case, equating the longitudinal fields at $y = \pm\frac{b}{2}$, the fields' penetration factor ϕ_y is found to be zero. As illustrated in the equivalent circuits shown in Figures 5.3 and 5.4, the sum of E_z and the sum of H_z at $y = \pm\frac{b}{2}$ for the strip and groundplane having surface impedance Z_{ss} and Z_{sg}, respectively, must be the same as that sharing an equal surface impedance of $\frac{\left(Z_{ss} + Z_{sg}\right)}{2}$. Applying voltage and current divider formula for E_z and H_z, the following is obtained

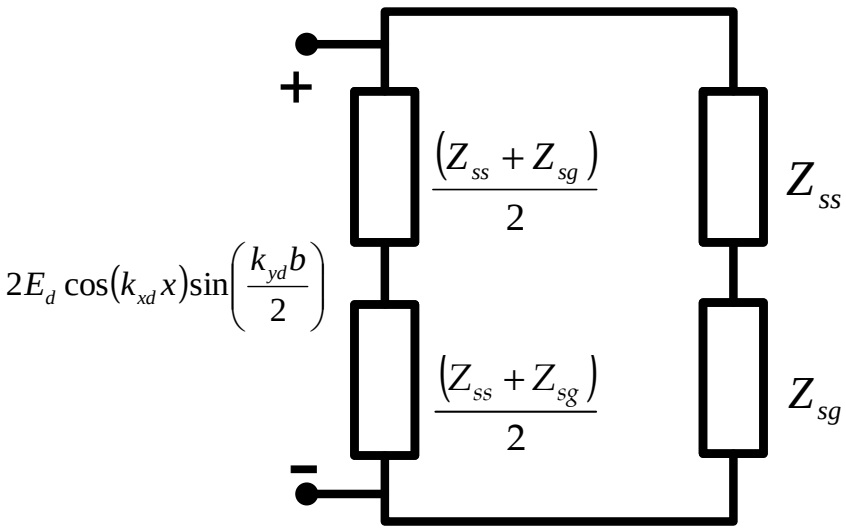

Figure 5.3. Equivalent circuit for the longitudinal electric fields at the substrate-strip and substrate-groundplane boundaries.

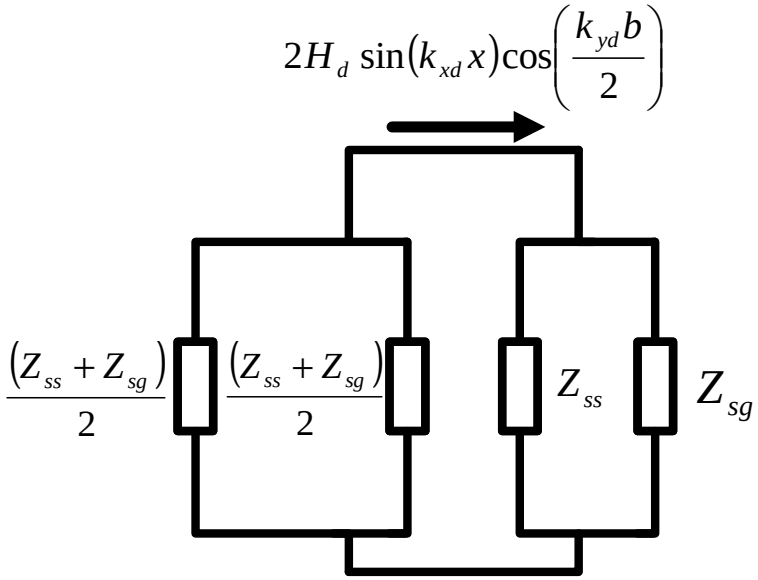

Figure 5.4. Equivalent circuit for the longitudinal magnetic fields at the substrate-strip and substrate-groundplane boundaries.

At $y = \frac{b}{2}$, it follows:

$$\begin{aligned} E_{zd} &= E_d \cos(k_{xd} x)\sin\left(\frac{k_{yd} b}{2} + \phi_y\right) \\ &= \frac{2Z_{ss}}{Z_{ss} + Z_{sg}}\left[E_d \cos(k_{xd} x)\sin\left(\frac{k_{yd} b}{2}\right)\right], \end{aligned} \tag{5.10}$$

$$\begin{aligned} H_{zd} &= H_d \sin(k_{xd} x)\cos\left(\frac{k_{yd} b}{2} + \phi_y\right) \\ &= \frac{2Z_{sg}}{Z_{ss} + Z_{sg}}\left[H_d \sin(k_{xd} x)\cos\left(\frac{k_{yd} b}{2}\right)\right], \end{aligned} \tag{5.11}$$

and at $y = -\frac{b}{2}$, one obtains:

$$\begin{aligned} E_{zd} &= E_d \cos(k_{xd} x)\sin\left(\frac{k_{yd} b}{2} - \phi_y\right) \\ &= \frac{2Z_{sg}}{Z_{ss} + Z_{sg}}\left[E_d \cos(k_{xd} x)\sin\left(\frac{k_{yd} b}{2}\right)\right], \end{aligned} \tag{5.12}$$

$$\begin{aligned} H_{zd} &= H_d \sin(k_{xd} x)\cos\left(\frac{k_{yd} b}{2} - \phi_y\right) \\ &= \frac{2Z_{ss}}{Z_{ss} + Z_{sg}}\left[H_d \sin(k_{xd} x)\cos\left(\frac{k_{yd} b}{2}\right)\right]. \end{aligned} \tag{5.13}$$

The transverse fields' expression can be obtained by substituting the longitudinal fields into Maxwell's source-free curl equations and expressing the transverse field components in terms of E_{zd} and H_{zd} (Cheng, 1989). Hence,

substituting (5.8) and (5.9) into (2.10) and (2.12), the transverse fields H_{xd} and E_{xd} can be expressed as follows

$$H_{xd} = -\frac{j}{h_d^2}\left[k_z k_{xd} H_d - \omega\varepsilon_d k_{yd} E_d\right]\cos(k_{xd}x)\cos(k_{yd}y+\phi_y)\ , \quad (5.14)$$

$$E_{xd} = \frac{j}{h_d^2}\left[k_z k_{xd} E_d + \omega\mu_d k_{yd} H_d\right]\sin(k_{xd}x)\sin(k_{yd}y+\phi_y)\ , \quad (5.15)$$

where μ_d and ε_d are the permeability and permittivity of the dielectric substrate, respectively, and $h_d^2 = k_{xd}^2 + k_{yd}^2$. Since (5.14) and (5.15) are derived from the substitution of longitudinal electric and magnetic fields, thus, unlike quasi-static methods, it accounts for the co-existence of hybrid modes.

5.3.2 Fields in Free Space

As shown in Figure 5.2, the air or the free space region is unbounded in the y direction. Thus, electromagnetic waves must assume to decay exponentially as y approaches infinity. At the x direction, the fields must satisfy the boundary condition of the perfectly conducting walls at $x = \pm\frac{a}{2}$ (Kowalski and Pregla, 1971; Zysman and Varon, 1969). Solving Helmholtz homogeneous equation and applying the boundary condition, the longitudinal fields can, thus, be expanded to

$$E_{za} = E_a \cos(k_{xa}x)\exp(-jk_{ya}y)\ , \quad (5.16)$$

$$H_{za} = H_a \sin(k_{xa}x)\exp(-jk_{ya}y)\ , \quad (5.17)$$

where E_a and H_a are constant amplitudes of the fields; while $k_{xa} = \frac{\pi}{a}$ and k_{ya} are the transverse wavenumbers in the x and y directions, respectively. The subscript a represents fields in the free space region.

Following the same procedure as that used to derive the transverse fields in the dielectric substrate, the following transverse fields' expressions in the free space region are obtained

$$H_{xa} = -\frac{1}{h_a^{\,2}}\left[jk_z k_{xa} H_a - \omega\varepsilon_a k_{ya} E_a\right]\cos(k_{xa}x)\exp(-k_{ya}y)\ , \qquad (5.18)$$

$$E_{xa} = \frac{1}{h_a^{\,2}}\left[jk_z k_{xa} E_a - \omega\mu_a k_{ya} H_a\right]\sin(k_{xa}x)\exp(-jk_{ya}y)\ , \qquad (5.19)$$

where μ_a and ε_a are the permeability and permittivity of free space, respectively and $h_a^{\,2} = k_{xa}^{\,2} + k_{ya}^{\,2}$.

Since the tangential fields are continuous at the boundary, the constant coefficients E_a and H_a can thus be expressed in terms of E_d and H_d, respectively, by matching E_{za} with E_{zd} using (5.15) and (5.19) and H_{za} with H_{zd} using (5.14) and (5.18), at the boundary $y = \frac{b}{2}$

$$E_a = E_d \exp\left(\frac{jk_{ya}b}{2}\right)\sin\left(\frac{k_{yd}b}{2}\right)\ , \qquad (5.20)$$

$$H_a = H_d \exp\left(\frac{jk_{ya}b}{2}\right)\cos\left(\frac{k_{yd}b}{2}\right)\ . \qquad (5.21)$$

5.3.3 Characteristic Equation for Microstrip Lines

In order to satisfy the boundary condition, E_t and H_t in the dielectric substrate and air region can be matched at the dielectric-air interface. As discussed in Section 2.5.2, E_t and H_t at the boundary of the dielectric-conductor interface can be related to the surface impedance Z_s of the conductor via the equation:

$$Z_s = \frac{E_t}{J_{st}}. \tag{5.22}$$

where $J_s = a_n \times H_t$ denotes the surface current density (Cheng, 1989).

From Kerr (1999), Z_{ss} and Z_{sg} can be expressed in terms of the electrical properties as:

$$Z_{ss} = \frac{jk_s}{\sigma_s}\left[\frac{\exp(jk_s t_s) + \dfrac{\sigma_s Z_\eta - jk_s}{\sigma_s Z_\eta + jk_s}\exp(-jk_s t_s)}{\exp(jk_s t_s) - \dfrac{\sigma_s Z_\eta - jk_s}{\sigma_s Z_\eta + jk_s}\exp(-jk_s t_s)}\right], \tag{5.23a}$$

$$Z_{sg} = \frac{jk_g}{\sigma_g}\left[\frac{\exp(jk_g t_g) + \dfrac{\sigma_g Z_\eta - jk_g}{\sigma_g Z_\eta + jk_g}\exp(-jk_g t_g)}{\exp(jk_g t_g) - \dfrac{\sigma_g Z_\eta - jk_g}{\sigma_g Z_\eta + jk_g}\exp(-jk_g t_g)}\right], \tag{5.23b}$$

where $Z_\eta = \sqrt{\frac{\mu_0}{\varepsilon_0}}$ is the intrinsic impedance of free space; while k_s and k_g are the wavenumbers in the strip and groundplane, respectively. It can be seen that when the thickness is large (i.e. t_s or $t_g \rightarrow \infty$), (5.23a) or (5.23b) reduces to the usual surface impedance formula shown in (2.38).

Assuming that an "imaginary window" with width c exists in the microstrip structure, as shown in Figure 5.2, it can be observed from (5.22) that the sum of the fields ratio $\frac{E_t}{J_{st}}$ at the boundary $y = \pm\frac{b}{2}$ can be computed using either of the following two methods:

(i) Integrating the ratio of the tangential fields in the substrate from $x = c/2$ to $-c/2$, i.e. $\int_{-c/2}^{c/2} \frac{E_t}{J_s} dx$, at $y = \pm\frac{b}{2}$. Here, c can be of any value from zero to the width of the perfectly conducting walls at both ends of the microstrip structure (i.e. $0 \leq c \leq a$).

(ii) Adding the integration of the ratio of the tangential fields in the air region, i.e. $\int_{w/2}^{c/2} \frac{E_t}{J_s} dx$ with the total surface impedance of the strip and grounplane from $c/2$ to $-\frac{c}{2}$ at $y = \pm\frac{b}{2}$.

At the boundary $y = \pm\frac{b}{2}$, applying (5.22), the surface impedance can be derived as $Z_s = \mp\frac{E_x}{H_z} = \pm\frac{H_x}{E_z}$. Hence, finding the sum of $\frac{E_t}{J_{st}}$ within the

window with width c using the two methods in (i) and (ii) mentioned above and matching them, the following sets of equations giving the total sum of surface impedance of the microstrip, can be obtained

$$\int_{-c/2}^{c/2} -\frac{E_{xd}\left(y=\frac{b}{2}\right)}{H_{zd}\left(y=\frac{b}{2}\right)}dx + \int_{-c/2}^{c/2} \frac{E_{xd}\left(y=-\frac{b}{2}\right)}{H_{zd}\left(y=-\frac{b}{2}\right)}dx$$
$$= 2\int_{0}^{w/2} Z_{ss}\left(y=\frac{b}{2}\right)dx + 2\int_{w/2}^{c/2} -\frac{E_{xa}\left(y=\frac{b}{2}\right)}{H_{za}\left(y=\frac{b}{2}\right)}dx + 2\int_{0}^{c/2} Z_{sg}\left(y=-\frac{b}{2}\right)dx \quad ,$$

(5.24a)

$$\int_{-c/2}^{c/2} \frac{H_{xd}\left(y=\frac{b}{2}\right)}{E_{zd}\left(y=\frac{b}{2}\right)}dx + \int_{-c/2}^{c/2} -\frac{H_{xd}\left(y=-\frac{b}{2}\right)}{E_{zd}\left(y=-\frac{b}{2}\right)}dx$$
$$= 2\int_{0}^{w/2} \frac{1}{Z_{ss}\left(y=\frac{b}{2}\right)}dx + 2\int_{w/2}^{c/2} \frac{H_{xa}\left(y=\frac{b}{2}\right)}{E_{za}\left(y=\frac{b}{2}\right)}dx + 2\int_{0}^{c/2} \frac{1}{Z_{sg}\left(y=-\frac{b}{2}\right)}dx \quad .$$

(5.24b)

It is worthwhile noting that, since only the right half of the microstrip structure is considered, the right hand side of (5.24) is multiplied by two in order to compute the total sum of fields ratio $\frac{E_t}{J_{st}}$ from $\frac{c}{2}$ to $-\frac{c}{2}$.

Substituting the field equations (5.10) to (5.19) into (5.24) and expressing E_a and H_a in terms of E_d and H_d using (5.20) and (5.21), respectively, the following equations are obtained

$$\left[jk_z k_{xd} \tan\left(\frac{k_{yd}b}{2}\right)\right]\left[\frac{c}{h_d^{\,2}}\left(\frac{Z_{ss}}{Z_{sg}}+\frac{Z_{sg}}{Z_{ss}}\right)+\frac{(w-c)}{h_a^{\,2}}\left(\frac{Z_{ss}}{Z_{sg}}\right)\right]E_d =$$
$$\left[\frac{(w-c)}{h_a^{\,2}}\omega\mu_a k_{ya} - wZ_{ss} - cZ_{sg} - j\frac{c}{h_d^{\,2}}\omega\mu_d k_{yd}\left(\frac{Z_{ss}}{Z_{sg}}+\frac{Z_{sg}}{Z_{ss}}\right)\tan\left(\frac{k_{yd}b}{2}\right)\right]H_d \quad ,$$

(5.25a)

$$\left[\frac{(w-c)}{h_a^{\,2}}\omega\varepsilon_a k_{ya} - \frac{w}{Z_{ss}} - \frac{c}{Z_{sg}} + j\frac{c}{h_d^{\,2}}\omega\varepsilon_d k_{yd}\left(\frac{Z_{sg}}{Z_{ss}}+\frac{Z_{ss}}{Z_{sg}}\right)\cot\left(\frac{k_{yd}b}{2}\right)\right]E_d =$$
$$\left[jk_z k_{xd} \cot\left(\frac{k_{yd}b}{2}\right)\right]\left[\frac{c}{h_d^{\,2}}\left(\frac{Z_{sg}}{Z_{ss}}+\frac{Z_{ss}}{Z_{sg}}\right)+\frac{(w-c)}{h_a^{\,2}}\left(\frac{Z_{sg}}{Z_{ss}}\right)\right]H_d \quad .$$

(5.25b)

In order to obtain nontrivial solutions, the determinant in (5.25a) and (5.25b) must be zero. By letting the determinant of the coefficients E_d and H_d in (5.25) vanish, the following set of transcendental equation is obtained

$$\left[jk_z k_{xd}\right]^2\left[\frac{c\left(\frac{Z_{ss}}{Z_{sg}}+\frac{Z_{sg}}{Z_{ss}}\right)}{h_d^{\,2}}+\frac{(w-c)\left(\frac{Z_{ss}}{Z_{sg}}\right)}{h_a^{\,2}}\right]\left[\frac{c\left(\frac{Z_{ss}}{Z_{sg}}+\frac{Z_{sg}}{Z_{ss}}\right)}{h_d^{\,2}}+\frac{(w-c)\left(\frac{Z_{sg}}{Z_{ss}}\right)}{h_a^{\,2}}\right] =$$
$$\left[wZ_{ss}+cZ_{sg}-\frac{(w-c)\omega\mu_a k_{ya}}{h_a^{\,2}}+\frac{jc\omega\mu_d k_{yd}\left(\frac{Z_{ss}}{Z_{sg}}+\frac{Z_{sg}}{Z_{ss}}\right)\tan\left(\frac{k_{yd}b}{2}\right)}{h_d^{\,2}}\right]\times$$
$$\left[\frac{w}{Z_{ss}}+\frac{c}{Z_{sg}}-\frac{(w-c)\omega\varepsilon_a k_{ya}}{h_a^{\,2}}-\frac{jc\omega\varepsilon_d k_{yd}\left(\frac{Z_{ss}}{Z_{sg}}+\frac{Z_{sg}}{Z_{ss}}\right)\cot\left(\frac{k_{yd}b}{2}\right)}{h_d^{\,2}}\right] \quad .$$

(5.26)

The propagation constant k_z for each mode can be expressed in terms of the transverse wavenumbers using either of the dispersion relation shown in (5.27) and (5.28) below

$$k_z = \sqrt{k_0^{\,2} - k_{xa}^{\,2} - k_{ya}^{\,2}}\ , \tag{5.27}$$

$$k_z = \sqrt{k_d^{\,2} - k_{xd}^{\,2} - k_{yd}^{\,2}}\ . \tag{5.28}$$

Since $k_{xa} = k_{xd} = \dfrac{\pi}{a}$, k_{ya} can thus be expressed in terms of k_{yd} by equating (5.27) and (5.28)

$$k_{ya} = \sqrt{k_0^{\,2} - k_d^{\,2} + k_{yd}^{\,2}}\ . \tag{5.29}$$

Substituting (5.27) or (5.28) and (5.29) into (5.26), it can be clearly seen that k_{yd} is the remaining unknown to be numerically solved for. The attenuation constant α_z can be computed by substituting the root of k_{yd} into (5.28) and extracting the imaginary component of $k_z = \beta_z - j\alpha_z$ in (2.2). For a lossless dielectric, the wavenumber in the dielectric substrate k_d is purely real. Close inspection on (5.28) shows that in order to compute the value of the complex propagation constant k_z, k_{yd} must be a complex variable as well, since both k_d and k_{xd} are real variables. Like the case of the lossy waveguides, the Powell Hybrid root-searching algorithm in a NAG routine has been used to find the root of k_{yd}. Since the fundamental mode is the HE_0 mode, the search

can thus start with values close to zero for both the real and imaginary components of k_{yd}.

5.3.4 The Superconducting Microstrip Lines

Several authors (Matick, 1969; Meyers, 1961; Swihart, 1961; Fingers and Kerr, 2008) considering superconducting transmission lines and striplines at low frequencies, have used the simple two-fluid model to characterize the superconductors. Nevertheless, Kautz (1978) has compared the results for the attenuation constant and phase velocity of striplines obtained using the two-fluid model and the Mattis-Bardeen theory. As shown by Kautz (1978), it is more realistic to apply the microscopic theory developed by Mattis and Bardeen (1958) since it takes into account the interactions of quasiparticles and Cooper pairs with the energy gap (as discussed in Chapter 4). Hence, in order to be able to give a more accurate prediction of loss, Mattis-Bardeen equations, i.e. equations (4.2) to (4.5), shall be applied here to calculate the loss in superconducting microstrip transmission lines.

5.4 Results and Discussion

In order to verify the new formulation, the attenuation constant of a microstrip line is computed using the transcendental equation in (5.26) based on two sets of parameters arbitrarily chosen from the results in Pucel *et al.* (1968a). Both the strip and groundplane of the normal microstrip structure are made of copper. The attenuation curve computed for rutile substrate with a

dielectric constant ε_r = 105 is illustrated in Figure 5.5 and for alumina substrate with ε_r = 9.35 in Figure 5.6. The attenuation constants are compared with those from equations derived using conformal transformations (Wheeler, 1964; Wheeler, 1965; Wheeler, 1977) and Wheeler's incremental inductance rule (Wheeler, 1942), by Hammerstad and Bekkadal (1975) (HB), Schneider, *et al.* (1969) (SGB), and Pucel *et al.* (1968b) (PMH). As shown in Figures 5.5 and 5.6, the attenuations computed using the new method are close, though somewhat higher than those from the three quasi-static methods. Close inspection on the experimental results published by Pucel *et al.* (1968a), it can be observed, however, that the measurement results showed higher loss than those suggested by PMH as well. Hence, this suggests strongly that the new

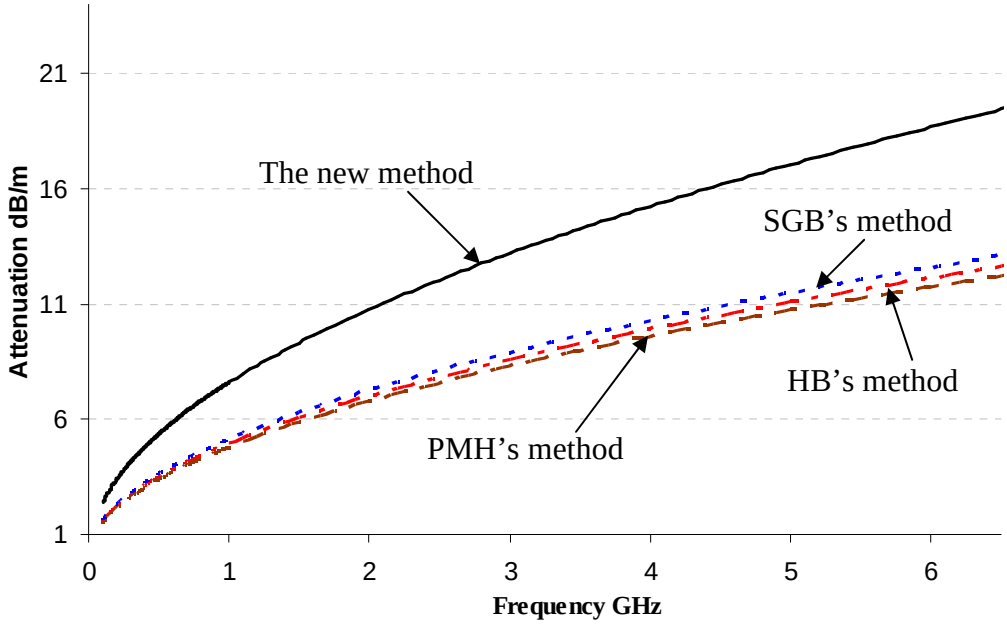

Figure 5.5. The loss in a copper microstrip transmission line with alumina substrate. Given $w = b$ = 508.0 μm, t_s = 8.382 μm, t_g = 300.0 μm, and ε_r = 105. (a) ····· SGB's method, - · - · - HB's method, – – – PMH's method, and ——— the new method.

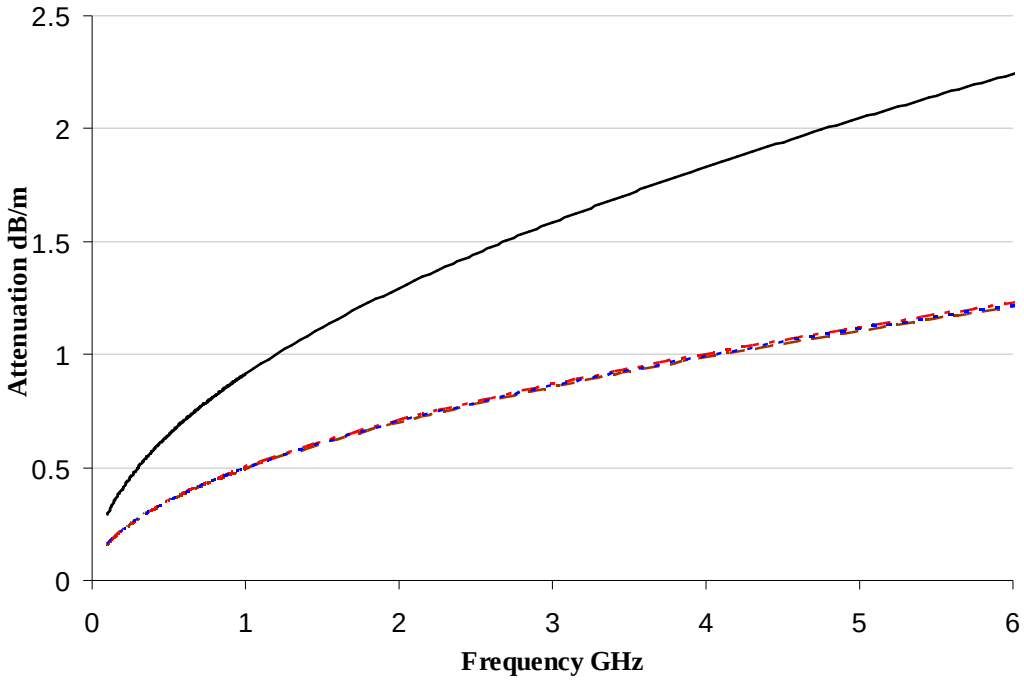

Figure 5.6. The loss in a copper microstrip line with rutile substrate. Given w = 3.048 mm, b = 1.27 mm, t_s = 9.906 μm, t_g = 300.0 μm, and ε_r = 9.35. (a) SGB's method, HB's method, PMH's method, and the new method.

full-wave method gives more accurate prediction of loss, which tallies closer with the experimental result shown in Pucel *et al.* (1968a).

Next, the attenuation of a Nb microstrip above and below the critical temperature T_c of 9.25 K is investigated. The dimensions of the superconducting microstrip structure are taken to be w = 750 nm, b = 250 nm, $t_s = t_g$ = 300 nm, ε_r = 3.8, and $c = a = \infty$. Figure 5.7 depicts the values of the attenuation constant α_z against a range of strip thickness to dielectric height ratio t_s/b, at frequency f = 100 GHz for the microstrip line at room

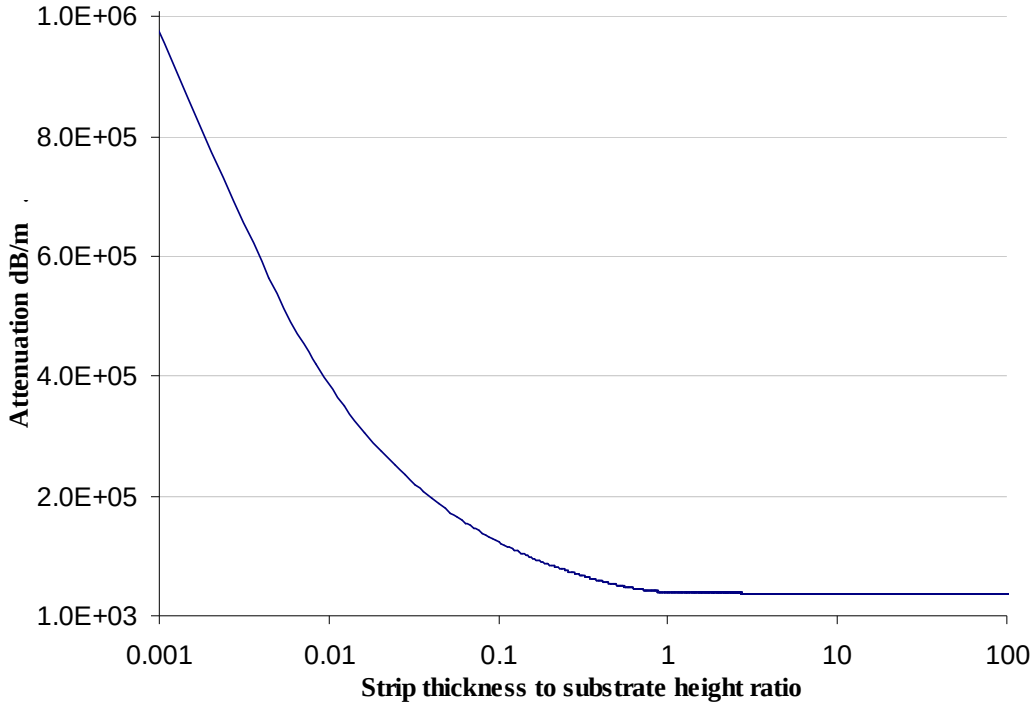

Figure 5.7. The loss in a Nb microstrip line at room temperature and f = 100 GHz as a function of strip thickness to substrate height ratio (t_s/b). Given w = 750 nm, b = 250 nm, and ε_r = 3.8.

temperature. As can be seen, when $\frac{t_s}{b}$ decreases below 0.1, the attenuation diverges to a very high value. Since the penetration depth of Nb is 85 nm at T = 0 K (Track *et al.*, 1989) and 40 nm at T = 4.2 K (Schelten *et al.*, 1971), it is apparent that a sharp increase of loss occurs when the thickness of the strip is less than the penetration depth (during superconducting state) or skin depth (during normal state) of Nb. Another factor contributing to the high loss in microstrips is that, when the strip becomes infinitesimally thin (i.e. $t_s \approx 0$), the current at the edges of the strip diverges to an extremely high rate resulting in the loss becomes unbounded (Heitkampar and Heinrich, 1991). Clearly, the

Spectral Domain Approach (SDA) which assumes zero thickness during formulation is not able in any formal way to calculate the behaviour of strips having finite thickness. In order to avoid singularities, however, Yassin and Withington (1995) have proposed limiting the number of basis function used to represent the current distribution to a finite set of values. Since the SDA is calibrated to yield the best agreement with the conformal mapping techniques, the calculation of the power loss could only, therefore, be as good as and no better than the equations used by HB, SGB, and PMH.

Figures 5.8 and 5.9 show the attenuation of Nb microstrip line at temperature T = 4.2 K, both below and above the frequency gap f_g, respectively. The sum of fields ratio, i.e. $\frac{E_t}{J_s}$ in (5.22) are integrated using the limits c = 750 nm, 1750 nm, 7500 nm, and 1.0×10^8 nm and (5.26) is computed based on these four sets of values of c. It can be seen from Figure 5.10 that when the fields ratio is integrated along the width of the strip (i.e. $c = w$ = 750 nm), the fringing fields beyond the width of the strip are excluded in the mathematical treatment. Hence, the sum of fields ratio resembles closely Matick's formulation which assumes a parallel plate capacitor with negligible fringing loss. Indeed, the attenuation obtained using the proposed method at $c = w$, tallies very closely with that computed using Matick's equation (Matick, 1969; Kautz, 1978), and is, in fact, indistinguishable as f exceeds f_g. As c increases, the attenuation increases accordingly as well. The attenuation, however, ceases to increase further when the fields ratio is integrated beyond some definite value of c. The additional loss predicted by the proposed method

when c approaches infinity can thus be attributed to the fringing effect at the edges of the strip.

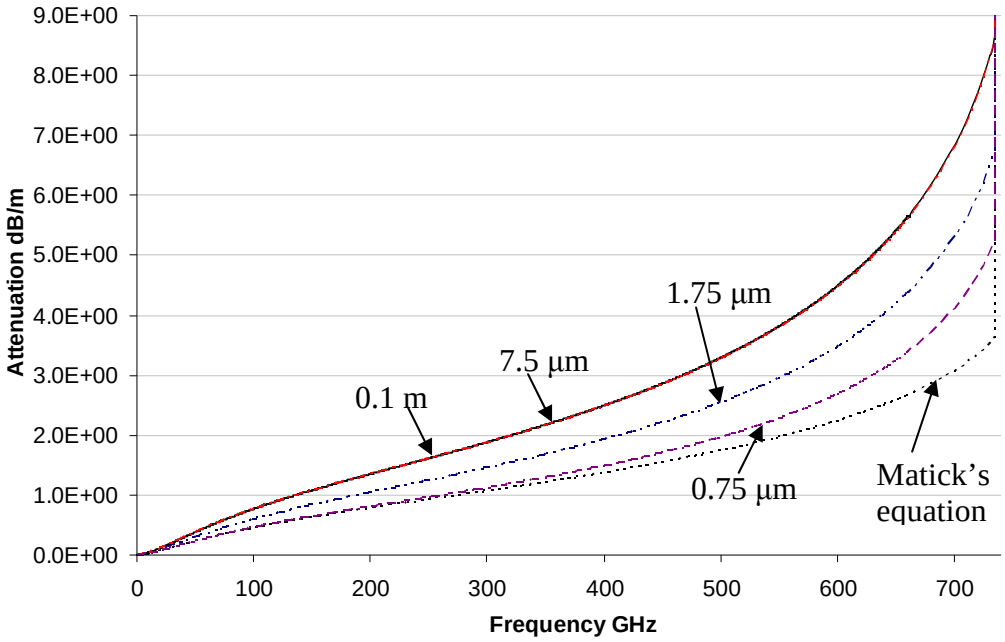

Figure 5.8. The loss in a superconducting microstrip line at T = 4.2 K below the gap frequency f_g. Equation (5.26) was integrated over c = 0.1 m (——), 7.5 µm (— · — · —), 1.75 µm (— · · —), and 0.75 µm (— — —). ····· was calculated using Matick's equation.

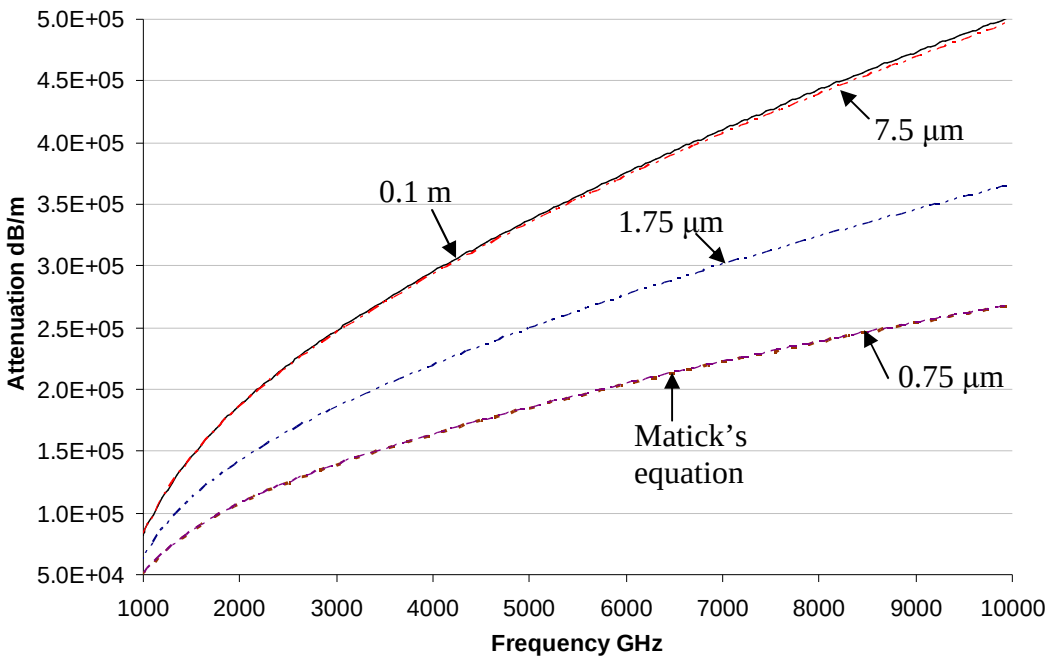

Figure 5.9. The loss in a superconducting microstrip line at T = 4.2 K above the gap frequency f_g. Equation (5.26) was integrated over c = 0.1 m (——), 7.5 μm (— · — · —), 1.75 μm (— · · —), and 0.75 μm (— — —). ····· was calculated using Matick's equation.

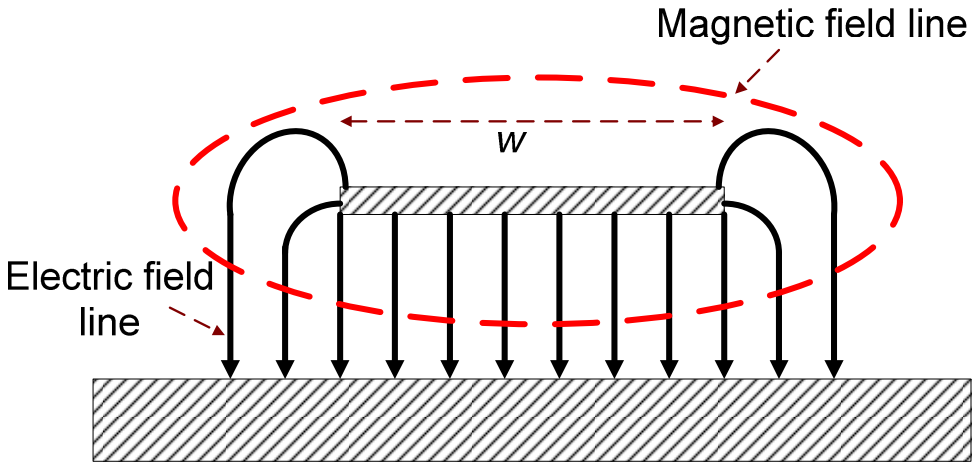

Figure 5.10. Field lines distribution in an air-filled microstrip.

An overall picture of the attenuation below and above the gap frequency f_g is shown in Figure 5.11. It is interesting to see that in this range, the attenuation computed by Yassin and Withington (1995) is even lower than Matick's method, indicating that Yassin-Withington's method underestimates the loss of a superconducting microstrip line significantly. Although both the new method and Yassin-Withington's method introduce a penetration factor into their formulations, it can be seen that the new method actually gives a more accurate result. This is however to be expected since the modification introduced by Yassin and Withington (1995) in the TEM mode transmission

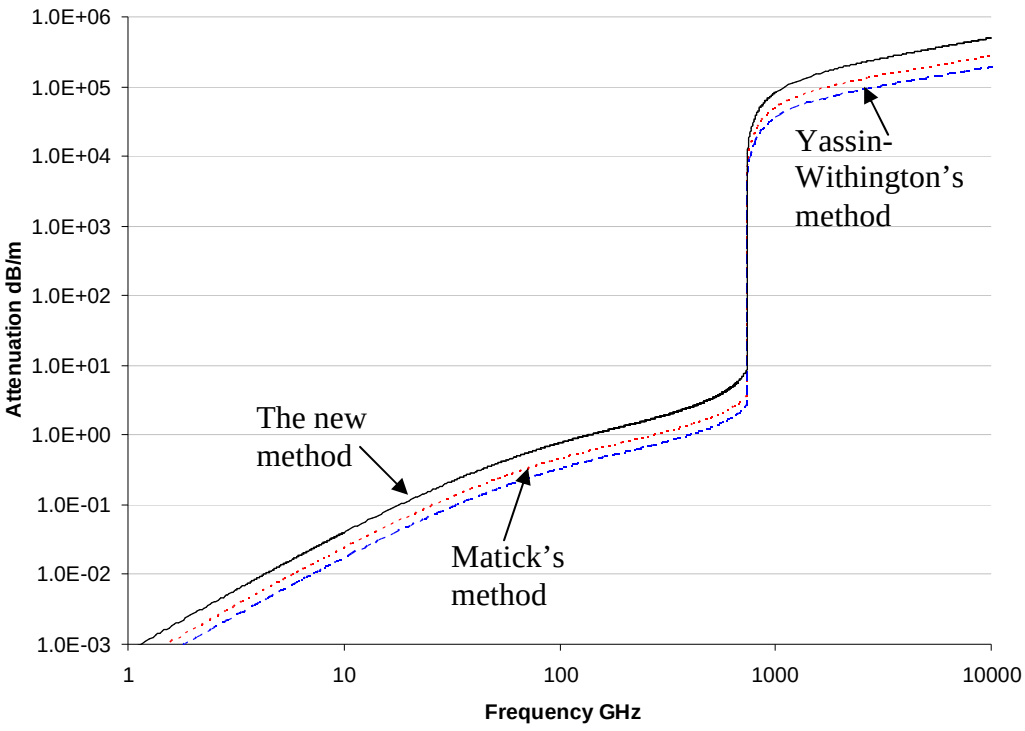

Figure 5.11. The loss in a superconducting Nb microstrip line at T = 4.2 K as a function of frequency. ——— was calculated using the new method in (5.53), ····· using Matick's equation, and – – – – using Yassin-Withington's equation.

line model, is based on an empirical approximation; while, the new formulation proposed here is developed from fundamental principles which accounts for the existence of both longitudinal fields.

A comparison of the attenuation constant and phase velocity of Nb microstrip line at room temperature and at T = 4.2 K are shown in Figures 5.12 and 5.13, respectively. As can be clearly seen in Figure 5.12, at f below f_g, the attenuation of the superconducting microstrip line is considerably lower than that at room temperature. The attenuation should in fact reduce further as the microstrip line cooled to a much lower temperature (Yassin and Withington, 1995; Yassin and Withington, 1996a; Withington and Yassin, 1996). Figure 5.13 shows that the phase velocity of the superconducting microstrip line

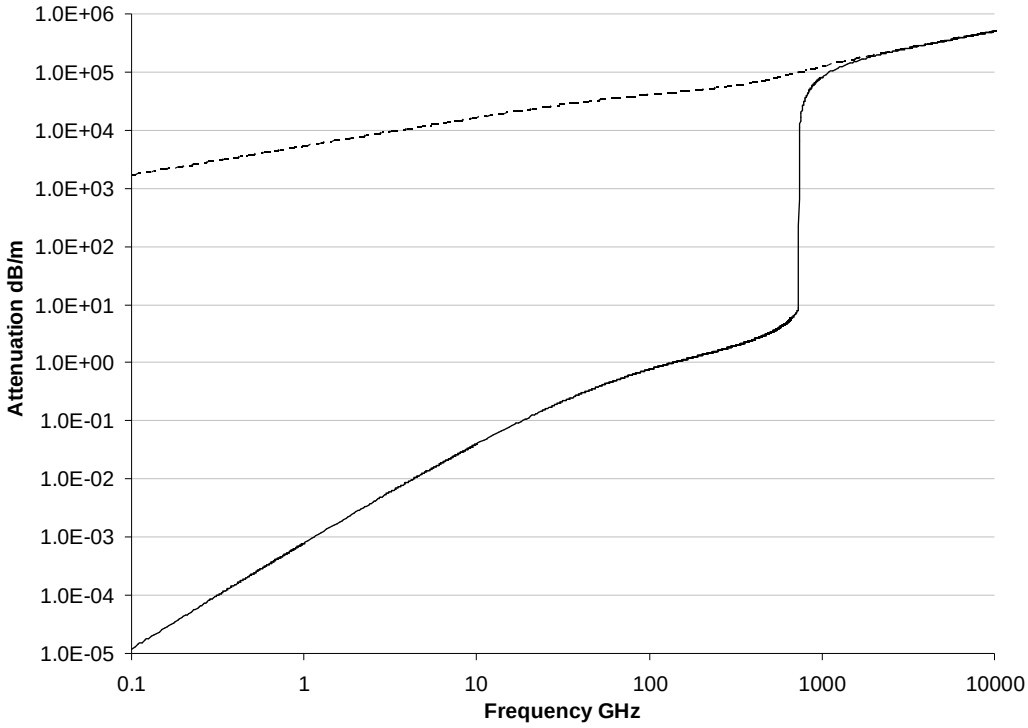

Figure 5.12. Comparison of the loss in a Nb microstrip line at room temperature (▪▪▪▪▪▪▪▪▪▪▪▪▪▪) and T = 4.2 K (▬▬▬▬▬▬▬▬).

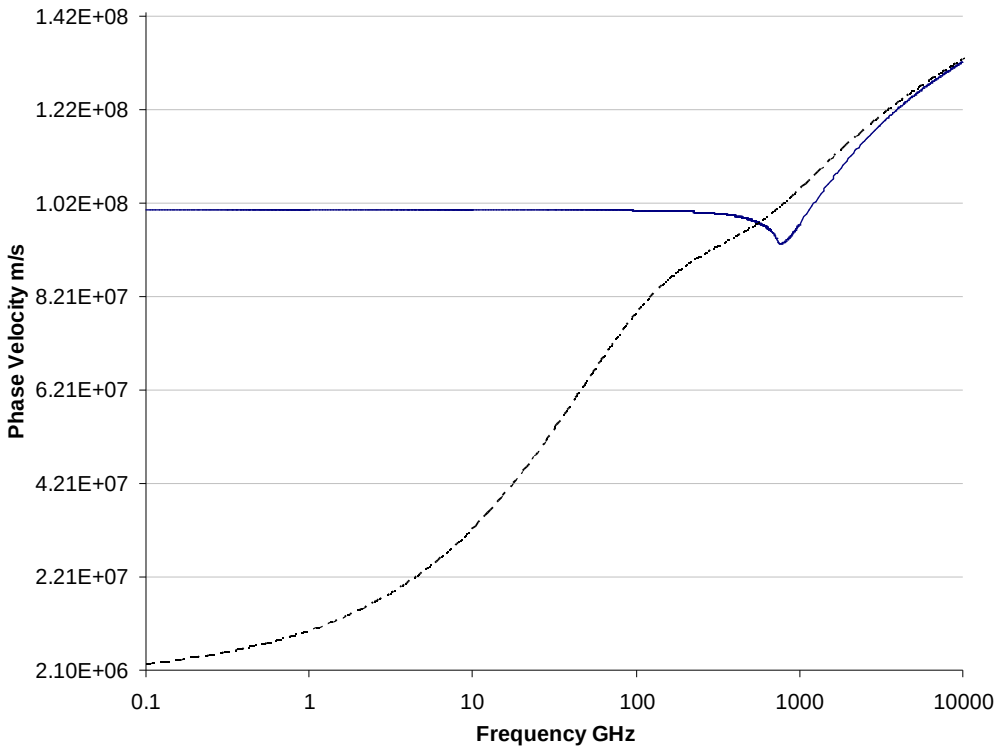

Figure 5.13. Comparison of the phase velocity in a Nb microstrip line at room temperature (.....) and T = 4.2 K (——).

below f_g stays almost constant at approximately 1.01×10^8 m/s. The fact that the phase velocity does not vary with frequencies indicates that the superconducting microstrip line is dispersionless. Above f_g, both the attenuation and the phase velocity approach those obtained from the microstrip line at room temperature. It can be observed that the phase velocity above f_g varies with frequencies and, thus, the microstrip line becomes dispersive. Such phenomenon is to be expected since Cooper-pair breaking becomes dominant at frequencies above the gap (Kittara *et al.*, 2002).

5.5 Summary

A new full-wave analysis to compute the propagation constant of waves in a normal and superconducting microstrip transmission line is proposed. The formulation is based on matching the tangential electric fields E_t and magnetic fields H_t at the dielectric-conductor and dielectric-air interfaces. Integrating the fields ratio along a definite width in the *x*-direction and solving for the determinant of the coefficients of the fields, a set of transcendental equation is obtained. The roots of the transcendental equation gives values for the transverse wavenumber k_{yd} in the substrate. Like the case of lossy waveguides discussed in Chapters 2 and 3, the wave propagation constant k_z could then be obtained by substituting k_{yd} into the dispersion relation.

The attenuation results computed using the new formulation are in good agreement with the quasi-static results in Hammerstad and Bekkadal (1975), Schneider *et al.* (1969), and Pucel *et al.* (1968b). Quasi-static techniques assume pure TEM mode of wave propagation and is, thus, valid only in the low frequency range where the dimensions of the microstrip structure is much smaller than the wavelength. The new method proposed here is a full-wave analysis which takes into account the presence of the longitudinal fields, as well as fringing loss. Thus, the new method gives more realistic result, especially for superconducting microstrip lines operating in the THz frequencies, where the dimensions of the structure is comparable with the wavelength.

CHAPTER 6

COPLANAR WAVEGUIDES

In this chapter, the loss of waves propagating in a coplanar waveguide and microstrip line is compared and analyzed. The performance of both devices, designed at different dimensions and operating at different range of frequencies is investigated.

6.1 Introduction

The conventional coplanar waveguide (CPW) proposed by C. P. Wen (1969) is basically a planar device consisting of a dielectric substrate with a layer of conductor deposited at the top surface, as shown in Figure 6.1. The metallization layer is separated into three sections, i.e. a center strip with a narrow gap at both sides, separating it from two ground planes on either side. To simplify the analysis of a CPW, Wen has assumed the thickness of the dielectric substrate b to approach infinity, i.e. $b \rightarrow \infty$. For practical application, however, the thickness of the CPW has to be finite. Indeed, it is the width w and thickness t_s of the center strip, the gap between the strip and the groundplane w_c, the permittivity ε_d, and the height b of the dielectric substrate which determine the characteristic impedance Z_0 and the attenuation α of wave in the CPW.

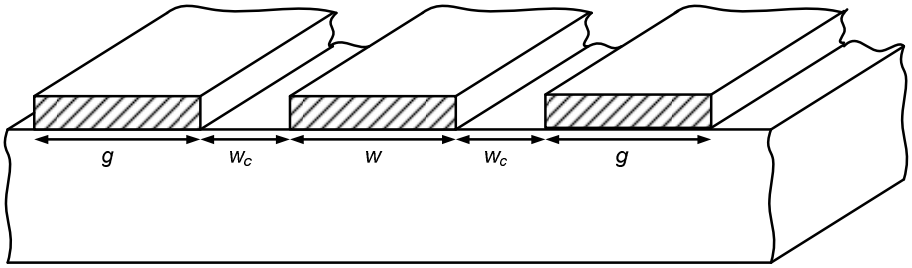

Figure 6.1 The cross section of a coplanar waveguide.

CPWs have been extensively used in the design of monolithic microwave integrated circuits (MMICs). This is because CPWs offer the following advantages over microstrip lines:

(i) Unlike microstrip structures which require via holes to ground active devices, CPWs allow ground connections to be conveniently made at the substrate edge (Browne, 1987a; Brown, 1987b). It is to be noted that, at high frequencies, via holes can introduce significant inductance and degrade circuit performance (Jackson, 1986).

(ii) CPWs are uniplanar devices which eliminate the additional steps for backside wafer processing and significantly lower the fabrication cost.

(iii) CPWs allow easy connection of shunt and series circuit elements (Brown, 1989; Browne, 1990; Browne, 1992). Hence, it is well suited for use with field effect transistors (FETs) such as MOSFETs and MESFETs, which are coplanar (Ahmad *et al.*, 2006) in nature as well.

Nevertheless, in spite of the above advantages, CPWs have not been commonly used in the coupling of waves in mixer circuits. Microstrips are still the preferred option for wave coupling. One most general reason for this is

that, CPWs are believed to inherently exhibit higher conduction loss than microstrips (Jackson, 1986). However, it was pointed out by Gopinath (1982) and Itoh (1989) that under special circumstances, the conduction loss in CPWs can be significantly lower than that in microstrip lines. In fact, Kittara *et al.* (2002) has performed a theoretical study on the losses in both superconducting CPWs and microstrips using the formulations developed by Gupta (1996) and Yassin and Withington (1995), respectively. In Kittara *et al.* (2002), the performance of CPWs and microstrips designed with different dimensions and material properties was compared. In their study, it was shown that CPWs with a higher dielectric constant and at dimensions much larger than the microstrip, the loss turned out to be much lower than that in a micrsotrip. It is not indicated in Kittara *et al.* (2002), however, which structures exhibit lower loss when the dielectric constant and dimensions (such as the width of the strip *w*, the thickness of the substrate *b*, etc.) of the structures are similar to each other. Hence, it is interesting to compare the loss between CPWs and microstrip lines, designed at similar dimensions and dielectric constants.

Furthermore, coplanar waveguides have also been extensively used as resonators in Kinetic Inductance Detectors (KIDs) to detect the increase of quasiparticles due to the coupling of millimeter and submillimeter signals (Day *et al.*, 2003; Calvo *et al.*, 2010; Schaerth *et al.*, 2008; Figer, 2010). The study of loss in superconducting CPWs is, hence, crucial for future development of such devices.

In this chapter, the loss of normal and superconducting coplanar waveguides is investigated. A comparison and analysis between the loss in coplanar waveguides and microstrip lines is performed. In order to show that the performance of both devices at large dimensions (such as those used in printed circuit technology) and small dimensions (such as those used in SIS mixer circuits) can be different, an analysis is made with the dimensions of both devices multiplied with a multiplication factor q varying from 0 to 5.

To determine the conduction loss for planar lines in an absolute sense is difficult. The loss depends to a large extent on the conductor surface roughness, which can vary from device to device, albeit being designed with the same geometry and dimensions (Jackson, 1986). As illustrated in Chapter 5, the loss is also highly affected by the behaviour of the current crowded at the edge of the strip with different thickness. Hence, in the comparison of microstrips and CPWs, the surface roughness for both CPWs and microstrip structures has been assumed to be zero. To account for the same current density in the strip, the strip thickness (t_s) of both devices has also been taken to be the same.

6.2 Attenuation in Coplanar Waveguides

Similar with the case of microstrip lines, three types of losses can be identified in coplanar waveguides, i.e. dielectric, ohmic, and radiation/surface wave losses. Very often, dielectric loss can be taken to be negligibly small by choosing a low loss substrate material. Power leakage due to surface waves

and radiation from unwanted modes can also be avoided by carefully designing the CPW circuit. Some of the steps which can be taken to minimize power leakage are listed below:

(i) Radiation due to the excitation of the parasitic odd modes can be minimized by maintaining the symmetry of the CPW or using air bridges at regular intervals to short it out (Jackson, 1986).

(ii) Surface wave loss can be suppressed if the cutoff frequency of the surface modes is "pushed" above the operating frequency. This can be done by choosing the appropriate substrate thickness b such that $b < \frac{0.12\lambda_0}{\sqrt{\varepsilon_r}}$, where λ_0 is the wavelength of a plane wave in free space (Riaziat *et al.*, 1990).

(iii) The parasitic parallel plate waveguide mode in a conductor-backed CPW can be controlled by introducing an additional layer of dielectric in between the metallization plane and the substrate. Power leakage due to this parasitic mode occurs when the dominant transmission line mode of the CPW travels faster than the parallel plate mode. Hence, the dielectric constant and dielectric thickness of this additional layer are chosen in such a manner that the CPW mode is slower than the parasitic mode (Liu and Itoh, 1992).

Since the loss from the above dielectric and radiation/surface waves could be suppressed, the ohmic loss in coplanar waveguides would only be considered in the subsequent analysis. To calculate the ohmic losses in CPWs,

the analytical solution published in Ghione (1993) shall be applied. In Ghione (1993), the power dissipated in the line was evaluated through a conformal approximation of the current density of the finite thickness structure, with the width of the groundplane g tending to infinity. The analytical equation of the attenuation constant was then derived using the power-loss method as

$$\alpha = \frac{R_s \sqrt{\varepsilon_{eff}(f)} \left\{ \frac{\left[\pi + \ln\left(\frac{8\pi w(1-k_1)}{2t_s(1+k_1)} \right) \right]}{w} + \frac{\left[\pi + \ln\left(\frac{4\pi(w+2w_c)(1-k_1)}{t_s(1+k_1)} \right) \right]}{(w+2w_c)} \right\}}{240\pi K(k_1)K'(k_1)(1-k_1^{\,2})}. \tag{6.1}$$

where R_s is the surface resistance of the conductor, $\varepsilon_{eff}(f)$ the frequency dependent effective dielectric constant, w the width of the strip, and $K(k_1)$ and $K'(k_1)$ are the complete elliptic integrals of the first kind and its complement, respectively. The argument of the elliptic integrals k_1 can be solved using a pair of conformal transformations (Veyres and Hanna, 1980)

$$k_1 = \frac{w}{w+2w_c}. \tag{6.2}$$

Here, the series expansion for $K(k_1)$ illustrated by Hilberg (1969) has been implemented, as given below

for $0 \le k_1 \le 0.707$,

$$K(k_1) = \frac{\pi}{2}\left\{1 + 2\left(\frac{{k_1}^2}{8}\right) + 9\left(\frac{{k_1}^2}{8}\right)^2 + 50\left(\frac{{k_1}^2}{8}\right)^3 + 306.25\left(\frac{{k_1}^2}{8}\right)^4 + \ldots\right\},$$

(6.3a)

and for $0.707 \le k_1 \le 1$,

$$K(k_1) = p + (p-1)\left(\frac{{k_1'}^2}{4}\right) + 9\left(p - \frac{7}{6}\right)\left(\frac{{k_1'}^4}{64}\right) + 25\left(p - \frac{37}{30}\right)\left(\frac{{k_1'}^6}{256}\right) + \ldots ,$$

(6.3b)

where $p = \ln(4/k_1')$ and $k_1' = \sqrt{1 - {k_1}^2}$.

A simpler expression which relates $K'(k_1)$ to $K(k_1)$ can be found in Jahnke *et al.* (1969) as

for $0 \le k_1 \le 0.707$,

$$K'(k_1) = \frac{K(k_1)}{\pi} \ln\left[\frac{2\left(1 + \sqrt{k_1'}\right)}{\left(1 - \sqrt{k_1'}\right)}\right], \qquad (6.4a)$$

and for $0.707 \leq k_1 \leq 1$,

$$K'(k_1) = \frac{K(k_1)\pi}{\ln\left[2\left(1+\sqrt{k_1}\right)\Big/\left(1-\sqrt{k_1}\right)\right]}\ , \tag{6.4b}$$

Ghione (1993) has applied an effective dielectric constant ε_{eff} which does not vary with frequency f in its calculation of loss. Here, to account for the dispersive effect in CPWs, however, a frequency dependent effective dielectric constant $\varepsilon_{eff}(f)$ has been incorporated into (6.1), instead. The $\varepsilon_{eff}(f)$ is found by curve fitting the results of numerical simulation (Hasnain *et al.*, 1986)

$$\varepsilon_{eff}(f) = \left[\sqrt{\varepsilon_{eff}} + \frac{\sqrt{\varepsilon_r} - \sqrt{\varepsilon_{eff}}}{1+G(f/f_{TE})^{-1.8}}\right]^2\ , \tag{6.5}$$

where ε_r is the dielectric constant of the substrate and f_{TE} the cutoff frequency for the TE_0 surface wave mode for the substrate. The variables G, u, and v are given respectively as

$$G = \exp[u \ln(w/w_c) + v]\ , \tag{6.6a}$$

$$u = 0.54 - 0.64\ln(2w/b) + 0.015[\ln(2w/b)]^2\ , \tag{6.6b}$$

$$v = 0.43 - 0.86\ln(2w/b) + 0.54[\ln(2w/b)]^2\ . \tag{6.6c}$$

It is to be noted that, ε_{eff} and $\varepsilon_{eff}(f)$ in (6.5) are different – with the former being independent of frequency. The effective dielectric constant ε_{eff} is

dispersionless and can be derived using quasi-static methods. Hence, the ε_{eff} formulated by Veyres and Hannas (1980) using the quasi-static conformal transformations has been applied in (6.5)

$$\varepsilon_{eff} = 1 + \frac{\varepsilon_r - 1}{2} \frac{K(k_2)}{K'(k_2)} \frac{K'(k_1)}{K(k_1)}. \tag{6.7}$$

Here, the argument k_2 of the elliptic integral is given as

$$k_2 = \frac{\sinh\left(\frac{\pi w}{4b}\right)}{\sinh\left[\frac{\pi\left(w/2 + w_c\right)}{2b}\right]}. \tag{6.8}$$

6.3 Comparison between Microstrip Lines and Coplanar Waveguides

In order to compare the loss in microstrip lines and CPWs at different dimensions, the strip width and substrate thickness of both devices operating at f = 100 GHz are varied. For the CPW, the conduction loss is computed using (6.1); whereas, for the microstrip line, the conduction loss is computed using (5.26) formulated in Chapter 5. In the analysis, the loss of the strip width w at 750 nm and substrate thickness b at 250 nm is first computed. Both strip width and substrate thickness are then increased by a multiplication factor q, i.e. strip width w = 750 nm × 10^q and substrate thickness b = 250 nm × 10^q. The exponent q is allowed to vary from 0 to 5. The strip thickness t_s for both the microstrip and CPW is taken to be 300 nm, while the groundplane

thickness t_g for the microstrip is the same as the strip thickness, i.e. $t_g = t_s$ = 300 nm. The strip and groundplane are made of Niobium (Nb) with conductivity $\sigma = 1.57 \times 10^7$ S/m at room temperature and the dielectric constant of the substrate ε_r is given as 3.8 for both the microstrip line and CPW. The distance between the strip and the ground plane for the coplanar waveguide w_c is taken to be 5 μm.

From Figure 6.2, it can be clearly seen that as q increases, the conduction loss of the microstrip line decreases at a higher rate than the CPW. Both curves intersect at $q = 2.2$. At large dimensions where $q > 2.2$, the loss of the microstrip line is much lower than the CPW. At $q < 2.2$, however, it can be observed that the conduction loss of the CPW turns out to be considerably lower. Such results give a strong implication especially in the design of SIS mixer circuits for the detection of millimeter and submillimeter waves, where microstrips are usually used for the coupling of waves. The dimensions of an SIS circuit are small, for eg. the substrate cross section for a microstrip used to couple a 100 GHz signal is around 610 × 150 μm^2 (Vassilev *et al.*, 2004). Due to the fact that a CPW features much lower attenuation in small dimensions (where $q < 2.2$), the result in Figure 6.2 actually suggests that CPWs can, hence, be considered as a better alternative for waves coupling.

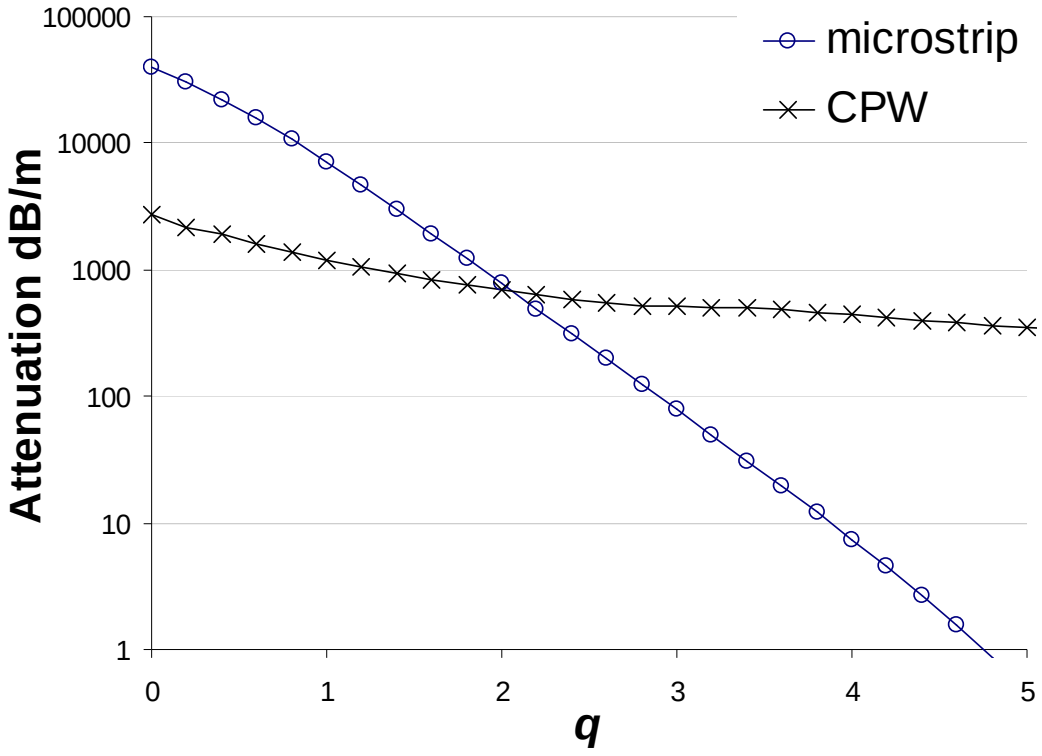

Figure 6.2. Comparison of conduction loss between microstrips and CPWs at strip width w = 750 nm × 10^q and substrate thickness b = 250 nm × 10^q, where q varies from 0 to 5.

An SIS mixer circuit, as well as a coplanar waveguide resonator used in a Kinetic Inductance Detector (KID) usually operates under the critical temperature of the superconductor. Hence, the performance of superconducting microstrips and coplanar waveguides are investigated as well. Figures 6.3 and 6.4 show the losses of waves in superconducting microstrips and CPWs operating at temperature T = 4.2 K, for "large" and "small" dimensions, respectively. For "large" dimensions where q > 2.2, the following parameters for both microstrips and CPWs have been taken: w = b = 200 μm, t_s = t_g = 300 nm. For "small" dimensions where q < 2.2, the parameters are: w = 750 nm, b = 250 nm, t_s = t_g = 300 nm. The distance between the strip and

groundplane in a coplanar waveguide w_c for “large” and “small” dimensions are 5 μm and 2 μm respectively.

From Figure 6.3, it can be clearly seen that the loss of wave in a superconducting CPW with “large” dimensions turns out to be higher than those in a microstrip line. The loss in the CPW is, however, much lower at “small” dimension, as shown in Figure 6.4. Hence, this shows that the result shown in Figure 6.2 for normal structures is also valid for the case of a superconductor. In other words, it can be seen that at “small” dimensions, i.e. the size of a probe usually used for wave coupling in an SIS mixer, a CPW exhibits much lower loss compared with a micrsotrip probe of a similar size.

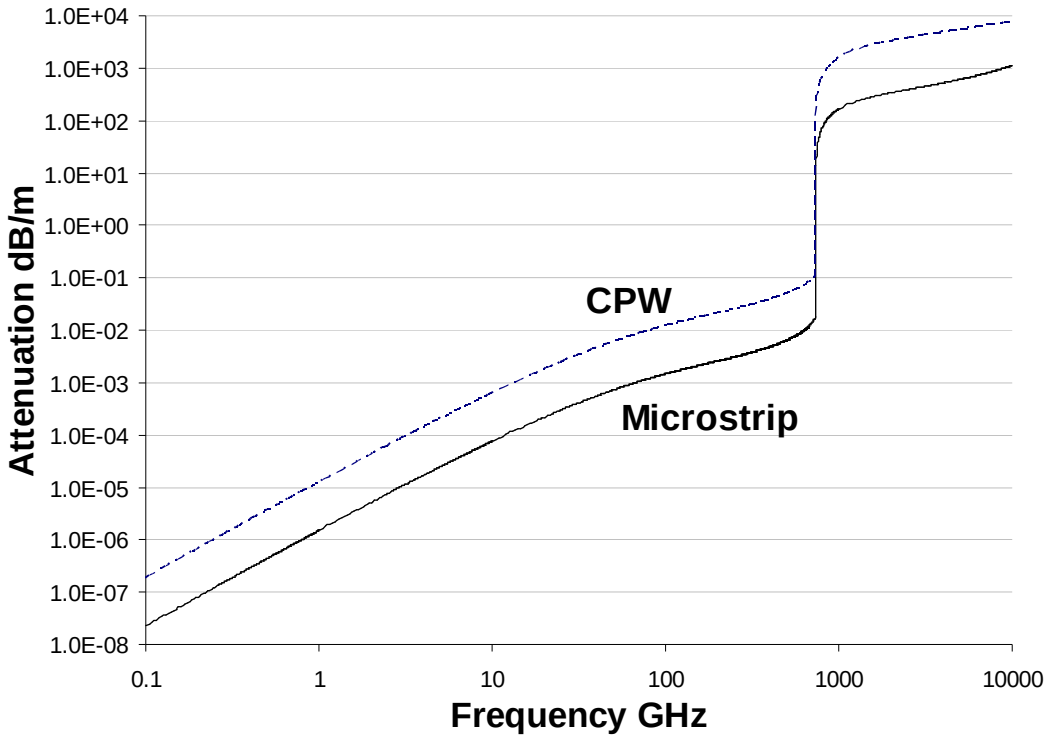

Figure 6.3. Conduction loss of superconducting microstrips and CPWs for “large” structures where $q > 2.2$.

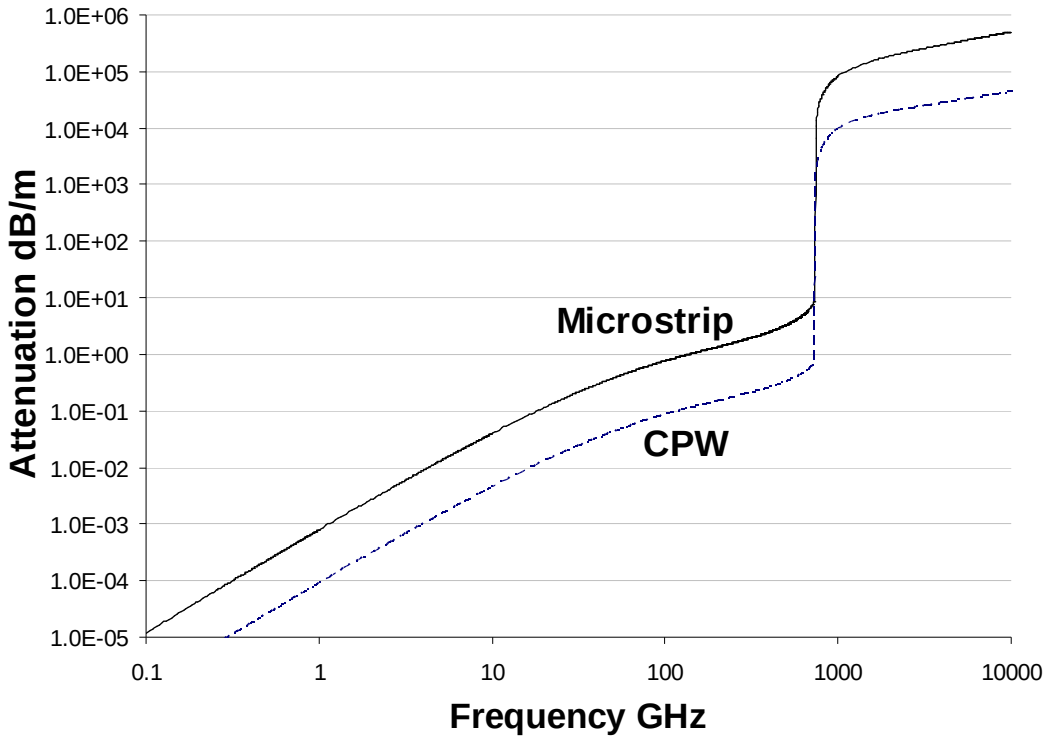

Figure 6.4. Conduction loss of superconducting microstrips and CPWs for "small" dimensions where $q < 2.2$.

6.5 Summary

A comparison between the attenuation of waves propagating in a microstrip line and coplanar waveguide (CPW) is performed. The results for both the normal and superconducting cases show that the conduction loss of a microstrip line decreases at a higher rate than the CPW as the dimensions for both devices increases. As the dimensions reduce to that comparable with the wavelength (i.e. $q < 2.2$), the loss in a CPW appears to be significantly lower.

Such result is very useful especially in the design of mixers. As shown in Vassilev and Belitsky (2001b), the size of a probe used in SIS mixer lies in

the range where $q < 2.2$. The preliminary result illustrated in Figures 6.2 and 6.4 actually suggests that CPWs can be considered as a better alternative device in the coupling of millimeter and submillimeter waves. Since superconducting coplanar waveguides are also commonly applied in Kinetic Inductance Detectors (KIDs) to measure the shift of resonant frequencies, the loss investigated here is certainly important for such devices as well.

CHAPTER 7

SUMMARY AND FUTURE WORK

In order for extremely weak millimeter and submillimeter waves to propagate and couple effectively to the SIS junction, it is important to minimize the loss in wave guiding structures that are built inside the receivers. A novel and accurate formulation is developed to compute the loss in different wave guiding structures made of different materials (normal conductors and superconductors) that can be implemented in radio astronomy receivers. Existing methods of calculations assume pure TE, TM or TEM mode propagation in wave guiding structures. Hence, they are only accurate up to the microwave range where the conducting material exhibits high loss tangent close to a perfect conductor. At millimeter and submillimeter wavelengths, however, the loss tangent of a conducting material decreases with increasing frequency. In other words, the co-existence of the longitudinal fields becomes significant at millimeter and submillimeter wavelengths. Since existing methods assume that fields in lossy structures are identical to those in a perfect waveguide, they fail to account for the additional loss induced by the mode-coupling effects of hybrid modes. The workhorse of this thesis is a new computational method that is derived from fundamental principles. The superposition of hybrid lossy modes and also the mode coupling effect of multimode propagation in lossy waveguides are accounted for in this new method by incorporating both the longitudinal electric and magnetic fields into

the solution when the Helmhotz's equation is solved. Penetration factors are introduced in the field equations to represent the presence of fields at the boundary of the lossy wall material. In addition, the transverse wavenumbers are allowed to take on a complex form in order to satisfy the dispersion relation of propagating fields in lossy guides. A set of characteristic equations is then derived by matching the fields with the surface impedance at the boundary and finding the determinant of the field coefficients. Finally, the characteristic equations are solved to obtain the attenuation in the waveguides. This new method is versatile and can be applied to guiding structures of differing geometries.

In the following, a summary on the analysis of both normal and superconducting wave guiding structures is made. This includes circular and rectangular waveguides, microstrip transmission lines, and coplanar waveguides. At the end of this chapter, some potential research areas worth investigating are proposed.

7.1 Summary

In chapters 2 and 3, the new method has been applied on the case of lossy rectangular and circular waveguides, respectively. The results have been validated with the experimental measurement for the propagation of dominant modes, at frequencies at the vicinity of cutoff. For higher order modes of propagation, the computed results show that the loss at millimeter and submillimeter frequencies is higher than the propagation of single mode alone,

i.e. the loss computed using the power-loss method (Stratton, 1941; Seida, 2003; Collin, 1991; Cheng, 1989). The additional loss obtained using the new method is induced by the mode coupling effect of the concurrent propagation of modes. This is an important discovery since most existing methods are derived from the perturbation of the lossless case, they fail to account for the interaction of different modes existing in practical lossy waveguides.

In chapter 4, the loss in superconducting waveguides has also been investigated. The complex conductivity of a superconducting Nb was solved using Mattis-Bardeen's equation (Mattis and Bardeen, 1958) and subsequently substituted into the characteristic equations developed using the new method. The results show that at f below the gap frequency f_g, the superconducting waveguide behaves like a lossless waveguide, i.e. the loss diverges to infinity at frequencies below cutoff and becomes zero above cutoff. Indeed, such discovery is significant since it suggests strongly that superconducting waveguides operating at this range can be used to channel waves to the detector circuit in a highly efficient manner and with minimum loss. Above f_g however, the waveguide loses its superconductivity and exhibits loss. This is to be expected since Cooper-pair breaking becomes dominant at f above f_g. In fact, it can be observed that the loss above the gap diverges at a higher rate and eventually surpasses the loss in a normal waveguide. This result can be attributed to the fast increase rate of surface resistance and fields' penetration in the waveguide when operating below the critical temperature.

In chapter 5, the new method is extended further to the case of normal and superconducting microstrip lines. Here, the electric to magnetic fields ratio, i.e. E_t/H_t in the substrate is matched with the ratios of the fields in free space and also the surface impedances of the strip and groundplane. To account for the finite thicknesses of the strip and groundplane, the surface impedance equation formulated by Kerr (1999) has been applied in the new formulation.

Comparison in normal microstrip transmission lines show that the loss computed using the new method is somewhat higher than those computed using the quasi-static methods. Indeed, it can be observed from Figures 5.5 and 5.6 that the experimental measurements performed by Pucel *et al.* (1968a) are higher than those estimated by the quasi-static methods as well. This suggests that the new method gives more accurate prediction of loss. The higher loss found using the new method can be attributed to those induced by the longitudinal components in hybrid modes.

For superconducting microstrip lines, the loss obtained from the new method is validated by comparing with Matick's (Matick, 1969; Kautz, 1978) and Yassin-Withington's (Yassin and Withington, 1995; Yassin and Withington, 1996a; Withington and Yassin, 1996) results. The field in the microstrip line at the boundaries of the substrate was integrated along the width of the substrate. When the field is integrated over the size of the strip, the loss from the new method is in close agreement with that from Matick's method. However, when it is integrated beyond the size of the strip, the loss

becomes higher than that using Matick's equation. Since Matick assumes the strip to be infinitely wide, the additional loss found in the new method can thus be attributed to the fringing loss at the edges of the strip. In the comparison, it could be seen that the loss obtained using Yassin-Withington's method is even lower than Matick's method, indicating that Yassin-Withington's method underestimates the loss of a superconducting microstrip. Compared with normal microstrips, superconducting microstrips show much lower loss below the gap frequency f_g. The new method also shows that the phase velocity below f_g is constant indicating that the superconducting microstrip is dispersionless.

In chapter 6, the performance of microstrips and coplanar waveguides (CPWs) was compared. Preliminary results showed that at wavelength comparable to the dimensions of the structures, CPWs exhibit lower loss than microstrip lines. Such result is very useful and actually suggests that, with modification made to the SIS receiver design, a CPW can be considered as a better alternative to be used for the coupling of waves.

7.2 Future Work

In this thesis, a new analytical approach to compute losses in uniform wave guiding structures have been presented. It is to be noted, however that, besides such losses, there are a number of other factors which affect the performance of waves channeling and coupling onto the detector circuit. Here,

a few key factors have been identified. To improve the efficiency of the guiding structures, these factors are worthwhile looking into in the future.

7.2.1 Full-Wave Analysis of Coplanar Waveguides

The loss in coplanar waveguides computed in Chapter 6 is based on the quasi-static method illustrated in Ghione (1993). As mentioned in Chapter 5, the accuracy of quasi-static methods start to deteriorate at high frequencies, since the signals can no longer be approximated to the propagation of pure TEM mode. Although full-wave analysis such as the mode-matching method (Heinrich, 1990) exists, it requires a significant amount of computer resources to carry out the computations. Thus far, a simpler and analytical full-wave analysis is not available. Therefore, it is worthwhile developing an analytical full-wave approach to compute the loss of waves in coplanar waveguides.

7.2.2 Bending Losses in Rectangular Waveguides

The waveguides that have been considered in this thesis, hitherto, are assumed to be uniformly straight. Studies have shown that an increase of loss occurs due to bends in waveguides (Miyagi *et al.*, 1984). It can be seen from Figures 1.2 and 1.3 that bends are inevitable while channeling the signals using waveguides to the microstrip probe. Miyagi *et al.* (1984) and Mercatili and Schmeltzer (1964) have formulated analytical solutions to compute bend losses in both conducting and dielectric circular waveguides. Although Kumar and Galawa (1994) and Deck *et al.* (1998) have derived equations to compute

bend losses in rectangular waveguides, their methods are only restricted to the case of dielectric waveguides. Moreover, a general approach applicable to both circular and rectangular waveguides is not available yet. To be able to compute losses in waveguides in a more "complete" sense, the new method presented in this thesis can thus be considered to be extended further so as to include bend losses in the formulation.

7.2.3 Input Impedance of a Microstrip Probe in Circular Waveguides

When constructing millimeter and submillimeter wave SIS mixers, it is important to design the mixer block in such a way that the incoming waveguide mode is coupled to the microstrip probe in a highly efficient manner. To allow the incident power to be coupled efficiently, the dimension of the probe must be designed in such a way that the input impedance of the probe is purely resistive (with the reactance reduced to zero) (Collin, 1991). The input impedance of a microstrip probe placed in rectangular waveguides has been extensively studied (Yassin and Withington, 1996b; Withington and Yassin, 1997; Withington *et al.*, 1999; Ho and Shih, 1989). However, literatures on microstrip probe in circular waveguides are, surprisingly, rare. This is because rectangular waveguide-to-microstrip transition is more commonly used in receiver circuits.

Although a circular waveguide is less popular than its rectangular counterpart, it finds many applications, especially in cases where a rotational symmetry is desirable. For eg. Bock (1999) and Grimes *et al.* (2007) have

used a circular waveguide with four microstrip probes to design an L-band orthomode transducer (OMT) to extract two orthogonal polarization modes in the waveguide.

Lee and Yung (1994) have developed an analytical equation to calculate the input impedance of a coaxial line probe in a circular waveguide. It is believed that with modification made on their method, their approach can be extended further to the case of a microstrip probe in a circular waveguide as well.

REFERENCES

Ahmad, I., Ho, Y. K., Majlis, B. Y. (2006). Fabrication and characterization of a 0.14 μm CMOS device using ATHENA and ATLAS simulators. *International Scientific Journal of Semiconductor Physics, Quantum Electronics, and Optoelectronics*, 9, 40 – 46.

Ahn, D., Park, J. -S., Kim, C. –S., Kim, J., Qian, Y., Itoh, T. (2001). A design of the low-pass filter using the novel microstrip defected ground structure. *IEEE Transactions on Microwave Theory and Techniques*, 49, 86 – 93.

Alley, G. D. (1970). Interdigital capacitors and their applications to lumped-element microwave integrated circuits. *IEEE Transactions on Microwave Theory and Techniques*, 18, 1028 – 1033.

Assadourian, F. and Rimai, E. (1952). Simplified theory of microstrip transmission systems. *Proceedings of IRE*, 1651 – 1657.

Balanis, C. A. (1989). Advanced Engineering Electromagnetics. In: *Rectangular Cross-Section Waveguides and Cavities*. (pp. 352 – 462). New York. John Wiley and Sons.

Bardeen, J., Cooper, L. N., and Schrieffer, J. R. (1957). Theory of superconductivity. *Physical Review*, 108, 1175 – 1204.

Barychev, A. M. (2005). *Superconductor-Insulator-Superconductor terahertz mixer integrated with a superconducting flux-flow oscillator*. Ph.D. Thesis, Delft University of Technology.

Baselmans, J. J. A., Hajenius, M., Gao, J. R., Klapwijk, T. M., Korte, P. A. J. D., Voronov, B., and Gol'tsman, G. (2004). Doubling of sensitivity and bandwidth in phonon cooled hot electron bolometer mixers. *Applied Physics Letters*, 84, 1958 – 1960.

Bladel, J. V. (1971). Mode coupling through wall losses in a waveguide. *Electronics Letters*, 7, 178 – 180.

Blundell, R. and Tong, C.-Y. E. (1992). Submillimeter receivers for radio astronomy. *Proceedings of the IEEE*, 80, 1702 – 1720.

Bock, D. (1999). Measurements of a scale-model ortho-mode transducer. *BIMA Memo*, 74.

Boifot, A. M., Lier, E., and Schaug-Petersen, T. (1990). Simple and broadband orthomode transducer. *Proceedings of IEE*, 137, 396 – 400.

Booker, H. (1982). Energy in Electromagnetism. 1st Edition. Peter Peregrinus.

Brenner, H. E. (1967a). Perturbations of the critical parameters of the quarter-wave directional couplers. *IEEE Transactions on Microwave Theory and Techniques*, 15, 384 – 385.

Brenner, H. E. (1967b). λ/4-Richtkoppler in inhomogenem medum mit abweichungen der gleich- und gegentaktparameter vom idealwert. *Frequenz*, 26, 156 – 165.

Browne, J. (1987a). Broadband amps sport coplanar waveguide. *Microwaves RF*, 26, 131 – 134.

Browne, J. (1987b). Coplanar MIC amplifier bridges 0.5 to 18.0 GHz. *Microwaves RF*, 26, 194 – 195.

Browne, J. (1989). Coplanar waveguide supports integrated multiplier systems. *Microwaves RF*, 28, 137 – 138.

Browne, J. (1990). Coplanar circuits arm limiting amp with 100-dB gain. *Microwaves RF*, 29, 213 – 220.

Browne, J. (1992). Broadband amp drops through noise floor. *Microwaves RF*, 31, 141 – 144.

Caloz, C. and Itoh, T. (2004). A novel mixed conventional microstrip and composite right/left-handed backward-wave directional coupler with broadband and tight coupling characteristics. *IEEE Microwave and Wireless Components Letters*, 14, 31 – 33.

Calvo, M., Giordano, C., Battiston, R., de Bernadis, P., Margesin, B., Masi, S., and Monfardini, A. (2010). Development of kinetic inductance detectors for cosmic microwave background experiments. *Experimental Astronomy*, 28, 185 – 194.

Carter, M. C., Baryshev, A., Harman, M., Lazareff, B., Lamb, J., Navarro, S., John, D., Fontana, A. -L., Ediss, G., Tham, C. Y., Withington, S., Tercero, F., Nesti, R., Tan, G. -H., Sekimoto, Y., Matsunaga, M., Ogawa, H., and Claude, S. (2004). ALMA front-end optics. *Proceedings of the Society of Photo Optical Instrumentation Engineers*, 5489, 1074 – 1084.

Chattopadhyay, G., Phihour, B., Carlstrom, J. E., Church, S., Lange, A., and Zmuidzinas, J. (1998). A 96-GHz ortho mode transducer for the polatron. *IEEE Microwave and Guided Wave Letters*, 8, 321 – 341.

Chattopadhyay, G., Schlecht, E., Maiwald, F., Dengler, R. J., Pearson, J. C., and Mehdi, I. (2002). Frequency multiplier response to spurious signals and its effects on local oscillator systems in millimeter and submillimeter wavelengths. *Proceedings of the Society of Photo-Optical Instrumentation Engineers*, 4855, 480 – 488.

Cheng, D. K. (1989). Field and Wave Electromagnetics. In: *Waveguides and Cavity Resonators*. 2nd Edition. (pp. 520 – 599). US. Addison Wesley.

Cherednichenko, S., Khosropanah, P., Kollberg, E., Kroug, M., and Merkel, M. (2002). Terahertz superconducting hot-electron bolometer mixers. *Physica C: Superconductivity*, 372 - 376, 407 - 415.

Chou, R. C. and Lee, S. W. (1988). Modal attenuation in multilayered coated waveguides. *IEEE Transactions on Microwave Theory and Techniques*, 36, 1167 – 1176.

Claricoats, P. J. B. (1960a). Propagation along unbounded and bounded dielectric rods: Part 1. Propagation along an unbounded dielectric rod. *IEE Monograph*, 409E, 170 – 176.

Claricoats, P. J. B. (1960b). Propagation along unbounded and bounded dielectric rods: Part 2. Propagation along a dielectric rod contained in a circular waveguide. *IEE Monograph*, 409E, 177 – 185.

Collin, R. E. (1991). Field Theory of Guided Waves. In: *Waveguides and Cavities*. 2nd Edition. (pp. 329 – 410). New York. IEEE Press.

Cooper, L. N. (1956). Bound electrons pairs in a degenerate Fermi gas. *IEEE Transactions on Microwave Theory and Techniques*, 104, 1189 – 1190.

Cresci, L., Ciappi, L., Nesti, R., Palagi, F., and Panella, D. (2002). C-band septum polarizer design. *Arcetri Technical Report*, 1 – 12.

Day, P. K., LeDuc, H. G., Mazin, B. A., Vayonakis, A., and Zmuidzinas, Z. (2003). A broadband superconducting detector suitable for use in large arrays. *Nature*, 425, 817 – 821.

Deck, R. T., Mirkov, M., and Bagley, B. G. (1998). Determination of bending losses in rectangular waveguides. *Journal of Lightwave Technology*, 16, 1703 – 1714.

Duzer, T. V., and Turner, C. W. (1981). Principles of superconductive devices and circuits. 1st Edition. Elsevier.

Edwards, T. C. (1981). Foundations for Microstrip Circuit Design. 1st Edition. John Wiley and Sons.

Ellison, B. N., and Miller, R. E. (1988). A low noise 230 GHz receiver. *International Journal of Infrared and Millimeter Waves*, 9, 361 – 370.

Endo, A., Noguchi, T., Kroug, M., Shitov, S. V., Shan, W. L., Tamura, T., Kojima, T., Uzawa, Y., Sakai, T., Inoue, H., and Kohno, K. (2009). A THz SIS mixer with a NbTiN-ground plane and SIS microtrilayers directly grown on a quartz substrate. *IEEE Transactions on Applied Superconductivity*, 18, 400 – 404.

Figer, D. F. (2010). Future detectors for astrophotonics. *Conference of Frontiers in Optics, Rochester*, New York.

Finger, R. And Kerr, A. R. (2008). Microwave loss reduction in cryogenically cooled conductors. *International Journal of Infrared and Millimeter Waves*, 29, 924 – 932.

Ghione, G. (1993). A CAD-oriented analytical model for the losses of general asymmetric coplanar lines in hybrid and monolithic MICs. *IEEE Transactions on Microwave Theory and Techniques*, 41, 1499 – 1510.

Glaser, J. I. (1969). Attenuation and guidance of modes on hollow dielectric waveguides. *IEEE Transactions on Microwave Theory and Techniques (Correspondence)*, 17, 173 – 176.

Gopinath, A. (1982). Losses in coplanar waveguide. *IEEE Transactions on Microwave Theory and Techniques*, 30, 1101 – 1104.

Green, H. F. (1965). The numerical solution of some important transmission-line problems. *IEEE Transactions on Microwave Theory and Techniques*, 13, 676 – 692.

Grimes, P. K., King, O. G., Yassin, G., and Jones, M. E. (2007). Compact broadband planar orthomode transducer. *Electronics Letters*, 43, 1146 – 1147.

Grunberger, G. K. and Meinke, H. H. (1971). Experimenteller und theoretischer nachweis der langsfeldstarken in der grundwelle der mikrowellen-streifenleitung. *Nachrichtentechnische Zeitschrift*, 24, 364 – 368.

Grunberger, G. K., Keine, V., and Meinke, H. H. (1970). Longitudinal field components and frequency-dependent phase velocity in the microstrip transmission line. *Electronics Letters*, 6, 683 – 685.

Gupta, K. C., Garg, R., Gahl, I., and Bhartia, P. (1996). Microstrip Lines and Slotlines. In: *Microstrip Lines II*. 2nd Edition. (pp. 61 – 151). London. Artech House.

Gustincic, J. J. (1963). A general power loss method for attenuation of cavities and waveguides. *IEEE Transactions on Microwave Theory and Techniques*, 62, 83 – 87.

Hammerstad, E. and Jansen, O. (1980). Accurate models for microstrip computer-aided design. *IEEE MTT-S International Microwave Symposium Digest*, 207 – 209.

Hammerstad, E. O. and Bekkadal, F. (1975). *Microstrip Handbook*, ELAB Report, University of Trondheim, Norway.

Hasnain, G., Dienes, A., and Whinnery, J. R. (1986). Dispersion of picosecond pulses in coplanar transmission lines. *IEEE Transactions on Microwave Theory and Techniques*, 34, 738 – 741.

Heinrich, W. (1990). Full-Wave Analysis of Conductor Losses on MMIC Transmission Lines. *IEEE Transactions on Microwave Theory and Techniques*, 38, 1468 – 1472.

Heitkamper, P. and Heinrich, W. (1991). On the calculation of conductor loss on planar transmission lines assuming zero strip thickness. *IEEE Transactions on Microwave Theory and Techniques*, 39, 586 – 588.

Hilberg, W. (1969). From approximations to exact relations for characteristic impedances. *IEEE Transactions on Microwave Theory and Techniques*, 17, 259 – 265.

Ho, T. Q. and Shih, Y. C. (1989). Spectral-domain analysis of E-plane waveguide to microstrip transitions. *IEEE Transactions on Microwave Theory and Techniques*, 37, 388 – 392.

Hong, J. -S. and Lancaster, M. J. (1997). Theory and experiment of novel microstrip slow-wave open loop resonator filters. *IEEE Transactions on Microwave Theory and Techniques*, 45, 2358 – 2365.

Hsu, C. -L., Hsu, F. -C., and Kuo, J. -T. (2005). Microstrip bandpass filters for ultra-wideband (UWB) wireless communication. *IEEE MTT-S International Symposium Digest*, 679 – 682.

Imbriale, W. A., Otoshi, T. Y., and Ceh, C. (1998). Power loss for multimode waveguides and its application to beam waveguide systems. *IEEE Transactions on Microwave Theory and Techniques*, 46, 523 – 529.

Itoh, T. (1989). Overview of quasi-planar transmission lines. *IEEE Transactions on Microwave Theory and Techniques*, 37, 275 – 280.

Itoh, T. and Mittra, R. (1972). Analysis of microstrip transmission lines. *Antenna Laboratory Report*, 72-5.

Itoh, T. and Mittra, R. (1973). Spectral domain for calculating the dispersion characteristics of microstrip lines. *IEEE Transactions on Microwave Theory and Techniques*, 21, 496 – 499.

Itoh, T. and Mittra, R. (1974). A technique for computing dispersion characteristics of shielded microstrip lines. *IEEE Transactions on Microwave Theory and Techniques*, 22, 896 – 898.

Jackson, R. W. (1986). Considerations in the use of coplanar waveguide for millimeter-wave integrated circuits. *IEEE Transactions on Microwave Theory and Techniques*, 34, 1450 – 1456.

Jahnke, E., Emde, F., and Losch, F. (1960). Tables of Higher Functions. 1st Edition. New York: McGraw-Hill.

Kautz, R. L. (1978). Picosecond pulses on superconducting striplines. *Journal of Applied Physics*, 49, 308 – 314.

Kerr, A. R. (1999). Surface impedance of superconductors and normal conductors in EM simulators. *MM Memo*, 245.

Kittara, P., Grimes, P., Yassin, G., Withington, S., Jacobs, K., and Wulff, S. (2004). A 700-GHz SIS antipodal finline mixer fed by a Pickett-Potter horn-reflector antenna. *IEEE Transactions on Microwave Theory and Techniques*, 52, 2352 – 2360.

Kittara, P., Yassin, G., and Withington, S. (2002). Analysis of superconducting coplanar waveguides for SIS mixer circuits. *Proceedings of the 13th International Symposium on Space Terahertz Technology*, Harvard University, US.

Kittel, C. (1986). Introduction to Solid State Physics. 1st Edition. John Wiley and Sons.

Kohler, M. and Bayer, H. (1964). Feld und ausbreitungskontante im rechteckhohlrohr bei endlicher leifahigkeit des wandmaterials. *Zeitschrift Fur Angewandte Physik*, 18, 16 – 22.

Komatsu, E., Smith, K. M., Dunkley, J., Bennett, C. L., Gold, B., Hinshaw, G., Jarosik, N., Larson, D., Nolta, M. R., Page, L., Spergel, D. N., Halpern, M., Hill, R. S., Kogut, A., Limon, M., Meyer, S. S., Odegard, N., Tucker, G. S., Weiland, G. L., Wollack, E., and Wright, E. L. (2010). Seven-year Wilkinson Microwave Anisotropy Probe (WMAP) observations: Cosmological interpretation. *The Astrophysical Journal Supplement*, 192, 18.

Kooi, J. W., Walker, C. K., LeDuc, H. G., Hunter, T. R., Benford, D. J., and Phillips, T. G. (1994). A low noise 665 GHz quasi-particle waveguide receiver. *International Journal of Infrared and Millimeter Waves*, 15, 477 – 492.

Kowalski, G. and Pregla, R. (1971). Dispersion characteristics of shielded microtrips with finite thickness. *Arch. Elek. Ubertragung*, 25, 193 – 196.

Krammer, H. (1976). Field configurations and propagation constants of modes in hollow rectangular dielectric waveguides. *IEEE Journal of Quantum Electronics (Correspondence)*, 505 – 507.

Kraus, J. D. (1986). *Radio Astronomy*. 2nd Edition. Cygnus-Quasar.

Kumar, A. and Galawa, R. L. (1994). Bending-induced loss in dual-mode rectangular waveguides. *Optics Letters*, 19, 707 – 709.

Lee, W. W. S. and Yung, E. K. N. (1994). The input impedance of a coaxial line fed probe in a cylindrical waveguide. *IEEE Transactions on Microwave Theory and Techniques*, 42, 1468 – 1473.

Liu, Y. and Itoh, T. (1992). Leakage phenomena in multilayered conductor-backed coplanar waveguide. *IEEE Microwave Guided Wave Letters*, 2, 426 – 427.

London, F. (1961). Superfluids: Macroscopic Theory of Superconductivity. New York. Dover Publications, Inc.

Ma, J. (1995). Properties of high-T_c superconducting circular waveguides with Meissner boundary. *International Journal of Infrared and Millimeter Waves*, 16, 147 – 157.

Ma, J. (1998). TM-properties of HTS's rectangular waveguides with Meissner boundary condition. *International Journal of Infrared and Millimeter Waves*, 19, 399 – 408.

Ma, J. (1999). Wave propagation properties in high-temperature superconducting parallel-plate waveguides. *IEEE Microwave and Guided Wave Letters*, 9, 183 – 185.

Marcuvitz, N. (1986). Transmission Line Modes. In: *Waveguide Handbook*. (pp. 56 – 71). London, UK. Peter Peregrinus Ltd.

Matick, R. E. (1969). Transmission Lines for Digital and Communication Networks. In: *Superconducting Transmission Lines*. 1st Edition. (pp. 211 – 266). US. McGraw-Hill.

Mattis, D. C. and Bardeen, J. (1958). Theory of the anomalous skin effect in normal and superconducting metals. *Physical Review*, 111, 412 – 417.

Mercatili, E. A. J. and Schmeltzer, R. A. (1964). Hollow metallic and dielectric waveguides for long distance optical transmission and lasers. *Bell System Technology Journal*, 43, 1783 – 1809.

Meyers, N. H. (1961). Inductance in thin film superconducting structures. *Proceedings of the IRE*, 49, 1640 – 1649.

Mittra, R. and Itoh, T. (1971). A new technique for analysis of dispersion characteristics of microstrip lines. *IEEE Transactions on Microwave Theory and Techniques*, 19, 47 – 56.

Miyagi, M., Harada, K., and Kawakami, S. (1984). Wave propagation and attenuation in the general class of circular hollow waveguides with uniform curvature. *IEEE Transactions on Microwave Theory and Techniques*, 32, 513 – 521.

Paine, S., Papa, D. C., Leombruno, R. L., Zhang, X., Blundell, R. (1994). Beam waveguide and receiver optics for the SMA. *Proceedings of the 5th International Symposium on Space Terahertz Technology*, University of Michigan, Ann Arbor, Michigan.

Papadopoulos, V. M. (1954). Propagation of electromagnetic waves in cylindrical waveguides with imperfectly conducting walls. *Quarterly Journal of Mechanics and Applied Mathematics*, 7, 325 – 334.

Phillips, T. G. and Keene, J. (1992). Submillimeter astronomy. *Proceedings of the IEEE*, 80, 1662 – 1678.

Pozar, D. M. (2005). Microwave Engineering. In: *Transmission Lines and Waveguides*. 3rd Edition. (pp. 91 – 154). US. John Wiley and Sons.

Pucel, R. A., Masse, D. J., and Hartwig, C. P. (1968a). Losses in microstrip. *IEEE Transactions on Microwave Theory and Techniques*, 16, 342 – 350.

Pucel, R. A., Masse, D. J., and Hartwig, C. P. (1968b). Correction to "losses in microstrip. *IEEE Transactions on Microwave Theory and Techniques*, 16, 1064.

Riaziat, M., Majidi-Ahy, R., Feng, I. J. (1990). Propagation modes and dispersion characteristics of coplanar waveguides. *IEEE Transactions on Microwave Theory and Techniques*, 38, 245 – 251.

Robson, P. N. (1963). A variational integral for the propagation coefficient of a cylindrical waveguide with imperfectly conducting walls. *Proceedings of IEE*, 110, 859 – 864.

Sadhir, V. K., Bahl, I. J., and Willems, D. A. (1994). CAD compatible accurate models of microwave passive lumped elements for MMIC applications. *International Journal Microwave and Millimeter-Wave Computer-Aided Engineering*, 4, 148 – 162.

Schaerth, S., Vayonakis, A., Day, P., Glenn, J., Columbia, S., Kumar, S., LeDuc, H., Masin, B., Vaillancourt, J., and Zmuidzinas, J. (2008). A millimetre and submillimeter kinetic inductance detector camera. *Journal of Low Temperature Physics*, 151, 684 – 689.

Schelten, J., Ullmaier, H., and Schmatz, W. (1971). Neutron diffraction by vortex lattices in superconducting Nb and Nb0.73Ta0.27. *Physica Status Solidi (b)*, 48, 619 – 628.

Schneider, M. V. (1965). Computation of impedance and attenuation of TEM-lines by finite difference methods. *IEEE Transactions on Microwave Theory and Techniques*, 13, 793 – 800.

Schneider, M. V. (1969). Microstrip lines for microwave integrated circuits. *Bell System Technical Journal*, 48, 1421 – 1444.

Schneider, V. M., Glance, B., and Bodtmann, W. F. (1969). Microwave and millimetre wave hybrid integrated circuits for radio systems. *Bell System Technical Journal*, 48, 1703 – 1726.

Seida, O. M. A. (2003). Propagation of electromagnetic waves in a rectangular tunnel. *Applied Mathematics and Computation*, 136, 405 – 413.

Serizawa, Y., Sekimoto, Y., Kamikura, M., Shan, W. L., and Ito, T. (2008). A 400 – 500 GHz balanced SIS mixer with a waveguide quadrature hybrid coupler. *International Journal of Infrared and Millimeter Waves*, 29, 846 – 861.

Shankar, N. U. (1986). *Application of digital techniques to radio astronomy measurements*, Ph.D. Thesis. Raman Research Institute. Bangalore University.

Somlo, P. I. and Hunter, J. D. (1996). On the TE10 mode cutoff frequency in lossy-walled rectangular waveguides. *IEEE Transactions on Instrumentation and Measurement*, 45, 301 – 304.

Stinehelfer, H. E. (1968). An accurate calculation of uniform microstrip transmission lines. *IEEE Transactions on Microwave Theory and Techniques*, 16, 439 – 444.

Stratton, J. A. (1941). Electromagnetic Theory. In: *Boundary-Value Problems*. 1st Edition. (pp. 482 – 588). New York. McGraw-Hill.

Swihart, J. C. (1961). Field solution for a thin-film superconducting strip transmission lines. *Journal of Applied Physics*, 32, 461 – 469.

Syahkal, D. M. and Davies, J. B. (1979). Accurate solution of microstrip and coplanar structures for dispersion and for dielectric and conductor losses. *IEEE Transactions on Microwave Theory and Techniques*, 27, 694 – 699.

Tarenghi, M. (2008). The Atacama Large Millimeter / Submillimieter Array: Overview and status. *Astrophysics and Space Science*. 313, 1 – 7.

Tham, C. Y., McCowen, A., and Towers, M. S. (2001). Efficient modelling of PCB transients via a full-wave 3d frequency domain integral equation. *IEEE Transactions on Magnetics*, 37, 3676 – 3679.

Tham, C. Y., McCowen, A., and Towers, M. S. (2003). Modelling of PCB transients with boundary elements/method of moments in the frequency domain. *Engineering Analysis with Boundary Elements*, 27, 315 – 323.

Track, E. K., Radparvar, M., and Faris, S. M. (1989). Modulation of the penetration depth of Nb and NbN films by quasiparticle injection. *IEEE Transactions on Magnetics*, 25, 1096 – 1099.

Vassilev, V. and Belitsky, V. (2001a). A new 3-dB power divider for millimetre-wavelengths. *IEEE Microwave and Wireless Components Letters*, 11, 30 – 32.

Vassilev, V. and Belitsky, V. (2001b). Design of sideband separation SIS mixer for 3 mm band. *Proceedings of the 12th International Symposium on Space Terahertz Technology*, Shelter Island, San Diego, California.

Vassilev, V., Belitsky, V., Risacher, C., Lapkin, I., Pavolotsky, A., and Sundin, E. (2004). Design and characterization of a sideband separating SIS mixer for 85 – 115 GHz. *Proceedings of the 15th International Symposium on Space Terahertz Technology*, Hotel Northampton, Northampton, Masachusetts.

Veyres, C. and Hanna, V. F. (1980). Extension of the application of conformal mapping techniques to coplanar lines with finite dimensions. *Int. Journal of Electron*ics, 48, 47 – 56.

Walker, C. K., Kooi, J. W., Chan, M., Leduc, H. G., Schaffer, P. L., Carlstrom, J. E., and Phillips, T. G. (1992). A low-noise 492 GHz SIS waveguide receiver. *International Journal of Infrared and Millimeter Waves*, 13, 785 – 798.

Wang, Y., Qiu, Z. A., Yalamanchili, R. (1994). Meissner model of superconducting rectangular waveguides. *International Journal of Electronics*, 76, 1151 – 1171.

Wen, C. P. (1969). Coplanar waveguide: A surface strip transmission line suitable for non-reciprocal gyromagnetic device application. *IEEE Transactions on Microwave Theory and Techniques*, 17, 1087 – 1090.

Wengler, M. J. (1992). Submillimeter waves detection with superconducting tunnel junctions. Proceedings of the *IEEE*, 80, 1810 – 1826.

Wheeler, H. A. (1942). Formulas for the skin effect. *Proceedings of IRE*, 30, 412 – 424.

Wheeler, H. A. (1964). Transmission-line properties of parallel wide strips by a conformal mapping approximation. *IEEE Transactions on Microwave Theory and Techniques*, 12, 280 – 289.

Wheeler, H. A. (1965). Transmission-line properties of parallel strips separated by a dielectric sheet. *IEEE Transactions on Microwave Theory and Techniques*, 12, 172 – 185.

Wheeler, H. A. (1977). Transmission-line properties of a strip on a dielectric sheet on a plane. *IEEE Transactions on Microwave Theory and Techniques*, 25, 631 – 647.

Winters, J. H. and Rose, C. (1991). High-T_c superconductors waveguides: Theory and applications. *IEEE Transactions on Microwave Theory and Techniques*, 39, 617 – 623.

Withington, S. (2003). Terahertz astronomical telescopes and instrumentation. *Philosophical Transactions of the Royal Society of London*, 362, 395 – 402.

Withington, S. and Yassin, G. (1996). Theoretical analysis of superconducting submillimetre wave microstrip transmission lines. *Proceedings of the 7th International Symposium on Space Terahertz Technology*, Charlottesville, US.

Withington, S. and Yassin, G. (1997). An investigation of the input impedance of a microstrip probe in waveguide. *Proceedings of the 8th International Symposium on Space Terahertz Technology*.

Withington, S., Campbell, E., Yassin, G., Tham, C. Y., Wolfe, S., and Jacobs, K. (2003). Beam combining superconducting detector for submillimetre-wave astronomical interferometry. *Electronics Letters*, 39, 605 – 606.

Withington, S., Yassin, G., Leech, J., and Isaak, K. G. (1999). An accurate expression for the input impedance of one-sided microstrip probes in waveguide. *Proceedings of the 10th International Symposium on Space Terahertz Technology*, Charlottesville, pp. 508 – 518.

Woody, D. P., Miller, R. E., and Wengler, M. J. (1985). 85 – 115 GHz receivers for radio astronomy. *IEEE Transactions on Microwave Theory and Techniques*, 33, 90 – 95.

Yalamanchili, R., Qiu, Z. A., Wang, Y. (1995). Rectangular waveguides with two conventional and two superconducting walls. *International Journal of Electronics*, 78, 715 – 727.

Yamashita, E. (1968). Variational method for the analysis of microstrip-like transmission-lines. *IEEE Transactions on Microwave Theory and Techniques*, 16, 529 – 535.

Yamashita, E. and Mittra, E. (1968). Variational method for the analysis of microstrip lines. *IEEE Transactions on Microwave Theory and Techniques*, 16, 251 – 256.

Yassin, G. and Withington, S. (1995). Electromagnetic models for superconducting millimetre-wave and submillimetre-wave microstrip transmission line. *Journal of Physics D: Applied Physics*, 28, 1983 – 1991.

Yassin, G. and Withington, S. (1996a). Loss in normal and superconducting millimetre-wave and submillimetre wave microstrip transmission line. *Proceedings of the 3rd IEE International Conference on Computation in Electromagnetics*, Bath, UK.

Yassin, G. and Withington, S. (1996b). Analytical expression for the input impedance of a microstrip probe in waveguide. *International Journal of Infrared and Millimeter Waves*, 17, 1685 – 1705.

Yassin, G., Jung, G., Dikovsky, V., Barboy, I., Kambara, M., Cardwell, D. A., and Withington, S. (2001). Investigation of microwave propagation in high-temperature superconducting waveguides. *IEEE Transactions on Microwave Theory and Techniques*, 11, 413 – 415.

Yassin, G., Padman, R., Withington, S., Jacobs, K., and Wulff, S. (1997). Broadband 230 GHz finline mixer for astronomical imaging arrays. *Electronic Letters*, 33, 498 – 500.

Yassin, G., Tham, C. Y., and Withington, S. (2003). Propagation in lossy and superconducting cylindrical waveguides. *Proceedings of* the *14th International Symposium on Space Terahertz Technology*, Tucson, Arizona.

Yassin, G., Withington, S., Buffey, M., Jacobs, K., and Wulff, S. (2000). A 350-GHz SIS antipodal finline mixer. *IEEE Transactions on Microwave Theory and Techniques*, 48, 662 – 669.

Zysman, G. I. and Varon, D. (1969). Wave propagation in microstrip transmission lines. *IEEE G-MTT International Microwave Symposium Digest*, 2 – 9.

APPENDIX A

DERIVATION OF HELMHOLTZ'S EQUATIONS

The electric $\vec{E}$ and magnetic $\vec{H}$ fields in Maxwell's equations can be expressed in phasor forms as

$$\nabla \times \vec{E} = -j\omega\mu \vec{H}, \tag{A.1}$$

$$\nabla \times \vec{H} = \vec{J} + j\omega\varepsilon \vec{E}, \tag{A.2}$$

$$\nabla \cdot \vec{E} = \rho, \tag{A.3}$$

$$\nabla \cdot \vec{H} = 0, \tag{A.4}$$

where $\vec{J}$ is the density of free current, ρ charge density, ω the angular frequency, and ε and μ are the permittivity and permeability of the medium, respectively.

For an electromagnetic wave propagating in a linear, isotropic, and homogeneous nonconducting medium, Maxwell's equations reduce to

$$\nabla \times \vec{E} = -j\omega\mu \vec{H}, \tag{A.5}$$

$$\nabla \times \vec{H} = j\omega\varepsilon \vec{E}, \tag{A.6}$$

$$\nabla \cdot \vec{E} = 0, \tag{A.7}$$

$$\nabla \cdot \vec{H} = 0. \tag{A.8}$$

In order to obtain a second order equation in $\vec{E}$ alone, the curl of (A.5) is taken, giving

$$\nabla \times \nabla \times \vec{E} = -j\omega\mu\left(\nabla \times \vec{H}\right). \tag{A.9}$$

Substituting (A.6) into (A.9), (A.9) can be expressed in term of $\vec{E}$ alone as

$$\nabla \times \nabla \times \vec{E} = \omega^2 \mu\varepsilon \vec{E}. \tag{A.10}$$

Using the vector identity $\nabla \times \nabla \times \vec{E} = \nabla\nabla \cdot \vec{E} - \nabla^2 \vec{E}$ (Cheng, 1989; Collin, 1991) and replacing $\nabla \cdot \vec{E}$ by (A.7) gives the desired result

$$\nabla^2 \vec{E} + k^2 \vec{E} = 0. \tag{A.11}$$

where $k = \omega\sqrt{\mu\varepsilon}$ is called the wavenumber.

Applying a similar procedure, an equation in $\vec{H}$ can be obtained as

$$\nabla^2 \vec{H} + k^2 \vec{H} = 0 . \qquad \text{(A.12)}$$

Both (A.11) and (A.12) are referred to as the homogeneous vector Helmholtz's equations.

APPENDIX B

DERIVATION OF THE TRANSVERSE FIELD COMPONENTS IN CARTESIAN COORDINATES

Maxwell's source free curl equations can be expanded in Cartesian coordinates to give

$$\nabla \times \vec{E} = -j\omega\mu \vec{H}, \tag{B.1}$$

$$\frac{\partial}{\partial y} E_z + jk_z E_y = -j\omega\mu H_x, \tag{B.1a}$$

$$-\frac{\partial}{\partial x} E_z - jk_z E_x = -j\omega\mu H_y, \tag{B.1b}$$

$$\frac{\partial}{\partial x} E_x - \frac{\partial}{\partial y} E_x = -j\omega\mu H_z, \tag{B.1c}$$

and

$$\nabla \times \vec{H} = j\omega\varepsilon \vec{E}, \tag{B.2}$$

$$\frac{\partial}{\partial y} H_z + jk_z H_y = j\omega\varepsilon E_x, \tag{B.2a}$$

$$-\frac{\partial}{\partial x} H_z - jk_z H_x = j\omega\varepsilon E_y, \tag{B.2b}$$

$$\frac{\partial}{\partial x} H_y - \frac{\partial}{\partial y} H_x = j\omega\varepsilon E_z, \tag{B.2c}$$

where $\vec{E}$ and $\vec{H}$ are the electric and magnetic fields, respectively, k_z the propagation constant, ω the angular frequency, ε and μ are the permittivity and permeability of the medium, respectively, and E_x, E_y, E_z, and H_x, H_y, H_z, are the electric and magnetic fields components in the x, y, and z directions, respectively. Here, the common factor $\exp[j(\omega t + k_z z)]$ have been omitted.

Expressing the transverse field components in terms of the longitudinal components E_z and H_z, the following equations can be obtained

$$H_x = -\frac{1}{h^2}\left(jk_z \frac{dH_z}{dx} - j\omega\varepsilon \frac{dE_z}{dy} \right), \tag{B.4}$$

$$H_y = -\frac{1}{h^2}\left(jk_z \frac{dH_z}{dy} + j\omega\varepsilon \frac{dE_z}{dx} \right), \tag{B.5}$$

$$E_x = -\frac{1}{h^2}\left(jk_z \frac{dE_z}{dx} + j\omega\mu \frac{dH_z}{dy} \right), \tag{B.6}$$

$$E_y = -\frac{1}{h^2}\left(jk_z \frac{dE_z}{dy} - j\omega\mu \frac{dH_z}{dx} \right). \tag{B.7}$$

APPENDIX C

DERIVATION OF THE TRANSVERSE FIELD COMPONENTS IN CYLINDRICAL COORDINATES

Maxwell's source free curl equations can be expanded in cylindrical coordinates to give

$$\nabla \times \vec{E} = -j\omega\mu \vec{H}, \tag{C.1}$$

$$\frac{1}{r}\frac{\partial}{\partial \phi} E_z + jk_z E_\phi = -j\omega\mu H_r, \tag{C.1a}$$

$$-\frac{\partial}{\partial r} E_z - jk_z E_r = -j\omega\mu H_\phi, \tag{C.1b}$$

$$\frac{\partial}{\partial r} E_\phi - \frac{1}{r}\frac{\partial}{\partial \phi} E_r = -j\omega\mu H_z, \tag{C.1c}$$

and

$$\nabla \times \vec{H} = j\omega\varepsilon \vec{E}, \tag{C.2}$$

$$\frac{1}{r}\frac{\partial}{\partial \phi} H_z + jk_z H_\phi = j\omega\varepsilon E_r, \tag{C.2a}$$

$$-\frac{\partial}{\partial r} H_r - jk_z H_r = j\omega\varepsilon E_\phi, \tag{C.2b}$$

$$\frac{\partial}{\partial r} H_\phi - \frac{\partial}{\partial \phi} H_r = j\omega\varepsilon E_z, \tag{C.2c}$$

where $\vec{E}$ and $\vec{H}$ are the electric and magnetic fields, respectively, k_z the propagation constant, ω the angular frequency, ε and μ are the permittivity and permeability of the medium, respectively, and E_r, E_ϕ, E_z, and H_r, H_ϕ, H_z, are the electric and magnetic fields components in the r, ϕ, and z directions, respectively. Here, the common factor exp[j($\omega t + k_z z$)] have been omitted.

Expressing the transverse field components in terms of the longitudinal components E_z and H_z, the following equations can be obtained

$$H_r = -\frac{1}{h^2}\left(jk_z \frac{dH_z}{dr} - \frac{j\omega\varepsilon}{r}\frac{dE_z}{d\phi} \right), \tag{C.4}$$

$$H_\phi = -\frac{1}{h^2}\left(\frac{jk_z}{r}\frac{dH_z}{d\phi} + j\omega\varepsilon\frac{dE_z}{dr} \right), \tag{C.5}$$

$$E_r = -\frac{1}{h^2}\left(jk_z \frac{dE_z}{dr} + \frac{j\omega\mu}{r}\frac{dH_z}{d\phi} \right), \tag{C.6}$$

$$E_\phi = -\frac{1}{h^2}\left(\frac{jk_z}{r}\frac{dE_z}{d\phi} - j\omega\mu\frac{dH_z}{dr} \right). \tag{C.7}$$

PUBLICATIONS

Book Chapter

Yeap, K. H., Tham, C. Y., Yassin, G., and Yeong, K. C. (2011). *Propagation in lossy rectangular waveguides*. Electromagnetic waves propagation in complex matter, Intech, 255 – 272.

Journal Papers

Yeap, K. H., Tham, C. Y., Yassin, G., and Yeong, K. C. (2011). Attenuation in rectangular waveguides with finite conductivity walls. *Radioengineering Journal*, 20, 472 – 478. (Indexed in ISI)

Yeap, K. H., Lai, K. C., Tham, C. Y., Yeong, K. C., and Lim, E. H. (2011). Electromagnetic wave propagation in microstrip transmission lines. *Journal of Applied Sciences*, 11, 1376 – 1380. (Indexed in Scopus)

Yeap, K. H., Tham, C. Y., Yeong, K. C., Yong, Y. T., and Chong, K. H. (2010). Propagation near cutoff frequency in a lossy rectangular waveguide. *International Journal of Electronics, Computer, and Communications Technologies*, 1, 26 - 30.

Yeap, K. H., Tham, C. Y., Yeong, K. C., and Woo, H. J. (2010). Wave propagation in lossy and superconducting circular waveguides. *Radioengineering Journal*, 19, 320 – 325. (Indexed in ISI)

Yeap, K. H., Tham, C. Y., Yeong, K. C., and Lim, E. H. (2010). Full wave analysis of normal and superconducting microstrip transmission lines. *Frequenz Journal of RF-Engineering and Telecommunications*, 64, 59 – 66. (Indexed in ISI)

Yeap, K. H., Tham, C. Y., Yeong, K. C., and Yeap, K. H. (2009). A simple method for calculating attenuation in waveguides. *Frequenz Journal of RF-Engineering and Telecommunications*, 63, 236 – 240. (Indexed in ISI)

Conference Papers

Yeap, K. H., Tham, C. Y., Yeong, K. C., Lim, E. H., and Lai, K. C. (2010). Electromagnetic wave propagation in microstrip transmission lines. *Proceedings of the 1st International Conference of Fundamental and Applied Sciences*, Kuala Lumpur Convention Centre, Malaysia.

Yeap, K. H., Tham, C. Y., and Yeong, K. C. (2009). Attenuation of the dominant mode in a lossy rectangular waveguide. *Proceedings of the IEEE 9th Malaysia International Conference on Communications*, KL., Malaysia. (Indexed in ISI)

Yeap, K. H., Tham, C. Y., Yeong, K. C., Woo, H. J., and Chong, K. H. (2009). Full wave analysis of a superconducting stripline with large width-to-separation ratio. *Proceedings of the IEEE 7th Student Conference on Research and Development*, UPM, Serdang, Malaysia. (Indexed in IEEExplore)